Stony Brook University

Dissolved Manganese in Bioturbated Marine Sediments:

a Multi-Dimensional Characterization

A Dissertation Presented

by

Jaime Patricio Soto Neira

to

The Graduate School

in Partial Fulfillment of the

Requirements

for the Degree of

Doctor of Philosophy

in

Marine and Atmospheric Sciences

Stony Brook University

August 2015

Stony Brook University

The Graduate School

Jaime Patricio Soto Neira

We, the dissertation committee for the above candidate for the

Doctor of Philosophy degree, hereby recommend

acceptance of this dissertation.

Qingzhi Zhu – Dissertation co-Advisor
Associate Professor, School of Marine and Atmospheric Sciences

Robert C. Aller – Dissertation co-Advisor
Distinguished Professor, School of Marine and Atmospheric Sciences

Cindy Lee – Committee Chairperson
Distinguished Professor, School of Marine and Atmospheric Sciences

Mary Scranton – Committee Member
Professor, School of Marine and Atmospheric Sciences

Franck Gilbert – External Committee Member
Senior Scientist, Centre National de la Recherche Scientifique, France.

This dissertation is accepted by the Graduate School

Charles Taber
Dean of the Graduate School

Abstract of the Dissertation

Dissolved Manganese in Bioturbated Marine Sediments:

a Multi-Dimensional Characterization

by

Jaime Patricio Soto Neira

Doctor of Philosophy

in

Marine and Atmospheric Science

Stony Brook University

2015

Manganese is widely distributed on Earth and is essential for almost all living organisms. It is a redox reactive metal and under natural conditions is commonly present as Mn(II), Mn(III), and Mn(IV). In marine environments, Mn is involved in a diverse set of organic and inorganic reactions, including use by phytoplankton as a micronutrient in the photic zone, as a shield against oxygen by anaerobic microorganisms, as well as an electron acceptor during organic matter remineralization by microbes in sedimentary deposits under suboxic conditions. Thus, manganese is directly linked to carbon, nitrogen and sulfur cycles by participating in the formation, preservation and remineralization of organic matter, as well as in the sequestration, remobilization, and transport of trace metals.

Measuring the concentrations of dissolved manganese in marine sedimentary environments is challenging. Chemical speciation of this element, adsorption and desorption processes, complexation with both organic and inorganic ligands, and physical reworking of sedimentary

deposits by macrofaunal activities, generate highly complex distributional patterns for Mn in space and time, which traditional one-dimensional analytical methods fail to resolve. For this reason, this research focused on both the development and use of a planar optode, with capabilities of measuring two- and three-dimensional distributions of dissolved manganese (Mn II) in marine pore waters. These multi-dimensional measurements provided a complement for the already available techniques to further elucidate Mn cycling and associated biogeochemical processes in the heterogeneous bioturbated zone of marine deposits.

This study followed a sequential three-stages approach for developing a planar optode to measure Mn(II) and using it to characterize Mn distribution patterns in marine sedimentary deposits. The first stage involved the identification of the complex formed by the metallation reaction of 4,4',4'',4''-(Porphine-5,10,15, 20-tetrayl) tetrakis (benzenesulfonic acid) with cadmium (Cd-TSPP) as a suitable chemical indicator for Mn(II), and its application in a wet-chemical spectrophotometric method for the detection of Mn(II) in marine pore waters. The second stage included the development of a planar transparent optical sensor film (planar optode) that is suitable for two-dimensional measurement in marine sedimentary deposits by immobilizing Cd-TSPP in a modified polyurethane matrix. The third stage involved the validation and use of the developed planar optode for 2- and 3-dimensional measurements of Mn(II) in marine sediments. Validation was performed by deploying membranes with traditional 1-dimensional techniques for Mn to compare results provided by both approaches under the same conditions of sampling; while applications of the sensor included Mn(II) flux estimations across the water sediment interface and deeper sediments, as well as, simultaneous deployment of manganese sensors with 2-dimensional planar optode for ferrous iron measurements, and basic 3-dimensional tomographic reconstructions. This allowed the elucidation of the effect of

bioturbation spatially and the visualization of the effect of changes in the overlying water oxygen regimes on Mn(II) and Fe(II) fluxes across the sediment water interface. Planar optodes are deployed during both incubation experiments and in situ, by using a submersible hyperspectral imaging system.

The results of this study yielded novel information about how natural processes such as bioturbation and/or changes in oxygen regimes affect spatial and temporal distributions of dissolved species of redox sensitive metals in marine bioperturbed sediments, with consequent changes in magnitude for fluxes of the elements across the sediment-water interface. In particular, they provides an insight into how Mn(II) fluxes develop and migrate from deeper sediments to the surface under simulated hypoxic events; these incubation experiments showed how active and complex biogeochemical cycling of redox elements are in those regions and built a basis for in-situ characterizations of this phenomena in coastal areas (e.g. oxygen minimum zones). Additionally, the 1-, 2- and 3-dimensional sensing schemes developed during this work represent an expansion of our analytical capabilities, provide a new perspective for the study of redox sensitive metal cycling in marine sedimentary deposits, and open new questions about the interactions between metals and other natural processes and their contribution to the global biogeochemistry.

Table of Contents

Conclusions and perspectives

List of Figures

Figure 2.2

(A) Normalized SORET bands of various metal-TSPP complexes. (B) Q band of Cd-TSPP and Mn-TSPP in the presence of different concentrations of Mn(II).

Figure 2.3

Absorbance spectra of Cd-TSPP from 450 – 500 nm as a function of Cd-TSPP concentration. The absorbance difference, $\Delta A_{469-490}$ (inset), increases exponentially with the increase of Cd-TSPP concentration in a 200 µL artificial sea water + 50 µL Cd-TSPP solution (35‰, pH 8), (n=2 for each concentration).

Figure 2.4

The effect of salinity on Mn(II) measurements in artificial seawater. [Mn(II)]: 16 µM.

Figure 2.5

The effect of temperature on the Mn(II) measurement. (A) Corrected absorbance at 469 nm at different temperature. [Mn(II)]: 1.0 µM, pH 8. (B) Linear relationship between ln(k) and reciprocal of temperature in Kelvin, expressed by eq. (6). The slope corresponds to an Arrhenius model activation energy of 22.12 kJ mol^{-1} defining the temperature dependence of indicator-analyte reaction.

Figure 2.6

Correlation of absorbance ($\Delta A_{469-490}$) measured for specific Mn(II) concentrations in seawater at pH 4, 6 and 8 ([Mn(II)]: 2.5 µM, 3.5 µM and 5.5 µM for pH 6 and 8, 15 µM and 30 µM for pH 4). pH is defined on the total [H+] scale.

Figure 2.7

Calibration graphs constructed with (A) single absorbance at 469 nm corrected by reference at 490 nm ($\Delta A_{469-490}$) versus Mn(II) concentration in artificial seawater, (B) the second derivative of absorbance at 469 nm using Gaussian curves fitted to Mn-TSPP Soret band manganese complex spectrum. Both curves are in the range of 0 to 7.5 nmol of Mn(II) in 200 µL samples.

Figure 2.8

Correlation of the single absorbance (a) and the 2nd derivative (b) methods with the atomic absorption spectrometric method (analyte: 0-40 µM).

Figure 3.1

Three-dimensional tomographic reconstructions of bioperturbed marine sediments contained in a cylindrical core, and measured using a CT-scanner, including: (A) reconstruction of surface sediments bioperturbed by *Macoma* sp. (B) reconstruction of burrowing structures generated by *Nereis* sp. and (C) reconstruction of sedimentary structures generated by *Macoma* sp. below surface.

Figure 3.2

Diagram depicting the general immobilization scheme used in this study, including the supporting material (S), immobilizing agent (IA) and the chemical indicator (I).

Figure 3.3

Schematic representation of the setup used for one-dimensional spectrophotometric measurements, depicting the light source orientation for characterizing both the spectrophotometric properties of sensing schemes and testing immobilization properties of each scheme by measuring residuals of indicator in the immersion solution.

Figure 3.4

Schematic representation of digitalized image numerical treatment for obtaining a single dataset for each channel in the HIS color space, using four image replicas.

Figure 3.5

Schematic representation of the procedure for deploying sensing schemes in contact with lateral box-core faces (e.g. 2-D measurements of Mn(II) in bioperturbed sediments).

Figure 3.6

Setup used during the comparison between 2-D vs 1-D measurements, depicting the deployment of both sensing scheme for 2-D measurements and syringe cores for traditional subsampling of pore water in incubated sediments.

Figure 3.7

Probability density function (φ) plots for H, I and S channels (HIS color space) obtained from digitalized images of S-IA schemes containing different concentrations of IA (0.025 g/ml, 0.05 g/ml, 0.1 g/ml, 0.2 g/ml and 0.4 g/ml).

Figure 3.8

Digitalized image of (A) the normal visual aspect of foils prepared using Sch6 sensing scheme and (C) visual aspect of a sensing foil prepared using the same scheme, but evidencing issues during the drying process (change of coloration due to gamma correction modifications used for easier visualization of wrinkles in the IA).and, their respective Quad tree tests of homogeneity (B and D).

Figure 3.9

Continuous spectrophotometric characterization of residuals released into the immersion solution from a sensing foil during 1-D measurements, oriented to detect immobilization issues during the entrapment of the chemical indicator in the IA.

Figure 3.10

Spectrophotometric characterization of Sch6 in the 350 nm to 820 nm range, depicting a peak in absorbance at 436 nm, as expected by the presence of cadmium cations located in the central ring of a porphyrin.

Figure 3.11

Slow reaction rates to Mn(II) shown by Sch2 (blue) and Sch3 (black) measured in a 24 hours period (ASW, s:35, pH:8, room temperature, [Mn(II)]: 1 mM).

Figure 3.12

Effect of additives as dextrose (A) or carboxymethyl cellulose (B) on internal diffusion patterns during reactivity test for Mn(II), as well as, visual changes in sensing foils homogeneity by heterogeneous distribution of additives during the preparation of sensing schemes and/or formation of indicator micelles.(sensing foil in B was exposed to UV radiation for 30 minutes to photoxidize non reacted indicator for visualization purposes).

Figure 3.13

Reaction progression between Sch6 and 15 µM Mn(II) solution tracked on time, depicting a initial decrease in absorbance at 469 nm during the first 3 to 4 minutes, followed by a sigmoidal increase on this parameter, evidencing the reaction of the sensing foil to the analyte.

Figure 3.14

(A) Visual image of sensing foil pieces used during the sensor calibration (Sch6) ordered from lower to higher Mn^{2+} concentration(0-150 µM) , (B) their conversion to the HIS colorspace (H channel shown), (C) the vertical averaging obtained from (B) and its standard deviation (D).

Figure 3.15

Calibration curve in the 0 to 150 μM of Mn^{2+} calculated using intensity units from digitalized image (Figure 3.14 A), and the fitting residuals (lower panel).

Figure 3.16

(A) Slopes and (B) disturbance terms for calibration curves calculated from the original digitalized image (iteration:0) and their convergence during the application of iterative method of noise reduction, as well as, the R^2 associated to each new calibration curve (C) and the reduction of standard deviation in intensity values during the calculations per each concentration (D).

Figure 3.17

Comparison between 2-D (A) and 1-D traditional method of Mn(II) determination(B,sed. cores). And 1-D horizontal averaging and standard deviation obtained from (A).

Figure 3.18

Visual image showing sedimentary structures created by *Nereis* sp. (A) and its effects over 2-D Mn(II) distributional patterns, depicted using 2-D determinations carried in the same section (B) by deploying a sensing foil as depicted in Figure 3.5.

Figure 3.19

(A) X-ray image showing five sensing foils deployed in parallel during incubation experiments with sediments bioperturbed by *Yoldia* sp., and (B) Mn(II) distributional patterns obtained from these foils, depicting how bioturbation modifies the distribution of the analyte.

Figure 4.1

Schematic model proposed by Sundby and Silverberg (1985). Marine sedimentary deposit and its overlying water column are sub-divided in five reservoirs, where particulate manganese is produced in the first three reservoirs (surface waters, bottom water and oxic sub-surficial sediments, respectively), and dissolved manganese is produced just in the fourth reservoir (deeper, sub-oxic sediments). Manganese burial into deeper sediments is represented by the fifth reservoir.

Figure 4.2

Schematic representation of the diffusive boundary layer, depicting the concentration gradient between pore water from sediments below the water-sediment interface (C_0) and overlying water (C_∞), as well as, depicting the thickness (δ_D) and effective thickness (δ_e)of the diffusive boundary layer.

Figure 4.3

Radial-diffusion tube model for bioirrigation proposed by Aller (1980), where the bioirrigated zone in marine sediments is represented by a group of closely packed hollow concentric cylinders, where the empty inside correspond to the burrow (in red).

Figure 4.4

Schematic representation of (A) method of planar optode deployment, and (B) setup of cores used for incubation experiments oriented to measure Mn(II) fluxes across the water-sediment interface during hypoxia development events in overlying waters.

Figure 4.5

Tomographic reconstruction carried using a rotatory table and a digital x-Ray screen. (A and B) General 3-D reconstruction of the first 5 cm of sediment using t0 core. (C) Reconstruction of the sediments after a planar optode deployment (sensing foil in green), and (D) filtered 3-D data showing no significant variations in density below the first centimeter of sediment (from the water-sediment interface) for t0 core.

Figure 4.6

Setup for simultaneous deployment of several planar optodes for three dimensional reconstructions of chemical distributions (A). Simple scheme of CT-scanning setup for tomographic reconstruction of round cores before and during the planar optode deployment (B).

Figure 4.7

Tomographic reconstruction of sediment inhabited by *Nereis* sp. during the simultaneous deployment of planar optodes (A). Close up of the same reconstruction depicting the animals and the sedimentary structures (burrows) they generated (B).

Figure 4.8

Changes in the Mn(II) concentration in the overlying water over time used to calculate total flux across the water-sediment interface. Vertical axis represents the conversion of concentration to mass units by multiplying the gradient by the volume of overlying water.

Figure 4.9

Two-dimensional distributional patterns of Mn(II) determined using planar optodes, where t0 represents initial oxic conditions, t1 depicts Mn(II) distributions after six hour of hypoxia development, and t2 corresponds to twelve hours of hypoxia development.

Figure 4.10

Two-dimensional distributional patterns of Mn(II) fluxes calculated using the multidimensional expression of Fick's law in Cartesian coordinates (eq. 27) with Mn(II) distributional patterns from planar optodes.

Figure 4.11

One-dimensional representation calculated from the two-dimensional distributions of Mn(II) fluxes, obtained by horizontally averaging the two-dimensional flux calculations for t0 (blue), t1 (red), and t2 (black).

Figure 4.12

Two-dimensional gradients of Mn(II) concentrations obtained during planar optodes deployment in bioturbated sediments by *Yoldia sp*. (2-D Mn(II) concentrations depicted in Figure 3.19, chapter 3).

Figure 4.13

Simultaneous deployment of Mn(II) and Fe(II) planar optodes depicting how differences in their precipitation rates affect their release across the water sediment interface under oxic conditions.

Figure 4.14

Three-dimensional reconstruction of Mn(II) distributional patterns depicting the increase of Mn(II) concentration from surface to bottom.

Figure 4.15

Fe(II) distribution provided by the simultaneous deployment of five planar optodes in a round core containing sediments bioperturbed by *Nereis sp*. (A), and two dimensional gradient calculations presented as a relative visualization of Fe(II) flux determinations (B).

Figure 4.16

Tomographic reconstruction depicting Macoma sp. and sedimentary structures created by its syphons (A). Fe(II) distributional patterns obtained from a planar optode deployed in the same location (B), and gradient calculations obtained from two dimensional Fe(II) distributional patterns (C).

List of Tables

97% (IN2), and modified porphyrin (IN3) utilized to prepare sensing foils for each tested immobilization sub-scheme.

Table 3.2

Summary of indicator release from entrapment attemps using the different sub-schemes proposed in this study (n.d: non detectable).

Table 4.1

Summarized schedule of core sealing (X), overlying water sampling (S), and opening & two dimensional sensor deployment (2DS) for cores used during flux experiments.

Acknowledgments

I would like to thank to my Ph.D advisors, Professors Qingzhi Zhu and Robert C. Aller, for their support during my Ph.D study and related research. Qing has been especially supportive and has given me the freedom to pursue various projects, and Bob has been enthusiastic, and energetic about my research.

In addition to my advisors, I would like to thank my thesis committee, Professors Cindy Lee, Mary Scranton and Frank Gilbert for their insightful comments and encouragement. I especially would like to express my gratitude to Mrs. Cindy and Mary for their patience, motivation, and immense knowledge. Besides their strong support for my career, I'm very lucky to have had the opportunity to learn from them on a daily basis about science and life, and I will consider myself accomplished if, in the future, I'm able to help and guide people as they did with me. I am very thankful for have them as mentors.

I also want to thank other faculty members at SoMAS, Drs. Gordon Taylor, David Black and Kirk Cochran, for inviting me to participate in valuable field experiences and sharing interesting ideas about science and life; also Drs. Rob Armstrong, Anne McElroy and Bruce Brownawell for their friendship and wise advice.

I especially thank Dr. Christina Heilbrun for her kindness, time and assistance in lab related issues. In addition, I would like to thank Mrs. Eileen Goldsmith, Carol Dovi, Christina Fink and Mr. Mark Lang, I appreciate their assistance in administrative and informatics issues.

I thank my fellow labmates, especially Meichen, Han and Zhenrui for sharing not only the office but also good and sad moments during those years. I would like to express my gratitude to my

fellow grad-students and friends at SoMAS Chris Martinez, Joe Tamborski, Liz Suter, Jungmin Lee, Claudia Hinrichs, and my dear friends Daniel and Elizabeth, for sharing experiences, conversations and creating good memories from those years at Stony Brook.

Funding for the first four years of my research came from a presidential scholarship provided by the Chilean government. The next years where funded by the Chemical Oceanography Division of NSF. I thank the funding agencies and all the people involved for my support.

Finally, I would like to thank my family, and especially to my wife Carolina for her unconditional love and never-ending support.

Chapter 1:

Introduction and Background

1 Introduction and Background

Manganese is essential for almost all living organisms. It is widely distributed in both terrestrial and marine environments and involved in various biological, physical and chemical processes. Its role in marine environments includes a diverse set of organic and inorganic reactions. Used by phytoplankton as micronutrient and/or during redox reactions by microbes in sedimentary environments, manganese is directly linked to carbon, nitrogen and sulfur cycles in the formation, preservation and remineralization of organic molecules (Froelich et al., 1979). Mn also plays a role in trace metal sequestration, remobilization, and transport. Metal ions can be adsorbed by oxidized manganese on particle surfaces in oxic environments and transported to the seafloor by sinking particles, or relocated by sediment reworking where they can be buried or released when manganese is dissolved under anoxic conditions (Murray, 1975; Murray et al., 1984; Stumm and Morgan, 1996; Miyata et al., 2007a,b).

1.1 Inorganic and organic chemistry of manganese in marine sediments

Manganese has multiple oxidation states, of which Mn(II), Mn(III) and Mn(IV) predominate in marine environments. Transition from one oxidation state to another depends on both inorganically and biologically mediated reactions. Reduced Mn(II) is thermodynamically favored in anoxic conditions, forming several soluble salts, insoluble carbonates and phosphate minerals (Nealson et al., 1988), while in oxic environments, manganese is present as solid Mn(IV) oxides and Mn(III) oxyhydroxides.

The rates of abiogenic oxidation of manganese at circumneutral pH are slow because of high activation energy, but rates increase at high pH. Abiogenic reduction of manganese can be

carried out by several organic and inorganic species such as Fe(II), nitrite, sulfide, pyruvate, etc. (e.g. Kessick and Thompson, 1974; Postma, 1985; Stone, 1987; Burdige et al., 1992; Bartlett and James, 1993).

Differences between reduced and oxidized manganese result in a cyclic redox process in sediments, where, in general terms, a sinking solid with oxidized forms of manganese are enriched on the surface, are eventually buried by deposition of new particles. Under anoxic conditions, manganese oxides are used by microbes as electron acceptors during organic matter remineralization (Figure 1.1), reducing them to dissolved forms (Mn(II) or Mn(III) as suggested by Madison et al., 2011). Dissolved Mn is redistributed by diffusive and/or advective processes depending on sedimentary structures and forces; some pathways will drive dissolved Mn to reach equilibrium with carbonate phases and be buried (Middelburg et al., 1987), or reach oxic conditions where it will be re-oxidized to Mn(III) and Mn(IV) forms (Sundby and Silverberg, 1985). Aller (1980) and Canfield et al. (1993) showed this cycle could be experienced several times by the same manganese pool before ultimate burial, with estimated turnover times of months for manganese in excess of background levels in the upper 5 cm of sediment.

In an idealized non-perturbed steady-state sedimentary environment overlain by oxic waters, dissolved and solid manganese phases profiles follow a classically described redox pattern (Figure 1.2). Across the first centimeters from the surface, dissolved Mn(II) concentrations are close to zero, or undetectable, while solid phases reflect Mn supply from sinking material in the water column. Mn (II) transported from deeper to shallower oxic sediments is reoxidized, generating a peak in solid phase Mn. Below the redoxcline, Mn (II) concentrations increase via microbial reduction of oxidized phases, but Mn(II) is depleted in deeper sediments due to removal by precipitation.

Adding nitrogen and sulfur species to the above depicted manganese cycle increases its complexity since Mn(II) production can increase due to reaction of NH_4^+ (eq. 2), FeS (eq. 3), S^0 (eq. 4) and HS^- (eq. 5) with Mn (III, IV) (Burdige et al.,1992; Luther et al.,1997; Hulth et al., 1999; Luther and Popp, 2002) , or decrease due to the reaction of NO_3^- with Mn(II) in suboxic environments (eq. 6) (Aller, 1990; Murray et al., 1995; Anschutz et al., 2000). These pathways are summarized in Figure 1.1A. Reactions such as ammonium oxidation to dinitrogen in anoxic conditions, or to nitrate in oxic sediments, could have direct implications for our understanding of biogeochemical cycles in marine sediments. These reactions have been observed in natural sedimentary environments such as the hemipelagic Panama Basin (Aller et al., 1998), fjords (Deflandre et al., 2002) and the Eastern Atlantic (Anschutz et al., 2002), as well as during incubation experiments (Hulth et al., 1999; Anschutz et al., 2005; Javanaud et al., 2011). Nevertheless, evidence for the absence of these reactions has been found in similar environments (Thamdrup and Dalsgaard, 2000; Engström et al., 2005; Bartlett et al., 2007). Sedimentary perturbation is the common condition in all the sites where ammonium oxidation involving manganese oxide has been reported. Therefore, Bartlett et al. (2008) suggest that the chemical imbalance produced by redistribution of manganese oxides during physical perturbation of sediments is the crucial condition to trigger this reaction, relegating the concentration of oxides as such to second place.

$$\tfrac{1}{2}\,CH_2O + \tfrac{3}{2}\,CO_2 + \tfrac{1}{2}\,H_2O + MnO_2 \rightarrow Mn(II) + 2\,HCO_3^- \quad ; \Delta G_{R\ pH\ 7\ and\ 8} = -190$$

(eq. 1)

$$4\,MnO_2 + NH^+ + 6\,H^+ \rightarrow 4\,Mn(II) + NO_3^- + 5\,H_2O \quad ; \Delta G_{R\ pH\ 7} = -175\ \Delta G_{R\ pH\ 8} = -141$$

(eq. 2)

$$\tfrac{5}{8}\,FeS + 4\,MnO_2 + NH^+ + 7\,H^+ \rightarrow \tfrac{1}{2}\,N_2 + 4\,Mn(II) + \tfrac{5}{8}\,SO_4^{2-} + \tfrac{5}{8}\,Fe(II) + \tfrac{11}{2}\,H_2O \; ; \Delta G_{R\ pH\ 7} = -175$$

$\Delta G_{R\ pH\ 8} = -141$ (eq. 3)

$$\tfrac{4}{3}\,H^+ + MnO_2 + \tfrac{1}{3}\,S^0 \rightarrow Mn(II) + \tfrac{1}{3}\,SO_4^{2-} + \tfrac{2}{3}\,H_2O; \quad \Delta G_{R\ pH\ 7} = -157 \quad \Delta G_{R\ pH\ 8} = -147$$

(eq. 4)

$$HS^- + MnO_2 + 3\,H^+ \rightarrow Mn(II) + S^0 + 2\,H_2O \; ; \Delta G_{R\ pH\ 7} = -136 \quad \Delta G_{R\ pH\ 8} = -119$$

(eq. 5)

$$\tfrac{5}{2}\,Mn(II) + NO_3^- + 2\,H_2O \rightarrow \tfrac{5}{2}\,MnO_2 + \tfrac{1}{2}\,N_2 + 4\,H^+ \; ; \quad \Delta G_{R\ pH\ 7} = -48.9 \quad \Delta G_{R\ pH\ 8} = -71.4$$

(eq. 6)

$$4S^0 + 4H_2O \rightarrow 3H_2S + SO_4^{2-} + 2H^+ \; ; \quad \Delta G_{0'\ pH\ 7} = 41$$

(eq. 7)

$$3H_2S + 2FeOOH \rightarrow S^0 + 2FeS + 4H_2O$$

(eq. 8)

(from Hulth et al., 1999 and Thamdrup et al.,1994; $\Delta G_{0'}$ and ΔG_R are in kJ mol^{-1})

The link between the sulfur cycle in marine sediments and manganese oxides depends on the endergonic nature of elemental sulfur disproportionation reactions (eq.7). The ΔGo' of 41 kJ

mol^{-1} is associated with the bacteria-mediated conversion of elemental sulfur to sulfides (e.g. FeS or H_2S), and sulfate, and is highly dependent on sulfide concentrations (Canfield and Thamdrup, 1994). Since sulfides are scavenged by reaction with iron and manganese oxides, forming FeS or elemental sulfur (eq. 5 and 8) (Aller and Rude, 1988; Canfield et al., 1993; Canfield and Thamdrup, 1994; Aller, 1994; Schippers and Jorgensen, 2001; Böttcher and Thamdrup, 2001), the presence of these oxides in anoxic sediments would enhance bacterial disproportionation.

Since bacterial sulfate reduction has been reported to account for at least 50% of organic matter remineralization in coastal sediments, and disproportionating bacteria have been reported as abundant and widely distributed in this environment (Jorgensen., 1982; Canfield et al., 1993; Thamdrup et al., 1993; Canfield and Thamdrup, 1994), the roles of manganese and iron oxides in carbon, nitrogen and sulfur cycles probably have been underestimated.

1.2 Role of microbial and macrobenthic organisms in the marine sedimentary manganese cycle.

Microbial activity plays a key role in the marine cycle of manganese. Reduction of Mn(III) and Mn(IV) to dissolved Mn(II) by microbes during organic matter remineralization in anoxic marine sediments is a widely accepted reaction (Lovley, 1991; Nealson and Myers, 1992). Furthermore, several studies suggest the biological nature of manganese oxidation since a diverse group of organisms, including bacteria and their spores (Johnston and Kipphut,1988; Myers and Nealson, 1988; Bratina et al., 1998; Francis et al., 2001; 2002; Chen et al., 2003; Bargar et al., 2005; Miyata et al., 2007a,b), fungi (by presence of manganese peroxidase) (Costa Bonugli-Santos et al., 2010) and microalgae (Marshall et al.,1979) that have manganese oxidizing or reducing capabilities have been isolated from natural marine environments.

Moreover, bacterial manganese oxide formation could not only be a residual of metabolic processes of these organisms, but also a protective shield against predation or pollution by coating the microbes' surface (Parikh et al., 2005; Tebo et al., 2005), as well, a way of turning humic substances into "edible" low molecular weight molecules (Sunda et al., 1994).

It remains unclear if extracellular bacterial manganese oxides are produced by consuming Mn or if they are related to intracellular/extracellular mechanisms for scavenging harmful reactive oxygen species during Mn(III) and Mn(IV) formation (Tebo et al., 2005). However, multicopper oxidase-like enzymes have been reported as a possible mechanism for bacterial Mn(III) and Mn(IV) production (e.g. Ehrlich, 1968, 1983; Jung et al.,1979; Okazaki, 1997). In a similar fashion, how fungi oxidize manganese is still unknown. Miyata et al. (2004) found a 54-kDa extracellular protein with Mn(II) oxidizing capabilities in *Acremonium*-like hyphomycete cultures, suggesting the participation of lactase and/or multicopper oxidase (MCO) in this reaction. Furthermore, heme-containing Mn peroxidase has been reported as an alternative Mn(II) oxidizing agent to MCO-like proteins. This non-specific oxidoreductase provides lignin degradation capabilities to fungal species (Glenn et al., 1983; Kuwahara et al., 1984). Manganese peroxidase has been reported for marine coastal sediments (e.g. Bonugli-Santos et al., 2010), but there are no studies quantifying its role in the marine manganese cycle.

Spatial distributions of manganese species in marine deposits are highly influenced by physically and biologically mediated sediment reworking. Macrobenthic organisms build sedimentary structures as a consequence of feeding, burrowing, secretion and excretion processes (e.g. Figure 1.3A), altering the assumed vertically stratified concentration profiles of electron acceptors produced by sequential use during organic matter remineralization or inorganic reactions in steady state sedimentary deposits (Aller, 1982).

Pore water composition is altered by macrobenthic animal activities such as feeding and burrowing, which increases the bidirectional sediment/water exchange between surface and deeper sediments, with the eventual input of oxygen and nutrients into the deposit and release of reduced species to overlying waters. Furthermore, worm tubes may act as a "piping" system for both gas and liquid exchange (e.g. Figure 1.3B). In addition, physical perturbation of sediments is carried out by macrobenthic animals. A closed cyclic particle transportation pattern between superficial and deeper sediments surrounding a single animal burrow has been reported, where an animal of a given size removes particles from deeper sediments during feeding and deposits them at the surface, where they are later buried by new material deposition (Rhoads, 1974; Aller and Dodge, 1974; Amiard-Triquet, 1974). This apparently simple process could be a building block to construct complex patterns of sedimentary reworking. Interconnections between individual particle fluxes from activities carried out by different animal species with heterogeneous size distributions and/or life stages and that live contiguously in the same area, could generate intricate sedimentary structures, with the consequent alteration in solid phase manganese distribution (Figure 1.3A, 1.3B). Gilbert et al. (2003) developed a novel technique to evaluate two-dimensional particle reworking in bioturbated sedimentary deposits by using luminophores as tracers of particle motion and computerizing image segmentation for motion detection and quantification. They found non-local mixing patterns in the particle reworking generated by *Amphiura filiformes*, as well as a general trend toward internal homogenization at longer time scales in the sedimentary deposit. These findings illustrate how benthic macrofaunal activities may modify boundaries of geochemical regions defined by the electron acceptors driving organic matter remineralization, as well as how these activities may generate apparently homogeneous sedimentary deposits from highly reworked sediments. Along with this process,

secretion and excretion of organic compounds such as mucus and fecal pellets by benthic macro fauna, modifies granulometry and sedimentary structures by forming aggregates (Aller, 1982). Thus, bioperturbed marine sedimentary deposits are highly dynamic and complex systems.

1.3 Manganese detection in marine sediments.

There are several analytical alternatives to quantify dissolved and solid phases of manganese in marine sediments. The most common methods are spectrophotometry, X-ray fluorescence, atomic absorption spectrometry and electroanalytical methods. During the last decade, improvements in accuracy and eliminating interference have been developed for all these methods (e.g. Chiswell et al.,1990; Crompton, 2006).

Spectrophotometric methods have been extensively used in marine sciences because of their simplicity, reliability, and accuracy, as well as their relatively low cost compared to other available techniques. Several variants to quantify dissolved Mn in marine environment have been reviewed extensively by Chiswell et al. (1990), covering a wide range of reagents, detection levels, operational pH ranges, interference issues, and advantages for each method. Formaldoxime, permanganate and pyridylazonaphthol are considered to be the most commonly used reagents for Mn detection in marine pore water, being the first the most commonly used (Marczenko, 1986).

Dioximes have been used as chemical indicator for several metal ions. For colorimetric determinations of Mn(II), formaldoxime alone provides an adequate dynamic range (0-3 µg/L), making unnecessary other dioximes that provide reliable measurements only in the mg/L range. In addition, the manganese-formaldoxime complex is very stable and stays unaltered in the

presence of compounds such as tartrate and oxalate. Nevertheless, its sensitivity has been reported as insufficient for quantification below 100 µg/L (Kastelan-Macan et al., 1987).

Azo dyes have also been extensively used as indicators for Mn(II) determination. Their general structure consists of terdentate ligands with phenolic groups and nitrogen atoms in aromatic heterocycles or amines. Although these indicators are insoluble in water, limiting their application, their solubility can be improved by adding non-chelating hydroxyl or sulphonic acid functional groups. The most representative indicator among the azo dyes is 1-(2'-pyridylazo)-2-naphtol (PAN) (Cheng and Bray, 1955). This indicator requires accurate pH control and the inclusion of masking agents, such as cyanide, then providing reliable measurements up to 2 mg/L. However, the ligand and complex absorbance peaks overlap when the analyte is below 100 µg/L (O'Halloran et al, 1986; Chiswell et al, 1987). Several variations of PAN have being developed for Mn(II) quantification with some success: 4-(2'-Pyridylazo)resorcinol (PAR) (Liu,1951)) and 1-(2'-thiazolylazo)-2-naphtol (TAR) (Nakagawa and Wada,1962). PAR and TAR show an adequate response to Mn(II) in the 0.1 to 1.1 mg/L and 0.04 to 1.4 µg/L range, respectively, but none of them has comparable properties to PAN (Shibata et al., 1973).

Taking advantage of the insolubility of azo compounds, Milani et al. (2015) developed a sensor based on the immobilization of PAN for measuring Mn(II) in marine environments; however, the necessity of adding masking agents and a strict control of pH in the samples requires further studies before the sensor can be validated.

X-ray fluorescence (XRF) is a useful method to estimate sediment composition (Wolfe et al., 1970; Ramsey et al., 1995; Stallard et al., 1995). It is based on the use of X-rays to excite electrons of manganese; ejection of electrons from inner atomic shells creates empty positions

that are filled when electrons fall back from the outer shells. These processes involve emission of characteristic fluorescence for specific elements in the sample (Weltje et al., 2008).

In 1988, the first XRF core scanner was introduced at the Netherlands Institute of Sea Research (Jansen et al., 1998). This device gives the relative intensity of elements during a high-resolution surface scanning of split sediment cores. However, this method measures only solid phases, and the determination is inaccurate due to uncertainties related to assumptions considered during the mass-balance and flux calculations used to convert intensities into element concentrations (Weltje et al., 2008). Additional problems related to element interactions, artifacts from specimen inhomogeneity, variable water content, and irregular response to sediment surface irregularities result in the XRF core scanner being a semi-quantitative method (Croudace et al., 2006; Richter et al., 2006).

Atomic absorption spectrometry (AAS) is a highly sensitive, specific and versatile technique to determine concentrations of trace metals (Liu et al., 1989). One of its common applications involves the use of 8-hydroxyquinoline (oxine), which forms complexes with manganese and other transition metals. The two main methods are based on oxine immobilization directly onto the inner walls of silicone tubing, or on the retention of complexes between manganese and oxine before quantification by the atomic absorption spectrophotometer (Sarzanini et al., 2001).

Direct quantification of Mn(II) in seawater using AAS is greatly affected by the sample matrix. Atomizing Mn(II) and its matrix at the same time and/or high chloride contents in the sample increase the background signal during the measurements. These issues have been approached by modifying the matrix (e.g. by adding ammonium nitrate or ascorbic acid) or adding extraction steps (e.g. Chelex 100 extraction) to separate the analyte, and heating at

steady-state to reduce the chloride interference (Crompton et al., 2006). The detection limit using Chelex is less than ng/L (Kingston et al.,1978), and the reported limit of detection for direct injection is ~0.3 µg/L; however, the state of the graphite tubes during the measurement influences this limit (McArthur, 1977). Using chelating agents such as ammonium pyrrolidinethiocarbamate or its combination with diethylammonium dithylthiocarbamate provides detection limits of 0.004 µg/L and 0.07 µg/L respectively (Lo et al., 1982).

An analytical alternative for determining dissolved manganese, as well as several other trace metals in marine environments, is the ICP-MS technique (e.g. Wu and Boyle, 1998; Saito and Schneider, 2006). Currently, there are three main approaches for using this technique for quantifying Mn in marine samples. The first is direct injection of seawater samples when the trace metal concentrations are expected to be high; but this method lacks the required sensitivity for the low trace metal concentrations expected in the open ocean. The other two approaches involve preconcentration of samples using metal affinity resins or magnesium hydroxide precipitation (e.g. Wu and Boyle, 1997; Field et al, 1999; Lohan et al., 2004; Saito and Schneider, 2006). While use of resins provides adequate levels of sensitivity and precision, some issues have been reported for ferrous iron measurements and other? dissolved redox-sensitive metals, and additional oxidation steps are required (Lohan et al, 2004). On the other hand, a technique based on precipitating the magnesium already present in seawater, by adding ammonium, provides a more straightforward technique. Reported precision for the ICP-MS technique using magnesium precipitation is approximately 1.2-2.4% R.S.D (Saito and Schneider, 2006).

Because of their sensitivity, selectivity and fast response, electroanalytical methods represent an excellent option for quantifying a wide range of metals in marine sediments (Van

Der Berg, 1991; Filipe and Brett, 2003). Anodic stripping voltammetry has been used to determine dissolved Mn. The most used ASV electrode is the mercury electrode, with detection limits of 0.01 µg/L (O'Halloran et al., 1982); however, the large reduction potential required to reduce Mn(II) to Mn(0) and the low solubility of manganese in mercury are problematic. Electrodes based on cathodic stripping voltammetry, such as carbon paste and boron doped diamond electrodes, have been more successful, with detection limits of 0.004 µg/L (Banks, 2005). In particular, Brendel and Luther (1995) developed a solid-state voltammetric gold amalgam microelectrode that is capable of measuring oxygen, S(-II), Fe(II) and Mn(II) in marine pore waters at sub-millimeter scales, providing a useful analytical tool for characterizing quantitatively the distribution of these analytes in the top millimeters of marine sedimentary deposits. Detection limits of 120 nM and 93 nM have been reported for anodic and cathodic stripping voltammetry determinations of Mn(II) (Yue et al., 2012).

Several factors, such as cost, portability, on-board implementation, time demand, specificity, detection limit, precision, reagent availability, number and volume of samples, etc. must be considered during selection of an appropriate technique for determining different manganese species in marine sedimentary deposits. Required sample volumes for the above described methodologies vary from µL to L, and preparation for analysis varies from direct measurement to intricate preconcentration stages; however, except for electroanalytical techniques, in-situ measurements in marine sediments are out of the scope of these techniques, as they are highly intrusive, limited to sample extraction and unable to fully resolve the complex distributional patterns as expected for bioperturbed systems. Nevertheless, advances in optical sensors capabilities of performing in-situ measurements of chemical parameters have been made,

offering a new perspective for the characterization of chemical environments in marine sedimentary deposits under different conditions.

1.4 Optical Sensors and their use in natural environments

Since the early 20th century, imaging techniques have been widely employed for descriptive analysis of sedimentary environments; submarine optical systems have been mainly focused on macrofaunal and sedimentary structure characterization (e.g. Petersen, 1913; Young and Rhoads, 1971; Rhoads and Cande, 1971, Rhoads and Germano, 1983; Solan, 2003). Technological advances in the last decades have broadened the use of imaging techniques to geochemical applications, where both identification and quantification of chemical species in natural environments have been accomplished by combining the use of optical systems with physical and/or chemical properties of the analytes. Some advantages of these techniques over conventional electrochemical approaches are their low electrical interference, lack of reference electrodes, low relative cost to other analytic methods, wider range of analytes, and possibility of carrying out two dimensional measurements, providing simultaneous measurements for multiple points. However, some optical sensors present limitations such as ambient light interference, photo degradation of indicators at high light intensities, long-term stability issues, delayed response in comparison with electrochemical techniques, or irreversible response (Seitz, 1984). Additionally, two dimensional sensors are susceptible to 1) heterogeneous responses at different locations in the sensing plane caused by uneven distribution of indicator and/or supporting layers, demanding individual calibrations for each pixel in the sensing plane (Oguri et al., 2006).

In addition, perturbations in sedimentary diffusive patterns during sensor emplacement can alter the thickness of the diffusive boundary layer (Viollier et al., 2003).

Optical sensors have been used to measure oxygen (Klimant et al., 1995, 1997; Glud et al., 1996; Wenzhofer et al., 2004), pH (Kohls et al., 1997; Zhu et al., 2005), pCO_2 (Hales et al., 1997; Neurauter et al., 2000; Zhu et al., 2006a), exo-enzymatic activity (Cao et al., 2011), ferrous iron (Zhu and Aller, 2012), and nitrate (Huber et al., 2001), as well as a wide variety of metals using indicators such as horseradish peroxidase (Shekhovtsova et al., 1994), porphyrins (Morales-Bahnik et al., 1993) and dithiocarbamate (Lerchi et al., 1992) for mercury; dithizone (De Oliveira and Narayanaswamy, 1992) and xylenol orange (Klimant and Otto, 1992) for lead; 2,4-dinitrosoresorcinol (DNR) (Malcik and Caglar, 1997) and urease (Andres and Narayanaswamy, 1995) for ferric iron; and both 1-nitroso-2-naphthol and 4-(2-pyridynazol)resorcinol for other metal ions including Co^{2+}, Cu^{2+}, Ni^{2+}, Fe^{3+}, Cd^{2+}, Zn^{2+} and Pb^{2+} (Malcik et al.,1998).

The working principle of chemical optical sensors is the use of electromagnetic radiation to excite a transducer which conditions its response to the amount of analyte reacting with it. The analytical signal can be absorbance, luminescence, reflectance, fluorescence lifetime, or even refractive index, scattering, diffraction and polarization, depending on the analyte and selected sensing scheme (Seitz et al., 1984; Jeronimo et al., 2007). Broadly speaking, five main sensing schemes have been described for determining chemical species in natural environments using optical systems. The first is based on measuring absorption or luminescence patterns generated by intrinsic optical properties of the analyte during its excitation by a wavelength-specific light source, taking advantage of the natural color differentiation between chemical species produced by pollution, organic content or oxidation states (e.g. Rhoads, 1995; Bull and Williamson, 2001;

Bona, 2006). Interferences by turbidity, masking agents or by the presence of chemical species with similar optical properties can cause the low specificity of this scheme (Oehme and Wolfbeis, 1997). However, extensive work has been done on improving image processing techniques to solve these problems. As a result, concentrations of iron oxide, copper, uranium radionuclides and other metals have been successfully determined (Malstrom, 1988; Freeman et al., 1985; Grygar et al., 2002; Viscarra Rossel et al., 2008).

The second sensing scheme used by optical systems is based on measuring changes in absorption or fluorescence patterns generated by chemical reactions between analytes and chromogenic compounds used as indicators. However, several reagents used as indicators in colorimetric methods are inappropriate for optical chemical sensors because of poor stability, low rates of reaction, pH sensitivity or unfavorable range of wavelengths at which measurements must be carried out (Bishop, 1972). For metal ion measurements, the chemical interaction between both chromogenic indicator and analyte could be an oxidation or reduction reaction, as well as a combination of both. Additionally, several reagents used to determine ion concentrations require buffers to maintain constant pH during measurements because many of them are acid-base indicators (Oehme and wolfbeis, 1997).

An alternative to previously described sensing schemes is using quenchable fluorophore compounds as indicators. This method relies on the static or dynamic quenching of indicator luminance by reaction with the analyte. In particular, the suggested source for quenching properties of heavy metals over luminescence from fluorophores is the heavy atom effect, and in particular, the quenching efficiency exposed by transitional metals is their numerous unpaired spins (Oehme and wolfbeis, 1997).

During static quenching, the analyte reacts with the fluorophore in its ground state with a conditional stability constant (Ks) described by:

$Ks=[MeI]/([Me][I])$ (eq.9)

where

[MeI]: concentration of quenched species.

[I] : concentration of fluorescent species.

[Me]: concentration of quenchers.

During dynamic quenching of an indicator's luminescence, the quencher reacts with the fluorophore in an excited state, and involves both fluorescence emission reduction and decreased lifetime. The main advantage of this scheme is the reversible nature of reactions, which means the indicator is not consumed during the reaction allowing real time tracking of concentrations (Oehme and wolfbeis, 1997).

Analyte quantification using dynamic quenchers is carried out using the numerical relationship between both luminescence quenching and analyte concentration described by the Stern-Volmer equation:

$(Io/I)-1=K_{sv}[Q]=K_q\tau o[Q]$ (eq.10)

where Io (I): fluorescence intensities in absence (presence) of the quencher Q.

[Q] : quencher concentration.

K_{sv} : overall quenching constant.

K_q : biomolecular quenching constant.

τo : lifetime of the emissive excited state of the analyte.

Some disadvantages of sensors based on dynamic quenching are the quencher's effect on luminescence lifetimes, linearity losses at high analyte concentrations and mixing of quenching types (static and dynamic) in the same sensor (Lakowicz et al., 1989).

The ionophore-based scheme uses lipophilic ion carriers and complexing agents capable of reacting in a reversible fashion with the analyte, transporting it through supporting membranes to the indicator by carrier translocation. One of the approaches used for this scheme involves the use of chromogenic or fluorogenic moieties into ionophores to obtain chromo- or fluoro-ionophores. This scheme could be used in both solution and bulk membrane sensors (Oehme and Wolfbeis, 1997).

Ionophore-potential sensitive dye mixtures and co-extraction techniques are two different approaches used in ionophore-based sensors, and have been mainly applied in bulk membranes instead of hydrophobic polymers due to the highly hydrophobic nature of the selected ionophores in those studies (Oehme and Wolfbeis, 1997). However, the most widely used scheme is the extraction of ions into membranes using neutral ion carriers, where metals are transported through supporting membranes by neutral ionophores and react with proton-selective chromo-ionophores. A disadvantage of this scheme is the high pH dependence demonstrated by ion-exchange based sensors due to relationships between parameters to be measured and the ratio of both analyte and proton activities (Lerchi et al., 1992).

Seitz (1991) indicated the gap between both empirical and theoretical reversibility of ion binding reactions in sensors using chelators as indicators. In practice, the ion binding reaction is irreversible because stability constants are outside the range where the sensor must work.

Considering the operational range of analyte concentration for a sensor as log(Ks)±1, the indicator will be saturated when -log(analyte concentration) < (log(Ks)-1); then, concentrations of analyte outside the range of log(Ks)±1 will not produce any change in the optical signal. Another problem developing reversible sensors arises from the difference between releasing and binding rates for some chelators. In some cases the reverse reaction is extremely slow, affecting the time response and reversibility of the sensor (Oehme and wolfbeis, 1997).

Simultaneously, biosensors have been developed to quantify analytes that traditional chemical or physical schemes are unable to incorporate. Their basic principle is the use of immobilized biological units such as DNA, RNA, bacteria, enzymes, proteins, antibodies or even whole cells as detecting agents, preserving biological functions and structural integrity, and producing highly stable systems in terms of response to chemical and thermal changes (Gill and Ballesteros, 2000 a, b and c). Several biological units used for sensing purposes in these schemes don't change their optical properties during recognition and/or consumption of the analyte, requiring transducers to generate the optical signal (Jeronimo et al., 2007).

A crucial aspect of biosensors is how biological units are immobilized. Several methods used in chemical sensors could damage the biological functions required for sensing because of their pH or toxicity; nevertheless, sol-gel technologies have been widely used to immobilize biological units retaining their structural integrity and biological functions (Gill and Ballesteros, 2000a, b and c).

Selecting the right option from the above described sensing schemes for specific applications and environments must take into account the requirements of signal stability, limit of detection, dynamic range and transducer lifetime, as well as possible limitations in size, weight, and energy supplies. Environmental characteristics like temperature, pH range,

interferences and physical conditions must be considered in choosing a sensing scheme, reagents or supporting materials (Ricco et al., 1998).

1.5 Establishing the Problem and Research Objectives

Several previous studies have been focused on elucidating the biological, physical and chemical processes that make up the manganese cycle in marine sediments, as well as the relationship of Mn to other elements such as nitrogen, carbon and sulfur. Studies regarding consumption of manganese solid phases by reactions like nitrification and sulfide scavenging in anoxic sediments, and how microbial communities use manganese during enzymatic degradation of lignin in coastal areas, give us a new perspective about the role of manganese in biogeochemical cycles. Nevertheless, available methods to determine both dissolved and solid phases of manganese are inadequate to quantify the role of these reactions in natural environments because of their unidimensional (usually averaged vertical pattern) and intrusive nature. Sedimentary perturbation by macrobenthic animals, and its effect on reactive particles and solute distributions, as described by Aller (1982), and as visually exposed using two-dimensional pH and O_2 sensors (Glud et al., 1996, 1999a,b, 2001; Wenzhöfer and Glud, 2004; Precht et al., 2004; Zhu et al., 2005, 2006b; Hakonen and Hulth, 2010), suggest that vertical manganese concentration profiles obtained using conventional techniques are far from representing the natural heterogeneity of perturbed marine coastal sediments; this difference from reality will impact our conceptual and quantitative modeling attempts. In particular, Aller (1980) showed how Fe(II) and Mn(II) concentration magnitudes depicted in vertical profiles in

coastal marine sediments can be lower than expected as a consequence of these species diffusion into burrowing structures. Thus, high resolution multi-dimensional measurements of Mn(II) distributional patterns become relevant to defining accurate boundary conditions, reflecting both heterogeneity and chemical zonation in bioperturbed sediments, during one or multidimensional modeling.

The development and use of two dimensional chemical optical sensors for measuring dissolved manganese in marine sedimentary deposits would represent a significant contribution to our understanding of the chemistry of coastal marine sedimentary deposits and the role benthic organisms play in the biogeochemical cycling of Mn. In combination with other optical planar sensor measurements of analytes such as pH, pCO_2, H_2S, Fe^{2+}, etc., the spatial and temporal measurements of Mn(II), Fe(II), S(-II) and pH can provide new insights into the interaction of manganese with the cycling and transport of other biogochemically active elements, and a basis for modeling their behavior at the seafloor. Therefore, the main objectives of this dissertation are to develop a rugged Mn planar optical sensor suitable for measuring 2-dimensional distribution patterns of dissolved Mn(II) in bioturbated surficial marine sediments, to establish 2- and 3-dimensional sensing techniques in marine sediments, to study Mn cycling and associated biogeochemical processes in the heterogeneous bioturbated marine deposits based on in-situ 2-D and 3-D Mn(II) distribution patterns, and to further elucidate the relationship of Mn cycling to the sediment geometry and benthic community properties such as the mobility and size of infauna.

1.6 The structure of the dissertation

In this dissertation, I investigate the multi-dimensional characterization of dissolved Mn(II) in bioturbated surficial marine sediments. Chapter 1 provides background information on Mn(II) cycling in marine sediments, the application of optical sensors in biogeochemistry, Mn(II) quantification techniques, and current research questions on these topics. Chapter 2 describes a new wet-chemical spectrophotometric method for sensitive and selective detection of Mn(II) in marine porewater samples. A new optical indicator for dissolved Mn(II) recognition and quantification, 4,4',4'',4'''-(Porphine-5,10,15,20-tetrayl) tetrakis (benzenesulfonic acid) with cadmium (Cd-TSPP), is selected. Its optical spectral properties in the presence/absence of Mn(II), and the effect of salinity, temperature and pH and other experimental conditions are investigated. Chapter 3 describes the development and optimization of a planar optode for measurements of Mn(II) in marine sedimentary deposits, testing the suitability of Cd-TSPP as a chemical indicator for multidimensional measurements in terms of the viability of its immobilization in a blocked urethane based polymer, and checking the effect of this process on its chemical response. Chemical and physical aspects of this sensor are optimized to provide a suitable response to the analyte under marine conditions, and to improve optical properties of the sensor for quantification purposes. The main goal of this optimization is to provide the planar optode the capability to depict distributional patterns of the analyte under different conditions of bioperturbation or/and oxygenation. Chapter 4 gives an account of applications of the developed Mn(II) planar optode during two- and three-dimensional Mn(II) measurements, coupling its use with a planar optode for ferrous iron, as well as with basic tomographic reconstructions, to quantitatively visualize the effect of bioturbation and /or changes in oxygenation regimes over

the chemistry of redox sensitive metals in marine sediments, depicting changes on its fluxes under and across the sediment-water interface. This chapter includes both in situ and ex situ measurements, as well as application to incubation experiments. Finally, Chapter 5 summarizes the achievements and findings of this research.

References

Aller, R. C. (1982), Carbonate Dissolution In Nearshore Terrigenous Muds - The Role Of Physical And Biological Reworking, Journal Of Geology, 90(1), 79-95.

Aller, R. C. (1990), Bioturbation And Manganese Cycling In Hemipelagic Sediments, Philosophical Transactions Of The Royal Society Of London Series A-Mathematical Physical And Engineering Sciences, 331(1616), 51-68, Doi:10.1098/Rsta.1990.0056.

Aller, R. C., And R. E. Dodge (1974), Animal-Sediment Relations In A Tropical Lagoon Discovery Bay, Jamaica, Journal Of Marine Research, 32(2), 209-232.

Aller, R. C., And P. D. Rude (1988), Complete Oxidation Of Solid Phase Sulfides By Manganese And Bacteria In Anoxic Marine Sediments, Geochim Cosmochim Acta, 52(3), 751-765.

Aller, R. C. (1980), Quantifying Solute Distributions In The Bioturbated Zone Of Marine-Sediments By Defining An Average Micro-Environment, Geochimica Et Cosmochimica Acta, 44(12), 1955-1965, Doi:10.1016/0016-7037(80)90195-7.

Aller, R. C. (1994), Bioturbation And Remineralization Of Sedimentary Organic-Matter - Effects Of Redox Oscillation, Chemical Geology, 114(3-4), 331-345, Doi:10.1016/0009-2541(94)90062-0.

Andres, R. T., And R. Narayanaswamy (1995), Effect Of The Coupling Reagent On The Metal Inhibition Of Immobilized Urease In An Optical Biosensor, Analyst, 120(5), 1549-1554, Doi:10.1039/An9952001549.

Anschutz, P., B. Sundby, L. Lefrançois, G. W. Luther Iii, And A. Mucci (2000), Interactions Between Metal Oxides And Species Of Nitrogen And Iodine In Bioturbated Marine Sediments, Geochimica Et Cosmochimica Acta, 64(16), 2751-2763, Doi:Http://Dx.Doi.Org/10.1016/S0016-7037(00)00400-2.

Anschutz, P., K. Dedieu, F. Desmazes, And G. Chaillou (2005), Speciation, Oxidation State, And Reactivity Of Particulate Manganese In Marine Sediments, Chem Geol, 218(3-4), 265-279.

Anschutz, P., F. J. Jorissen, G. Chaillou, R. Abu-Zied, And C. Fontanier (2002), Recent Turbidite Deposition In The Eastern Atlantic: Early Diagenesis And Biotic Recovery, Journal Of Marine Research, 60(6), 835-854, Doi:10.1357/002224002321505156.

Banks, C. E., J. Kruusma, R. R. Moore, P. Tomčík, J. Peters, J. Davis, Š. Komorsky-Lovrić, And R. G. Compton (2005), Manganese Detection In Marine Sediments: Anodic Vs. Cathodic Stripping Voltammetry, Talanta, 65(2), 423-429.

Bargar, J. R., B. M. Tebo, U. Bergmann, S. M. Webb, P. Glatzel, V. Q. Chiu, And M. Villalobos (2005), Biotic And Abiotic Products Of Mn(Ii) Oxidation By Spores Of The Marine Bacillus Sp. Strain Sg-1, Am. Miner., 90(1), 143-154, Doi:10.2138/Am.2005.1557.

Bartlett, R., R. J. G. Mortimer, And K. Morris (2008), Anoxic Nitrification: Evidence From Humber Estuary Sediments (UK), Chemical Geology, 250(1-4), 29-39, Doi:10.1016/J.Chemgeo.2008.02.001.

Bartlett, R. J., And B. R. James (1993), Redox Chemistry Of Soils, In Advances In Agronomy, Edited, Pp. 151-208, Academic Press.

Bishop, E. (1972), Mass And Charge-Transfer Kinetics And Coulometric Current Efficiencies .3. Pattern Theory And Its Application To Oxidation-Reduction Electrode Processes, Analyst, 97(1159), 761-&, Doi:10.1039/An9729700761.

Bona, F. (2006), Effect Of Seaweed Proliferation On Benthic Habitat Quality Assessed By Sediment Profile Imaging, Journal Of Marine Systems, 62(3-4), 142-151, Doi:10.1016/J.Jmarsys.2006.01.007.

Bonugli-Santos, R. C., L. R. Durrant, M. Da Silva, And L. D. Sette (2010), Production Of Laccase, Manganese Peroxidase And Lignin Peroxidase By Brazilian Marine-Derived

Fungi, Enzyme And Microbial Technology, 46(1), 32-37, Doi:10.1016/J.Enzmictec.2009.07.014.

Bottcher, M. E., And B. Thamdrup (2001), Anaerobic Sulfide Oxidation And Stable Isotope Fractionation Associated With Bacterial Sulfur Disproportionation In The Presence Of MnO_2, Geochimica Et Cosmochimica Acta, 65(10), 1573-1581, Doi:10.1016/S0016-7037(00)00622-0.

.

Bratina, B. J., B. S. Stevenson, W. J. Green, And T. M. Schmidt (1998), Manganese Reduction By Microbes From Oxic Regions Of The Lake Vanda (Antarctica) Water Column, Applied And Environmental Microbiology, 64(10), 3791-3797.

Brendel, P. J., And G. W. Luther (1995), Development Of A Gold Amalgam Voltammetric Microelectrode For The Determination Of Dissolved Fe, Mn, O(-2), And S(-2) In Porewaters Of Marine And Fresh-Water Sediments, Environmental Science & Technology, 29(3), 751-761, Doi:10.1021/Es00003a024.

Bull, D. C., And R. B. Williamson (2001), Prediction Of Principal Metal Binding Solid Phases In Estuarine Sediments From Color Image Analysis, Environmental Science & Technology, 35(8), 1658-1662, Doi:10.1021/Es0015646.

Burdige, D. J., S. P. Dhakar, And K. H. Nealson (1992), Effects Of Manganese Oxide Mineralogy On Microbial And Chemical Manganese Reduction, Geomicrobiol J, 10(1), 27-48, Doi:10.1080/01490459209377902.

Canfield, D. E., And B. Thamdrup (1994), The Production S-34-Depleted Sulfide During Bacterial Disproportionation Of Elemental Sulfur, Science, 266(5193), 1973-1975.

Canfield, D. E., B. Thamdrup, And J. W. Hansen (1993), The Anaerobic Degradation Of Organic Matter In Danish Coastal Sediments: Iron Reduction, Manganese Reduction, And Sulfate Reduction, Geochim Cosmochim Acta, 57(16), 3867-3883.

Cao, Z., Q. Zhu, R. C. Aller, And J. Y. Aller (2011), A Fluorosensor For Two-Dimensional Measurements Of Extracellular Enzyme Activity In Marine Sediments, Marine Chemistry, 123(1–4), 23-31, Doi:Http://Dx.Doi.Org/10.1016/J.Marchem.2010.09.002.

Chiswell, B., G. Rauchle, And M. Pascoe (1990), Spectrophotometric Methods For The Determination Of Manganese, Talanta, 37(2), 237-259, Doi:10.1016/0039-9140(90)80029-F.

Cheng, K. L. and R. H. Bray (1955). 1-(2-Pyridylazo)-2-Naphthol As A Possible Analytical Reagent. Analytical Chemistry 27(5): 782-785.

Crompton, T. R. (2006). Analysis of Seawater: A Guide For The Analytical And Environmental Chemist, Springer-Verlag Berlin, Heidelberger Platz 3, D-14197 Berlin, Germany.

Croudace, I. W., A. Rindby, And R. G. Rothwell (2006), Itrax: Description And Evaluation Of A New Multi-Function X-Ray Core Scanner, Geol. Soc. Spec. Publ., 267, 51-63, Doi:10.1144/Gsl.Sp.2006.267.01.04.

De Oliveira, W. A., And R. Narayanaswamy (1992), A Flow-Cell Optosensor For Lead Based On Immobilized Dithizone, Talanta, 39(11), 1499-1503, Doi:Http://Dx.Doi.Org/10.1016/0039-9140(92)80132-W.

Deflandre, B., A. Mucci, J. P. Gagne, C. Guignard, And B. Sundby (2002), Early Diagenetic Processes In Coastal Marine Sediments Disturbed By A Catastrophic Sedimentation Event, Geochimica Et Cosmochimica Acta, 66(14), 2547-2558, Doi:10.1016/S0016-7037(02)00861-X.

Ehrlich, H. L. (1968), Bacteriology Of Manganese Nodules .2. Manganese Oxidation By Cell-Free Extract From A Manganese Nodule Bacterium, Applied Microbiology, 16(2), 197-&.

Ehrlich, H. L. (1983), Manganese-Oxidizing Bacteria From A Hydrothermally Active Area On The Galapagos Rift, Ecological Bulletins(35), 357-366.

Engström, P., T. Dalsgaard, S. Hulth, And R. C. Aller (2005), Anaerobic Ammonium Oxidation By Nitrite (Anammox): Implications For N2 Production In Coastal Marine Sediments, Geochim Cosmochim Acta, 69(8), 2057-2065.

Field, M. P., J. T. Cullen, And R. M. Sherrell (1999), Direct Determination Of 10 Trace Metals In 50 Mu L Samples Of Coastal Seawater Using Desolvating Micronebulization Sector Field Icp-Ms, Journal Of Analytical Atomic Spectrometry, 14(9), 1425-1431, Doi:10.1039/A901693g.

Filipe, O. M. S., And C. M. A. Brett (2003), Cathodic Stripping Voltammetry Of Trace Mn(Ii) At Carbon Film Electrodes, Talanta, 61(5), 643-650, Doi:10.1016/S0039-9140(03)00327-8.

Francis, C. A., K. L. Casciotti, And B. M. Tebo (2002), Localization Of Mn(II)-Oxidizing Activity And The Putative Multicopper Oxidase, Mnxg, To The Exosporium Of The Marine Bacillus Sp Strain Sg-1, Archives Of Microbiology, 178(6), 450-456, Doi:10.1007/S00203-002-0472-9.

Francis, C. A., And B. M. Tebo (2001), Enzimatic Manganese(II) Oxidation By A Marine A-Proteobacterium, Appl Environ Microbiol, 67, 4024-4029.

Froelich, P. N., G. P. Klinkhammer, M. L. Bender, N. A. Luedtke, G. R. Heath, D. Cullen, P. Dauphin, D. Hammond, B. Hartman, And V. Maynard (1979), Early Oxidation Of Organic

Matter In Pelagic Sediments Of The Eastern Equatorial Atlantic: Suboxic Diagenesis, Geochim Cosmochim Acta, 43(7), 1075-1090.

Gilbert, F., S. Hulth, N. Strömberg, K. Ringdahl, And J.-C. Poggiale (2003), 2-D Optical Quantification Of Particle Reworking Activities In Marine Surface Sediments, Journal Of Experimental Marine Biology And Ecology, 285–286, 251-263, Doi:Http://Dx.Doi.Org/10.1016/S0022-0981(02)00531-2.

Gill, I., And A. Ballesteros (2000a), Bioencapsulation Within Synthetic Polymers (Part 1): Sol-Gel Encapsulated Biologicals, Trends In Biotechnology, 18(7), 282-296, Doi:10.1016/S0167-7799(00)01457-8.

Gill, I., And A. Ballesteros (2000b), Bioencapsulation Within Synthetic Polymers (Part 2): Non-Sol-Gel Protein-Polymer Biocomposites, Trends In Biotechnology, 18(11), 469-479, Doi:10.1016/S0167-7799(00)01493-1.

Gill, I., And A. Ballesteros (2000c), Degradation Of Organophosphorous Nerve Agents By Enzyme-Polymer Nanocomposites: Efficient Biocatalytic Materials For Personal Protection And Large-Scale Detoxification, Biotechnology And Bioengineering, 70(4), 400-410, Doi:10.1002/1097-0290(20001120)70:4<400::Aid-Bit5>3.0.Co;2-2.

Glenn, J. K., M. A. Morgan, M. B. Mayfield, M. Kuwahara, And M. H. Gold (1983), An Extracellular H_2O_2-Requiring Enzyme Preparation Involved In Lignin Biodegradation By The White Rot Basidiomycete Phanerochaete Chrysosporium, Biochemical And Biophysical Research Communications, 114(3), 1077-1083, Doi:10.1016/0006-291x(83)90672-1.

Glud, R. N., I. Klimant, G. Holst, O. Kohls, V. Meyer, M. Kühl, And J. K. Gundersen (1999a), Adaptation, Test And In Situ Measurements With O_2 Micro-optodes On Benthic Landers, Deep Sea Research Part I: Oceanographic Research Papers, 46(1), 171-183, Doi:10.1016/S0967-0637(98)00068-5.

Glud, R. N., M. Kuhl, O. Kohls, And N. B. Ramsing (1999b), Heterogeneity Of Oxygen Production And Consumption In A Photosynthetic Microbial Mat As Studied By Planar Optodes, Journal Of Phycology, 35(2), 270-279, Doi:10.1046/J.1529-8817.1999.3520270.X.

Glud, R. N., N. B. Ramsing, J. K. Gundersen, And I. Klimant (1996), Planar Optrodes: A New Tool For Fine Scale Measurements Of Two-Dimensional O2 Distribution In Benthic Communities, Marine Ecology Progress Series, 140, 217-226.

Glud, R. N., A. Tengberg, M. Kühl, P. O. J. Hall, I. Klimant, And G. Holst (2001), An In Situ Instrument For Planar O2 Optode Measurements At Benthic Interfaces, Limnology And Oceanography, 46(8), 2073-2080.

Grygar, T., P. Bezdicka, D. Hradil, A. Domenech-Carbo, F. Marken, L. Pikna, And G. Cepria (2002), Voltammetric Analysis Of Iron Oxide Pigments, Analyst, 127(8), 1100-1107, Doi:10.1039/B205199k.

Hakonen, A., And S. Hulth (2010), A High-Performance Fluorosensor For pH Measurements Between 6 And 9, Talanta, 80(5), 1964-1969, Doi:10.1016/J.Talanta.2009.10.055.

Hales, B., L. Burgess, And S. Emerson (1997), An Absorbance-Based Fiber-Optic Sensor For CO_2(Aq) Measurement In Porewaters Of Sea Floor Sediments, Marine Chemistry, 59(1-2), 51-62, Doi:10.1016/S0304-4203(97)00065-0.

Huber, C., I. Klimant, C. Krause, T. Werner, And O. S. Wolfbeis (2001), Nitrate-Selective Optical Sensor Applying A Lipophilic Fluorescent Potential-Sensitive Dye, Analytica Chimica Acta, 449(1-2), 81-93, Doi:10.1016/S0003-2670(01)01363-0.

Hulth, S., R. C. Aller, And F. Gilbert (1999), Coupled Anoxic Nitrification/Manganese Reduction In Marine Sediments, Geochim Cosmochim Acta, 63(1), 49-66.

Jansen, J. H. F., S. J. Van Der Gaast, B. Koster, And A. J. Vaars (1998), Cortex, A Shipboard Xrf-Scanner For Element Analyses In Split Sediment Cores, Marine Geology, 151(1-4), 143-153, Doi:10.1016/S0025-3227(98)00074-7.

Javanaud, C., V. Michotey, S. Guasco, N. Garcia, P. Anschutz, M. Canton, And P. Bonin (2011), Anaerobic Ammonium Oxidation Mediated By Mn-Oxides: From Sediment To Strain Level, Res. Microbiol.162:9,pp 848-857.

Jeronimo, P. C. A., A. N. Araujo, And M. Montenegro (2007), Optical Sensors And Biosensors Based On Sol-Gel Films, Talanta, 72(1), 13-27, Doi:10.1016/J.Talanta.2006.09.029.

Johnston, C. G., And G. W. Kipphut (1988), Microbially Mediated Mn(II) Oxidation In An Oligotrophic Arctic Lake, Applied And Environmental Microbiology, 54(6), 1440-1445.

Jorgensen, B. B. (1982), Mineralization Of Organic Matter In The Sea Bed: The Role Of Sulphate Reduction, Nature, 296(5858), 643-645.

Jung, W. K., And R. Schweisfurth (1979), Manganese Oxidation By An Intracellular Protein Of A Pseudomonas Species, Zeitschrift Fur Allgemeine Mikrobiologie, 19(2), 107-115, Doi:10.1002/Jobm.3630190206.

Kaštelan-Macan, M., L. Bokić, Š. Cerjan-Stefanović, And K. Moskaliuk (1986), Separation And Detection Of Traces Of Copper, Iron And Manganese In Cotton Materials By TLC, Chromatography, 22(1-6), 19-20, Doi:10.1007/Bf02257290.

Kessick, M. A., And B. M. Thomson (1974), Reaction Between Manganese Dioxide And Aqueous Sulfide, Environ. Lett., 7, 163-173.

Kingston, H. M., Et Al. (1978). "Separation Of 8 Transition-Elements From Alkali And Alkaline-Earth Elements In Estuarine And Seawater With Chelating Resin And Their Determination By Graphite Furnace Atomic-Absorption Spectrometry." Analytical Chemistry 50(14): 2064-2070.

Klimant, I., G. Holst, And M. Kuhl (1995), Oxygen Microoptrodes And Their Application In Aquatic Environment, 375-386 Pp., Doi:10.1117/12.221753.

Klimant, I., G. Holst, And M. Kuhl (1997), A Simple Fiberoptic Sensor To Detect The Penetration Of Microsensors Into Sediments And Other Biogeochemical Systems, Limnology And Oceanography, 42(7), 1638-1643.

Klimant, I., And M. Otto (1992), A Fiber Optical Sensor For Heavy-Metal Ions Based On Immobilized Xylenol Orange, Mikrochimica Acta, 108(1-2), 11-17, Doi:10.1007/Bf01240367.

Kohls, O., I. Klimant, G. Holst, And M. Kuhl (1997), Development And Comparison Of pH Microoptodes For Use In Marine Systems, SPIE Proceedings 82-91, Doi:10.1117/12.269958.

Kuwahara, M., J. K. Glenn, M. A. Morgan, And M. H. Gold (1984), Separation And Characterization Of Two Extracelluar H_2O_2-Dependent Oxidases From Ligninolytic Cultures Of Phanerochaete Chrysosporium, Febs Letters, 169(2), 247-250, Doi:10.1016/0014-5793(84)80327-0.

Lakowicz, J. R., G. Laczko, I. Gryczynski, H. Szmacinski, W. Wiczk, And M. L. Johnson (1989), Frequency-Domain Fluorescence Spectroscopy - Principles, Biochemical Applications And Future-Developments, Ber. Bunsen-Ges. Phys. Chem., 93(3), 316-327.

Lerchi, M., E. Bakker, B. Rusterholz, And W. Simon (1992), Lead-Selective Bulk Optodes Based On Neutral Ionophores With Subnanomolar Detection Limits, Analytical Chemistry, 64(14), 1534-1540, Doi:10.1021/Ac00038a007.

Liu, Y., And J. D. Ingle (1989), Automated On-Line Ion-Exchange Trace Enrichment System With Flame Atomic Absorption Detection, Analytical Chemistry, 61(6), 520-524, Doi:10.1021/Ac00181a004.

Lo, J. M., et al. (1982). Solvent-Extraction Of Dithiocarbamate Complexes And Back-Extraction With Mercury(II) For Determination Of Trace-Metals In Sea-Water By Atomic-Absorption Spectrometry. Analytical Chemistry 54(14): 2536-2539.

Lohan, M. C., And K. W. Bruland (2008), Elevated Fe(Ii) And Dissolved Fe In Hypoxic Shelf Waters Off Oregon And Washington: An Enhanced Source Of Iron To Coastal Upwelling Regimes, 42(17), 6462-6468.

Lovley, D. R. (1991), Dissimilatory Fe(III) And Mn(IV) Reduction, Microbiological Reviews, 55(2), 259-287.

Luther, III, G. W., And J. I. Popp (2002), Kinetics Of The Abiotic Reduction Of Polymeric Manganese Dioxide By Nitrite: An Anaerobic Nitrification Reaction, Aquatic Geochemistry, 8(1), 15-36.

Luther III, G. W., B. Sundby, B. L. Lewis, P. J. Brendel, And N. Silverberg (1997), Interactions Of Manganese With The Nitrogen Cycle: Alternative Pathways To Dinitrogen, Geochimica Et Cosmochimica Acta, 61(19), 4043-4052, Doi:10.1016/S0016-7037(97)00239-1.

Madison, A. S., B. M. Tebo, And G. W. Luther, Iii (2011), Simultaneous Determination Of Soluble Manganese(III), Manganese(Ii) And Total Manganese In Natural (Pore)Waters, Talanta, 84(2), 374-381, Doi:10.1016/J.Talanta.2011.01.025.

Malcik, N., And P. Caglar (1997), The Operational Parameters Of A New Fibre-Optic Sensor For Ferric Ions In Aqueous Media, Sensors And Actuators B-Chemical, 39(1-3), 386-389, Doi:10.1016/S0925-4005(97)80239-0.

Malcik, N., O. Oktar, M. E. Ozser, P. Caglar, L. Bushby, A. Vaughan, B. Kuswandi, And R. Narayanaswamy (1998), Immobilised Reagents For Optical Heavy Metal Ions Sensing, Sensors And Actuators B-Chemical, 53(3), 211-221, Doi:10.1016/S0925-4005(99)00004-0.

Malstrom, B. G. (1988), Redox Loops And Prot Malstrom, B. G. (1988), Redox Loops And Proton Pumps, Febs Letters, 231(1), 268-269.on Pumps, Febs Letters, 231(1), 268-269.

Marczenko, Z. 1986. Separation and Spectrophotometric Determination of Elements. Horwood, Chichester.

Marshall, K. C. (1980), The Role Of Surface Attachment In Manganese Oxidation By Freshwater Hyphomicrobia, In Biogeochemistry Of Ancient And Modern Environments, Edited By P. A. Trudinger, M. R. Walter And B. J. Ralph, Pp. 333-337, Springer Berlin Heidelberg, Doi:10.1007/978-3-642-48739-2_35.

McArthur, J. M. (1977). Determination Of Manganese In Natural-Waters By Flameless Atomic-Absorption Spectrometry. Analytica Chimica Acta 93(1): 77-83.

Middelburg, J. J., G. J. De Lange, And C. H. Van Der Weijden (1987), Manganese Solubility Control In Marine Pore Waters, Geochim Cosmochim Acta, 51(3), 759-763.

Milani, A., P. J. Statham, M. C. Mowlem, And D. P. Connelly (2015), Development And Application Of A Microfluidic In-Situ Analyzer For Dissolved Fe And Mn In Natural Waters, Talanta, 136(0), 15-22.

Miyata, N., D. Sugiyama, Y. Tani, H. Tsuno, H. Seyama, M. Sakata, And K. Iwahori (2007a), Production Of Biogenic Manganese Oxides By Repeated-Batch Cultures Of Laboratory Microcosms, Journal Of Bioscience And Bioengineering, 103(5), 432-439, Doi:10.1263/Jbb.103.432.

Miyata, N., Y. Tani, K. Iwahori, And M. Soma (2004), Enzymatic Formation Of Manganese Oxides By An Acremonium-Like Hyphomycete Fungus, Strain Kr21-2, Fems Microbiology Ecology, 47(1), 101-109, Doi:10.1016/S0168-6496(03)00251-4.

Miyata, N., Y. Tani, M. Sakata, And K. Iwahori (2007b), Microbial Manganese Oxide Formation And Interaction With Toxic Metal Ions, Journal Of Bioscience And Bioengineering, 104(1), 1-8, Doi:10.1263/Jbb.104.1.

Morales-Bahnik, A., R. Czolk, J. Reichert, And H. J. Ache (1993), An Optochemical Sensor For Cd(II) And Hg(II) Based On A Porphyrin Immobilized On Nafion(R) Membranes, Sensors And Actuators B-Chemical, 13(1-3), 424-426, Doi:10.1016/0925-4005(93)85417-9.

Murray, J. (1975), The Interaction Of Metal Ions At The Manganese Dioxide-Solution Interface, Geochim. Cosmochim. Acta, 39(4), 505-519.

Murray, J. W., L. S. Balistrieri, And B. Paul (1984), The Oxidation State Of Manganese In Marine Sediments And Ferromanganese Nodules, Geochim Cosmochim Acta, 48(6), 1237-1247.

Murray, J. W., L. A. Codispoti, And G. E. Friederich (1995), Oxidation-Reduction Environments - The Suboxic Zone In The Black-Sea, In Aquatic Chemistry: Interfacial And Interspecies Processes, Edited By C. P. O. C. R. M. J. J. Huang, Pp. 157-176, Doi:10.1021/Ba-1995-0244.Ch007.

Myers, C. R., And K. H. Nealson (1988), Bacterial Manganese Reduction And Growth With Manganese Oxide As The Sole Electron-Acceptor, Science, 240(4857), 1319-1321, Doi:10.1126/Science.240.4857.1319.

Nealson, K. H., And C. R. Myers (1992), Microbial Reduction Of Manganese And Iron - New Approaches To Carbon Cycling, Applied And Environmental Microbiology, 58(2), 439-443.

Nealson, K. H., B. M. Tebo, And R. A. Rosson (1988), Occurrence And Mechanisms Of Microbial Oxidation Of Manganese, In Advances In Applied Microbiology, Edited, Pp. 279-318, Academic Press.

Neurauter, G., I. Klimant, And O. S. Wolfbeis (2000), Fiber-Optic Microsensor For High Resolution pCO_2 Sensing In Marine Environment, Fresenius Journal Of Analytical Chemistry, 366(5), 481-487, Doi:10.1007/S002160050097.

Oehme, I., And O. S. Wolfbeis (1997), Optical Sensors For Determination Of Heavy Metal Ions, Mikrochimica Acta, 126(3-4), 177-192, Doi:10.1007/Bf01242319.

Oguri, K., H. Kitazato, And R. N. Glud (2006), Platinum Octaetylporphyrin Based Planar Optodes Combined With An UV-LED Excitation Light Source: An Ideal Tool For High-Resolution O_2 Imaging In O_2 Depleted Environments, Marine Chemistry, 100(1-2), 95-107, Doi:10.1016/J.Marchem.2005.11.005.

Okazaki, M., T. Sugita, M. Shimizu, Y. Ohode, K. Iwamoto, E. W. Devrinddejong, J. P. M. Devrind, And P. Corstjens (1997), Partial Purification And Characterization Of Manganese-Oxidizing Factors Of Pseudomonas Fluorescens Gb-1, Applied And Environmental Microbiology, 63(12), 4793-4799.

O'Halloran, R. J. (1982). Anodic Stripping Voltammetry Of Manganese In Seawater At A Mercury Film Electrode. Analytica Chimica Acta 140(1): 51-58.

Parikh, S. J., And J. Chorover (2005), FTIR Spectroscopic Study Of Biogenic Mn-Oxide Formation By Pseudomonas Putida Gb-1, Geomicrobiology Journal, 22(5), 207-218, Doi:10.1080/01490450590947724.

Petersen, C. G. J. (1913), Determination Of The Quantity Of Animal Life On The Sea Bottom, Ann Inst Ocean Paris, 6(1), Unpaginated.

Precht, E., U. Franke, L. Polerecky, And M. Huettel (2004), Oxygen Dynamics In Permeable Sediments With Wave-Driven Pore Water Exchange, Limnology And Oceanography, 49(3), 693-705.

Postma, D. (1985), Concentration Of Mn And Separation From Fe In Sediments—I. Kinetics And Stoichiometry Of The Reaction Between Birnessite And Dissolved Fe(II) At 10°C, Geochim Cosmochim Acta, 49(4), 1023-1033.

Ramsey, M. H., P. J. Potts, P. C. Webb, P. Watkins, J. S. Watson, And B. J. Coles (1995), An Objective Assessment Of Analytical Method Precision: Comparison Of -ICP-AES And Xrf For The Analysis Of Silicate Rocks, Chemical Geology, 124(1-2), 1-19, Doi:10.1016/0009-2541(95)00020-M.

Rhoads, D. C. (1995), Measuring Hydrocarbon Contaminants On The Sea-Floor, Sea Technol., 36(8), 37-&.

Rhoads, D. C., And S. Cande (1971), Sediment Profile Camera For In-Situ Study Of Organism-Sediment Relations, Limnology And Oceanography, 16(1), 110-&.

Rhoads, D. C., J. Germano, L. Boyer, R. Mcgrath, And G. L. Chase (1983), Benthic Habitat Evaluation In An Urban Estuarine Ecosystem And Its Relationship To Dredging And Disposal Operations, Estuaries, 6(3), 268-268.

Rhoads, D. C. (1974), Organism-Sediment Relations On The Muddy Sea Floor, Oceanography Mar Biol, 12, 263-300.

Ricco, A. J., And R. M. Crooks (1998), Chemical Sensors, Accounts Of Chemical Research, 31(5), 200-200, Doi:10.1021/Ar980479o.

Richter, T. O., S. Van Der Gaast, B. Koster, A. Vaars, R. Gieles, H. C. De Stigter, H. De Haas, And T. C. E. Van Weering (2006), The Avaatech Xrf Core Scanner: Technical Description And Applications To Ne Atlantic Sediments, Geol. Soc. Spec. Publ., 267, 39-50, Doi:10.1144/Gsl.Sp.2006.267.01.03.

Saito, M. A. and D. L. Schneider (2006). Examination Of Precipitation Chemistry And Improvements In Precision Using The $Mg(OH)_2$ Preconcentration Inductively Coupled Plasma Mass Spectrometry (ICP-MS) Method For High-Throughput Analysis Of Open-Ocean Fe And Mn In Seawater. Analytica Chimica Acta 565(2): 222-233.

Sarzanini, C., O. Abollino, And E. Mentasti (2001), Flow-Injection Preconcentration And Electrothermal Atomic Absorption Spectrometry Determination Of Manganese In Seawater, Analytica Chimica Acta, 435(2), 343-350, Doi:10.1016/S0003-2670(01)00856-X.

Schippers, A., And B. B. Jørgensen (2001), Oxidation Of Pyrite And Iron Sulfide By Manganese Dioxide In Marine Sediments, Geochim Cosmochim Acta, 65(6), 915-922.

Seitz, W. R. (1984), Chemical Sensors Based On Fiber Optics, Analytical Chemistry, 56(1), A16-&, Doi:10.1021/Ac00265a001.

Seitz, W. R. (1991), Sensors Provide Immediate Analytical Results On A Continuous Or Repetitive Basis, Talanta, 38(5), R5-R5, Doi:10.1016/0039-9140(91)80163-T.

Shekhovtsova, T. N., S. V. Chernetskaya, N. V. Belkova, And I. F. Dolmanova (1994), The Use Of Immobilized Enzymes For Determination Of Metal-Ions, Journal Of Analytical Chemistry, 49(8), 709-714.

Shibata, S., et al. (1973). Syntheses And Spectrophotometric Studies Of Azo Dyes Containing Meta-Dimethylaminophenol As Analytical Reagents. Analytica Chimica Acta 66(3): 397-409.

Solan, M., et al. (2003), Towards A Greater Understanding Of Pattern, Scale And Process In Marine Benthic Systems: A Picture Is Worth A Thousand Worms, Journal Of Experimental Marine Biology And Ecology, 285-286(0), 313-338, Doi:10.1016/S0022-0981(02)00535-X.

Stallard, M. O., S. E. Apitz, and C. A. Dooley (1995), X-Ray Fluorescence Spectrometry For Field Analysis Of Metals In Marine Sediments, Marine Pollution Bulletin, 31(4-12), 297-305, Doi:10.1016/0025-326x(95)00147-F.

Stone, A. T., And J. J. Morgan (1987), Reductive Dissolution Of Metal Oxides, In Aquatic Surface Chemistry, Edited, Pp. 221-254, Chichester.

Stumm, W., and J. J. Morgan (1996), Aquatic Chemistry, 3rd Ed, Wiley, New York.

Sunda, W. G., and D. J. Kieber (1994), Oxidation Of Humic Substances By Manganese Oxides Yields Low-Molecular-Weight Organic Substrates, Nature, 367(6458), 62-64, Doi:10.1038/367062a0.

Sundby, B., and N. Silverberg (1985), Manganese Fluxes In The Benthic Boundary Layer, Limnol Oceanogr, 30, 372-381.

.

Tebo, B. M., H. A. Johnson, J. K. Mccarthy, and A. S. Templeton (2005), Geomicrobiology Of Manganese(Ii) Oxidation, Trends Microbiol., 13(9), 421-428, Doi:10.1016/J.Tim.2005.07.009.

Thamdrup, B., and T. Dalsgaard (2000), The Fate Of Ammonium In Anoxic Manganese Oxide-Rich Marine Sediment, Geochim Cosmochim Acta, 64(24), 4157-4164.

Thamdrup, B., K. Finster, H. Fossing, J. W. Hansen, and B. B. Jørgensen (1994), Thiosulfate And Sulfite Distributions In Porewater Of Marine Sediments Related To Manganese, Iron, And Sulfur Geochemistry, Geochim Cosmochim Acta, 58(1), 67-73.

Thamdrup, B., K. Finster, J. W. Hansen, and F. Bak (1993), Bacterial Disproportionation Of Elemental Sulfur Coupled To Chemical-Reduction Of Iron Or Manganese, Applied And Environmental Microbiology, 59(1), 101-108.

Van Den Berg, C. M. (1991), Potentials And Potentialities Of Cathodic Stripping Voltammetry Of Trace Elements In Natural Waters, Analytica Chimica Acta, 250, 265-276.

Viollier, E., Et Al. (2003), Benthic Biogeochemistry: State Of The Art Technologies And Guidelines For The Future Of In Situ Survey, Journal Of Experimental Marine Biology And Ecology, 285, 5-31, Doi:10.1016/S0022-0981(02)00517-8.

Viscarra Rossel, R. A., Y. Fouad, And C. Walter (2008), Using A Digital Camera To Measure Soil Organic Carbon And Iron Contents, Biosystems Engineering, 100(2), 149-159, Doi:Http://Dx.Doi.Org/10.1016/J.Biosystemseng.2008.02.007.

Weltje, G. J., and R. Tjallingii (2008), Calibration Of XRF Core Scanners For Quantitative Geochemical Logging Of Sediment Cores: Theory And Application, Earth And Planetary Science Letters, 274(3-4), 423-438, Doi:10.1016/J.Epsl.2008.07.054.

Wenzhofer, F., and R. N. Glud (2004), Small-Scale Spatial And Temporal Variability In Coastal Benthic O_2 Dynamics: Effects Of Fauna Activity, Limnology And Oceanography, 49(5), 1471-1481.

Wolfe, L. A., and H. Zeitlin (1970), An X-Ray Fluorescence Spectroscopic Method For The Determination Of Total Manganese In Rocks And Marine Sediments, Analytica Chimica Acta, 51(3), 365-372, Doi:10.1016/S0003-2670(01)95730-7.

Wu, J. F. and E. A. Boyle (1997). Low Blank Preconcentration Technique For The Determination Of Lead, Copper, And Cadmium In Small-Volume Seawater Samples By Isotope Dilution ICPMS. Analytical Chemistry 69(13): 2464-2470.

Wu, J. F. and E. A. Boyle (1998). Determination Of Iron In Seawater By High-Resolution Isotope Dilution Inductively Coupled Plasma Mass Spectrometry After $Mg(OH)_2$ Coprecipitation. Analytica Chimica Acta 367(1-3): 183-191.

Young, D. K., And D. C. Rhoads (1971), Animal-Sediment Relations In Cape Cod Bay, Massachusetts .1. Transect Study, Mar. Biol., 11(3), 242-&, Doi:10.1007/Bf00401272.

Zhu, Q., And R. C. Aller (2012), Two-Dimensional Dissolved Ferrous Iron Distributions In Marine Sediments As Revealed By A Novel Planar Optical Sensor, Marine Chemistry, 136–137, 14-23, Doi:Http://Dx.Doi.Org/10.1016/J.Marchem.2012.04.002.

Zhu, Q., R. C. Aller, And Y. Fan (2006a), A New Ratiometric, Planar Fluorosensor For Measuring High Resolution, Two-Dimensional pCO_2 Distributions In Marine Sediments, Marine Chemistry, 101(1-2), 40-53, Doi:10.1016/J.Marchem.2006.01.002.

Zhu, Q., R. C. Aller, And Y. Fan (2006b), Two-Dimensional pH Distributions And Dynamics In Bioturbated Marine Sediments, Geochimica Et Cosmochimica Acta, 70(19), 4933-4949, Doi:10.1016/J.Gca.2006.07.033.

Zhu, Q. Z., R. C. Aller, And Y. Z. Fan (2005), High-Performance Planar pH Fluorosensor For Two-Dimensional pH Measurements In Marine Sediment And Water, Environmental Science & Technology, 39(22), 8906-8911, Doi:10.1021/Es051023m.

Chapter 2:

A new spectrophotometric method to quantify Mn (II) in marine pore waters

Abstract

This study explores the use of Cadmium (II) meso-tetrakis(4-sulfophenyl) porphyrin complex (Cd-TSPP) as an indicator for the spectrophotometric determination of dissolved manganese (II) in pore waters from marine sediments. Both single absorbance and second derivative based methods were evaluated with a multifunctional plate reader. Cd-TSPP has a maximum absorbance at 433 nm in solution, but the core Cd(II) ion in the complex can be quickly replaced by Mn(II) at pH 4 – 8 to form a new Mn porphyrin complex (Mn-TSPP) with maximum absorbance at 469 nm. The absorbance of Mn-TSPP at 469 nm and its second derivative spectra at the same wavelength show excellent linear relationships with Mn(II) concentrations (R^2=0.997 and R^2=0.999, respectively) in the 0 - 37.5 µM range for 200 µL samples. The detection limits using single absorbance and the second derivative are 0.4 and 0.3 µM Mn (II), respectively. A correction subtracting reference absorbance at 490 nm from 469 nm signal was required in the single absorbance approach in order to eliminate the effect of baseline fluctuations. In contrast, the second derivative approach shows higher selectivity, accuracy and precision for Mn (II) determination in pore water. The reaction is not affected by pH (4 – 8) or salinity but is temperature sensitive in the range of 10 – 45 °C with an activation energy of 22.12 kJ mol^{-1}. No interferences from metal ions such as Pb(II), Cu(II), Fe(II), Zn(II) etc. were found. The proposed method, which is rapid and suitable for small size samples, was successfully applied to the determination of Mn (II) in pore water.

2.1 Introduction

Manganese is a key redox reactive element in marine environments, particularly sedimentary deposits. In the oxic zones of marine sediment, manganese is commonly present as solid phase Mn(IV) and Mn(III) oxides and oxyhydroxides (Post 1999). Oxidized manganese can be readily reduced to more soluble Mn (II) in anoxic regions by electron donors such as organic matter, and rapidly reoxidized during subsequent transport and re-exposure to oxidants. Thus, cyclic manganese redox reactions are closely coupled to multiple biogeochemical and physical processes, for example, the degradation of organic matter, oxidation of reduced metabolites, and consumption of oxygen (Takamatsu et al., 1985; Sunby et al., 1986; Burdige et al., 1992; Canfield et al., 1993; Aller, 1994; Luther et al., 1997; Hulth et al., 1999; Thamdrup, 2000). The quantification of dissolved Mn (II) concentrations and distributions is an essential aspect of understanding redox reaction - transport processes in sedimentary deposits.

Several viable analytical techniques have been reported for Mn (II) determination, including atomic absorption spectroscopy (Porta et al., 1991), electroanalytical chemistry (Ma et al., 2008), and spectrophotometric methods (Chiswell et al., 1990). Spectrophotometric methods are particularly useful due to simplicity, sensitivity, stability, comparative low cost and suitability for both automation and field research. Various reagents and sensing schemes have been proposed for colorimetric measurements of manganese in natural environments using permanganate and formaldoxime, the latter being the most used method since the 1960's (Chiswell et al., 1990). Here, we examine the use of the porphyrin complex: cadmium (II) meso-tetrakis(4-sulfophenyl) porphyrin, as an alternative basis for spectrophotometric determination of dissolved Mn (II).

Porphyrins show high sensitivity and selectivity as indicators for metal ion determinations. Typically, the reaction of free porphyrins with metals is slow and thus difficult to incorporate directly into an analytical scheme. However, substitution reactions of dissolved metal ions with metalloporphyrins containing large complexed ions (e.g. Hg^{2+}, Pb^{2+} or Cd^{2+}) can be fast. Of critical importance is that in the process of exchanging the metal ion core of metalloporphyrin complexes, absorption spectra change (Biesaga et al., 2000). Both porphyrins and metalloporphyrins show intense absorption and molar absorptivities in the Soret band (400-500 nm), a metal specific property that is highly useful for optical quantification of metalloporphyrins, and which can be further optimized for analytical applications by use of derivative spectrophotometry (e.g. Ishii et al., 1982b).

Successive formation of metalloporphyrin from metal-free porphyrin (MP) reacting with a divalent metal ion (M^{2+}) and the substitution of a second metal (Mb^{2+}) into the metalloporphyrin nucleus can be generally depicted by equations 11 and 12:

$$M^{2+} + H_2P \leftrightarrow MP + 2H^+ \qquad \text{(eq. 11)}$$

$$MP + Mb^{2+} \rightarrow MbP + M^{2+} \qquad \text{(eq.12)}$$

Many studies have characterized the formation of metalloporphyrins (e.g. Gharib et al., 2009; Kilian & Pyrzynska, 2003; Tabata, 1987; Shamim & Hambright, 1980) and have demonstrated that metal ions typically form a 1:1 complex with porphyrins, excepting Na, Li and K ions which form complexes in a 2:1 ratio with the metal ions projecting slightly out of the macrocyclic plane (Biesaga et al., 2000). A second special case is complexation with large metal ions like mercury, lead and cadmium which are bound just on the central surface of the porphyrin. The resulting deformation of the porphyrin nucleus makes it possible for rapid

substitution reactions with other smaller divalent metal ions, forming complexes with spectroscopic properties specific to the substituting metal and thus potential target analytes (Tanaka, 1983).

Several porphyrins and metalloporphyrins have been used in different analytical schemes involving spectrophotometric, potentiometric, capillary electrophoresis and HPLC techniques to measure a wide range of divalent metal ions in plant and water samples (Ishii et al. 1982a; Xu et al. 1991; Almeda et al. 2009; Okutani et al. 1994). In particular, the most commonly used porphyrins for manganese ions determination are meso-Tetrakis(3-bromo-4-sulfophenyl) porphyrin (m-BrTPPS4), meso-tetrakis(4-sulfophenyl) porphyrin, meso-tetrakis(4-carboxyphenyl) porphyrin [T(4-CP)P] and its cadmium complex (Cd-T(4-CP)P) (Biesaga et al., 2000; Ishii & Kohata, 1987; Ishii et al., 1982a).

Given that meso-tetrakis(4-sulfophenyl) porphyrin has been successfully used in determination of metal ions in both terrestrial and fresh water samples, and the highly convenient isolation of the absorbance peak associated with the manganese complex versus other metalloporphyrin spectra inside the Soret band, we further investigated the suitability of its cadmium complex (Cd-TSPP, Figure 2.1) as a new indicator for rapid spectrophotometric quantification of dissolved manganese in pore water from marine sediments. Because modern multichannel plate readers permit rapid acquisition of continuous spectra on multiple samples, we also evaluated the efficacy of the second derivative technique and adaptation of the spectrophotometric Mn(II) method to common 96-well microplates. The effects of pH, temperature, salinity and potential interferences from foreign divalent ions on the measurement were studied and conditions were optimized. The second derivative approach provides for substantial improvements in the selectivity and sensitivity in measurement relative to single

wavelength absorbance methods (e.g. Han et al, 2011). The Cd-TSPP method has been successfully applied for Mn(II) measurements in sediment porewater samples, allowing measurement of hundreds of samples within a half hour.

2.2 Experimental

2.2.1 Equipment and reagents

A POLARstar Omega multifunctional plate reader with UV/VIS absorbance spectra capabilities was used to perform both kinetic and endpoint measurements at specific wavelengths (469 and 490nm) and obtain wavelength scans (250-700 nm). Reaction and measurement temperatures (25±0.1 °C) were monitored and controlled using the incubation mode of this equipment, and a 4 second double orbital (400 rpm) shaking sequence was performed before each measurement to avoid possible variation between replicates due to mixing processes inside wells, as previously described in the literature (Weiss et al. 2002). The number of Xenon lamp flashes per measurement was fixed at 50 to increase signal stability.

Atomic absorption measurements were carried out using a Graphite Furnace/Flame Perkin Elmer A Analyst 800 Atomic Absorption Spectrometer equipped with an automated motorized atomizer and a hollow cathode lamp for manganese. The graphite furnace mode was selected for all measurements with a sample injection volume of 20 μL, and each sample was measured three times.

The 5,10,15,20-Tetrakis(4-sulfonatophenyl) porphyrin (TSPP) was obtained from SIGMA-Aldrich (88074) and a 0.48 mM stock solution was prepared by dissolving 245.5 mg TSPP in

500ml of 0.01M sodium hydroxide solution. Cadmium porphyrin (Cd-TSPP) complex solutions were prepared according to the method reported by Kilian and Pyrzynska (2003). Briefly, cadmium ion was mixed with TSPP at a molar ratio of 4:1 (Cd^{2+}/TSPP) in a 250 ml amber flask. The reaction was carried out in the dark, and the concentrations of reactant TSPP and product Cd-TSPP were spectrophotometrically determined at 412 nm (ε=3.47x105; Inamo et al., 1997) and 433 nm, respectively. The reaction was stopped when the TSPP absorption peak at 412 nm disappeared. All Cd-TSPP working solutions were prepared the day before use. The stock solutions used to study interference from other metal ions (Fe(II), Pb(II), Cu(II) and Zn(II)) were treated with hydroxylamine hydrochloride (0.32 M in each well) as reductant. Reductant addition assured stable oxidation states for interference evaluations. All pH adjustments were carried out using the total [H^+] scale.

2.2.2 Procedures

A clear polystyrene microplate with optical glass bottom (Whatman) was used for measurements of Mn(II). Samples (200 μL) with different Mn(II) concentrations (pH 4 – 8) were transferred into each microplate well (maximum capacity 370 μL), and then 50 μL of 0.24 mmol/L Cd-TSPP solution was added. The mixture was allowed to stand for 15 min at room temperature and the absorbances of each well at 469 nm and at 490 nm (reference) were then measured. The absorbance difference ($\Delta A_{469-490} = A_{469}-A_{490}$) and the second derivative at 469 nm (described below) were used to construct calibrations and perform measurements. For the studies of pH effect and foreign ion interferences, 0.32 M of hydroxylamine hydrochloride in each well

was used to ensure that the oxidation state of redox metal ions was stable and also consistent with that under anoxic conditions (the latter important for possible in situ applications).

Pore water samples used for this precision and accuracy studies were obtained from surface marine sediments (0 – 1 cm) that were collected in July 2010 from Flax Pond, Great Peconic Bay and West Meadow Beach, Long Island, NY. Porewater was separated by centrifugation of sediment. These porewater samples were stirred, oxygenated and filtered through 0.2 µm pore polysulfone filters and spiked with a specific amount of Mn(II) standard prior to the determination.

Marine sediment samples used for Mn(II) determinations were obtained from Great Peconic Bay in July 2010 and Long Island Sound in Nov. 2007 and stored at 15°C. Porewater samples were separated by centrifugation of sediment, filtered through 0.2 µm pore polysulfone filters and acidified to pH 2 with HCl (trace metal grade) before storage. Sample pH was adjusted to 4 using NaOH solution immediately before analysis. Subsamples (200 µL) diluted in distilled water (dilution factor: 1.5) were used to ensure absorbance in the 0-1 range and a final total volume of 250 µL per well after adding 50 µL of indicator.

2.2.3 Second derivative determination

Application of the second derivative approach in spectrophotometric determinations of Mn (II) using Cd-TSPP was tested. The general Gaussian curve (eq. 13) was centered on the manganese metalloporphyrin peak (469 nm) in the absorption spectra and optimally fit using Least Squares, squaring the distance between data points and curves to estimate errors in the

curve fitting (eq. 14). The second derivative of the Gaussian model (eq.15) was evaluated at 469 nm for each Mn(II) concentration to obtain a calibration curve.

$$A = A_0 e^{-\frac{d(x-x_0)^2}{w^2}} + q \qquad \text{(eq.13)}$$

$$err = \sum_i^n d_i^2 = \sum_i (y_i - f(x_i))^2 \qquad \text{(eq.14)}$$

$$\frac{\partial^2 A}{\partial (x-x_0)^2_{x=469}} = \left[\frac{2dA_0}{w^2} - \left(\frac{2d(x-x_0)^2}{w^2} - 1\right) e^{\frac{-d(x-x_0)^2}{w^2}} \right]_{x=469} = \frac{2d\,A_0}{w^2} + 1 \qquad \text{(eq.15)}$$

where

A_o : maximum band height at wavelength x_o (469nm).

d : constant equal to -4Ln(2).

w : bandwidth at half maximum band height.

A : absorbance at wavelength x.

q : constant representing the baseline.

f(x) : fitted model.

2.2.4 Effect of temperature

The temperature dependence of the analyte-indicator reaction was studied in the range of 298.15 to 318.15 °K using both the temperature control incorporated in the POLARstar system

and the kinetic operational mode. The changes in absorbance of the reaction system at 469 nm and 490 nm were measured with a temporal resolution of 1 min., and reaction rates were estimated using the slope of the initial linear segment (~ first 7 min.) of reaction progression with time to validate the use of an Arrhenius model (equation 16) of temperature dependence for this reaction.

$$\ln(k) = \ln(B) - \left(\frac{E_a}{R}\right)\left(\frac{1}{T}\right) \qquad \text{(eq. 16)}$$

where

k : reaction rate (mol/sec).

B : pre-exponential factor.

Ea : activation energy (J).

R : gas constant (8.314472 J $K^{-1}mol^{-1}$).

T : absolute temperature (Kelvin).

2.3 Results and Discussion

2.3.1 Absorption spectra

The typical absorption spectrum of metalloporphyrins consists of a strong absorption band at about 400 nm (the Soret band or B band) and several weaker absorption bands located at 500 – 650 nm (the Q band) (Ishii et al., 1978; 1982a; Ishii & Kohata, 1987; Gharib et al., 2009). In agreement with this typical porphyrin characteristic, metallo-TSPP complexes also show the Soret and Q bands. As shown in Figure 2.2 A, the Soret band of TSPP complexes with cations

such as Pb(II), Cu(II), Fe(II), Zn(II) and Cd (II) are centered at wavelengths shorter than 430 nm, while Mn-TSPP has a Soret band centered at 469 nm, well separated from the Soret peaks of the other metalloporphyrins by the absorption peak of Cd-TSPP at 433 nm. This feature is highly useful for manganese determination because the reaction of Cd-TSPP with possible metal interferents will decrease the Cd-TSPP peak closest to the Mn signal rather than increase overlap.

In the present application, the Cd(II) in the indicator Cd-TSPP is quickly replaced by Mn(II), forming Mn-TSPP with maximum absorbance at 469 nm (Figure 2.2 A). The oxidation state of Mn in the Mn-TSPP complex after reaction was not determined in this work; however, no differences were found between absorbance behavior in the presence or absence of NH_2OH (range 0.1 – 0.32 M) implying a Mn(II) complex . The absorbance of Mn-TSPP at 490 nm is used as a reference to counter any baseline fluctuations, and the absorbance difference A469 – A490 is used to quantify Mn(II). In order to further improve the method selectivity and sensitivity, the second derivative spectra of Mn-TSPP at 469 nm is also used and compared with single absorbance (A469-A490) detection method.

The Q band Mn-TSPP complex peak was not used due to its poor sensitivity and significant overlap with peaks from other metal ions (Figure 2.2 B). Similarly, the absorbance in the Cd-TSPP peak at 433 nm in the Soret band, which decreases in proportion to the quantity of Mn(II) present, was not used.

2.3.2 Cd-TSPP concentration optimization

To optimize its concentration for Mn(II) determination, the indicator Cd-TSPP concentrations in the range of 19.2 to 144 μM prepared in artificial sea water (35‰, pH 8) were tested. The results summarized in Figure 2.3 indicate that the absorbance of the Cd-TSPP Soret band extending to 469 nm increased exponentially as concentration increased, and that the blank adsorption of Cd-TSPP at 469 nm potentially overlaps with any Mn-TSPP absorption band. Because the optical signal in Figure 2.3 is corrected by subtraction of a reference absorbance at 490 nm, the exponential rise of absorbance at 469 nm implies that the baseline distortion is directly related to the Cd-TSPP concentration increase (Figure 2.3 inset) and is not affected by baseline shifts. Selection of the indicator's optimal concentration must therefore consider and balance many aspects of the method such as dynamic range, sensitivity, detection limit and instrumental error related to the absorbance range. In the present case, a concentration of 48 μM Cd-TSPP was chosen because at this Cd-TSPP concentration, the proposed method can cover the normal range of manganese concentrations reported for marine pore waters (based on a 1:1 stoichiometry of reaction), with a low baseline disturbance at the Mn-TSPP absorption peak 469 nm (0.04 unit of absorbance over the reference at 490 nm, Figure 2.3 inset panel).

2.3.3 Salinity, temperature, and pH effects

The effect of salinity on the reaction of the Cd-TSPP complex with the analyte Mn(II) was tested. No difference was observed at a fixed Mn(II) of 16 μM when the salinity was varied from 22 to 44‰. When the reaction time was fixed at 15 min, the variation in the absorbance signal

(ΔA469-490) was 1.85% (RSD) for measuring Mn(II) in salinity 22, 35 and 44‰ solutions (Figure 2.4).

The effect of reaction temperature on the Mn(II) determination was evaluated by measuring the corrected absorbance $\Delta A_{469\text{-}490}$ of 1.0 µM Mn(II) solutions after reacting for 15 min at different temperatures. The results show that the Mn-TSPP absorbance linearly increases when temperature increases from 10 to 45°C (other temperatures were not tested) (Figure 2.5A). Temperature affects the reaction and thus Mn(II) concentration. A second temperature experiment also showed a linear relationship (R^2=0.998, $p<0.001$) between the natural logarithm of reaction rate (k) against the reciprocal of temperature in the range of 295.15° to 318.15° K (Figure 2.5 B), demonstrating that an Arrhenius relationship (eq. 16) describes the temperature dependence of the transmetallation reaction between Cd-TSPP and Mn(II). The activation energy for this reaction calculated from the slope of the model fit is 22.12 kJ mol^{-1}. This temperature dependence could be used experimentally to reduce the time of reaction by using a higher reaction temperature, and also indicates that for highest accuracy all samples should be maintained at a similar temperature during analysis. Practically, however, temperature variation during analysis will have minor impact. For example, the results in Figure 2.5 A show that the absorbance change is <5 % when reaction temperature fluctuates in the range of ±2 °C during the course of an analysis at 22 °C. In this work, all the Mn(II) kinetic reaction and endpoint measurements were performed in the plate reader with temperature controlled at 25±0.1 °C . Standards were also included in all plates, providing additional checks on calibration.

The effect of pH on Mn(II) determination using Cd-TSPP was assessed by comparing the absorbance signals obtained from three calibration curves at pH 4, 6, and 8 in seawater solutions, respectively. Hydroxylamine hydrochloride (0.32 M final concentration) was added into each

well in order to maintain the Mn(II) oxidation state at high pH values (for example pH 8) and to prevent any precipitation of Fe(III) which might scavenge Mn in natural samples. As noted previously, no interference from 0.32 M hydroxylamine hydrochloride was observed. A linear relationship between these three curves (R^2=0.99; n=4 for each Mn(II) concentration) with a slope of 1.171, indicates that the absorbance signals after 15 min reaction are not impacted by pH in the range of 4 to 8 (Figure 2.6). The reaction does not proceed at pH 2, and in this work the pH values of acidified samples were adjusted to 4 using NaOH just before analysis. The addition of 50 µL of indicator reagent to a 200 µL pH 4 sample does not affect pH. Although the optimal pH range is wide and encompasses most values commonly observed in natural samples, addition of buffer (e.g., tris or phosphate buffer, pH ~5) to plate wells can be easily incorporated as a regular step in a standardized procedure when sample pH variations below or above 4 – 8 may occur.

2.3.4 Reaction time and operational stability

At room temperature (22 °C), absorbance of the reaction solution at 469 nm increased with time, reaching a maximum value after reacting for 15 min at optimal conditions (data not shown). The maximum signal was stable for 4 hours in the dark at room temperature. A 15 min reaction time was adopted for measurements reported in the present study.

2.3.5 Calibration graph

Two calibration graphs were constructed based on different treatments of the data (Figure 2.7). The first approach is a calibration graph of the baseline-corrected-absorbance at 469 nm ($\Delta A_{469-490}$) versus Mn(II) concentration in 200 µL of artificial seawater (35‰, pH 8). The $\Delta A_{469-490}$ for Mn-TSPP shows good linearity with Mn(II) concentration in the range of 0 – 37.5 µM (Figure 2.7 A, R^2=0.997, n=4 for each concentration) with a detection limit of 0.4 µM Mn(II) (3σ) for a 200 µL sample volume. Higher concentrations of Mn(II) were not tested because absorbance of the highest concentration in our calibration curve (37.5 µM in microplate well) reached 1.76. Even though linearity is maintained across the concentration range, the high absorbance number (> 1) may result in increased measurement uncertainty. The range of Mn mass per plate well with this particular method modification is therefore 0.08 – 7.5 nmol, but sample size can be further manipulated to extend the concentration range (e.g., decrease sample size for high Mn concentration solutions and dilute the volume in the well to total 200 µL + 50 µL Cd-TSPP).

A second calibration curve was made using the second derivative of absorbance at 469 nm against Mn(II) concentration (Figure 2.7B). The Gaussian curve was fitted as described previously to the Mn-TSPP peak at 469 nm considering the spectra in the 469-500 nm range, with an error in the range of 1.9×10^{-4} to 1.3×10^{-2} optical density unit (equation 13and 14, Table 2.1). The second derivative at 469 nm (equation 15) shows an excellent linear relationship (R^2 = 0.999, $p<0.001$) with Mn(II) in the concentration range of 0 - 37.5 µM in the solution, with a detection limit of 0.3 µM (3σ). For the second derivative calculation, a reference absorbance correction at 490 nm is not necessary because the correction is implicit to the Gaussian fit, and

the constant representing the baseline of the spectrum in this model is removed during mathematical differentiation. Because the second derivative method can significantly improve method selectivity, and eliminate or decrease any possibility of error from spectrum distortions, its calibration graph shows a better linearity than the direct use of $\Delta A_{469-490}$ (compare Figure 2.7A and B). In addition, the second derivative method has the advantages of higher sensitivity, precision and selectivity compared with the single absorbance method ($\Delta A_{469-490}$).

2.3.6 Interferences

Interferences from various foreign ions on Mn(II) determination were studied and results summarized in Table 2.2. An ion was considered not to interfere if the relative error it caused was less than 5%. Because the Mn-TSPP Soret band absorbance does not overlap with those of other metal-TSPP complexes, the potential interference from foreign ions may come from the competitive consumption of the amount of indicator Cd-TSPP with analyte Mn(II). If the indicator Cd-TSPP is in excess, the interference from foreign cations can be depressed. The results in Table 2.2 indicate that for determination of 10 μM Mn(II), 1 μM of Zn(II), Cu(II), Cr(III) and Co(II) may interfere when the single absorbance (ΔA469-490) method is used. However, the concentration of these foreign cations in natural pore water sample is likely much lower than 1 μM (e.g., Westerlund et al. 1986; Shaw et al., 1990; Zhang et al., 1995). No interference was observed if the second derivative method was used to measure Mn(II) at the same relative concentrations, and the results in Table 2.2 clearly show that the selectivity is significantly improved by use of the second derivative method. One simple analytical option to

check for interferences, for any significant competition for Cd-TSPP reagent, and to ensure that Mn(II) is in an optimal range for analysis is to utilize two or more sample sizes when loading a well plate and check for equivalent or discrepant results (for example: 50 µL sample diluted to 200 µL; 100 µL sample diluted to 200 µL; 200 µL sample).

2.3.7 Accuracy and precision

Accuracies of the second derivative and single absorbance methods were evaluated by testing the recoveries of standard additions of Mn(II) in natural porewater matrices, including naturally present dissolved organic matter (DOM). Porewater samples 1, 2 and 3 were obtained from surface marine sediments (0 – 1 cm) that were collected in July 2010 from Flax Pond, Great Peconic Bay and West Meadow Beach, Long Island, NY, respectively. These porewater samples were stirred and oxygenated to precipitate any initial Fe(II) and Mn(II) present, filtered (0.2 µm) and spiked with Mn(II) standard prior to analysis. The recovered Mn(II) concentration in each porewater sample was measured four times and the results are listed in Table 2.3. The recoveries of standard addition Mn(II) in three different oxidized real porewater samples are 99.9 – 100.4% and 100.9 – 102% for the second derivative and single absorbance methods, respectively. The good agreement of the added and recovered amount of Mn(II) in the natural samples confirmed the method's accuracy, and the lack of interference from foreign ions or DOM under the analytical conditions. The proposed methods were compared with a traditional formaldoxime method. With this latter we obtained recoveries of 97.9 – 121.3% Mn(II) (Goto et al., 1962). The results in Table 2.3 show that the recovery of Mn(II) by the proposed method can be superior to that of formaldoxime. A further comparison of the proposed method with atomic

absorption spectroscopy (AAS) was also performed for the determination of 0.016 – 36.7 μM Mn(II) in artificial seawater samples. The results in Figure 2.8 showed excellent agreement between these methods. The correlation coefficients of AAS with both direct measurement ($\Delta A_{469-490}$) and 2nd derivative methods are 0.99, further confirming the analytical accuracy of the proposed methods (Figure 2.8 A and 2.8 B respectively).

Precisions of the proposed Mn(Cd)-TSPP methods were evaluated by calculating standard deviation (SD) and relative standard deviation (RSD) (n=4). Results in Table 2.3 show that RSDs are in the range of 1.31 – 4.05% and 1.28 – 4.18% for the second derivative and single absorbance method, respectively. Other advantages of the Mn(Cd)-TSPP methods include simplicity and speed.

2.3.8 Application

The proposed method has a suitable dynamic range and detection limit for application to the determination of Mn(II) in sediment porewater samples. Dilution may be required to minimize error from high absorbance. By using a 96-well microplate and a plate reader, large numbers of samples can be measured quickly. For example: one measurement set may evaluate about 90 independent samples, depending on the number of included blanks and standards. In the present case, two natural porewater samples were analyzed as examples of practical application. Sediment was obtained from Great Peconic Bay in July 2010 and Long Island Sound in Nov. 2007 and stored at 15 °C. Comparative analytical results between methods are listed in Table 2.4. No buffer was used during our measurements due to the wide working pH range.

However, a buffer (e.g., Tris-HCl) with a pH value 4 to 8 can be used depending on analytical requirements.

2.4 Conclusion

We have developed a quick spectrophotometric method for the determination of dissolved Mn(II) in porewater without interference from matrix foreign ions and salinity under typical circumstances. Analytical results are consistent with alternative methods such as formaldoxime or atomic absorption. The second derivative technique used to derive correlations between Mn(II) and spectral response significantly improved the selectivity, precision and accuracy compared with the traditional formaldoxime method. Combined with 96 or 384-well microplate and multifunction plate readers, the proposed method can readily measure hundreds of samples within a half hour. This method has been successfully applied to the determination of Mn(II) in natural pore water samples.

References

Aller, R.C., 1994. The sedimentary Mn cycle in Long Island Sound: Its role as intermediate oxidant and the influence of bioturbation, O2, and Corg flux on diagenetic reaction balances. Journal of Marine Research, 52: 259-295.

Almeda, S., Gandolfi, H.E., Arce, L. and Valcarcel, M., 2009. Potential of porphyrins as chromogenic reagents for determining metals in capillary electrophoresis. Journal of Chromatography A, 1216(34): 6256-6258.

Biesaga, M., Pyrzynska, K. and Trojanowicz, M., 2000. Porphyrins in analytical chemistry. A review. Talanta, 51(2): 209-224.

Burdige, D.J., Dhakar, S.P. and Nealson, K.H., 1992. Effects of Manganese Oxide Mineralogy on Microbial and Chemical Manganese Reduction. Geomicrobiology Journal, 10(1): 27-48.

Canfield, D.E., Thamdrup, B. and Hansen, J.W., 1993. The Anaerobic Degradation of Organic-Matter in Danish Coastal Sediments - Iron Reduction, Manganese Reduction, and Sulfate Reduction. Geochimica Et Cosmochimica Acta, 57(16): 3867-3883.

Chiswell, B., Rauchle, G. and Pascoe, M., 1990. Spectrophotometric Methods for the Determination of Manganese. Talanta, 37(2): 237-259.

Gharib, F., Soleimani, F., Farajtabar, A. and Aghaei, H., 2009. Complexation of 5,10,15,20-Tetrakis(4-sulfonatophenyl)porphyrin with the Cadmium(II) Ion at Different Ionic Strengths. Journal of Chemical and Engineering Data, 54(7): 2060-2066.

Goto, K., Komatsu, T. and Furukawa, T., 1962. Rapid Colorimetric Determination of Manganese in Waters Containing Iron - a Modification of Formaldoxime Method. Analytica Chimica Acta, 27(4): 331-&.

Han, Y., Y. Li, W. Si, D. Wei, Z. Yao, X. Zheng, B. Du, And Q. Wei (2011), Simultaneous Determination Of Cu2+, Zn2+, Cd2+, Hg2+ And Pb2+ By Using Second-Derivative Spectrophotometry Method, Spectrochimica Acta Part A: Molecular And Biomolecular Spectroscopy, 79(5), 1546-1551, Doi:Http://Dx.Doi.Org/10.1016/J.Saa.2011.04.086.

Hulth, S., Aller, R.C. and Gilbert, F., 1999. Coupled anoxic nitrification manganese reduction in marine sediments. Geochimica Et Cosmochimica Acta, 63(1): 49-66.

Inamo, M. et al., 1997. Equilibria, kinetics and mechanism of complexation of 5,10,15,20-tetrakis(4-sulfonatophenyl)porphyrin and its N-methylated derivative with cadmium(II) and zinc(II) ions in aqueous solution at various temperatures and pressures. Effects of metal ion size and porphyrin ring deformation on metal ion incorporation. Inorganica Chimica Acta, 256(1): 77-85.

Ishii, H., Koh, H. and Mizoguchi, T., 1978. Spectrophotometric Determination of Ultramicro Amounts of Copper with Alpha,Beta,Gamma,Delta-Tetraphenylporphine in Presence of a Surfactant. Analytica Chimica Acta, 101(2): 423-427.

Ishii, H., Koh, H. and Satoh, K., 1982a. Spectrophotometric Determination of Manganese Utilizing Metal-Ion Substitution in the Cadmium-Alpha,Beta,-Gamma,Delta-Tetrakis(4-Carboxyphenyl)Porphine Complex. Analytica Chimica Acta, 136(Apr): 347-352.

Ishii, H. and Kohata, K., 1987. Spectrophotometric and Analog Derivative Spectrophotometric Determination of Trace Amounts of Iron Using Sulfonated 5-(3,4-Dihydroxyphenyl)-10,15,20-Triphenylporphine. Analyst, 112(8): 1121-1126.

Ishii, H., Satoh, K., Satoh, Y. and Koh, H., 1982b. Spectrophotometric and Analog Derivative Spectrophotometric Determination of Ultramicro Amounts of Cadmium with Cationic Porphyrins. Talanta, 29(7): 545-550.

Kilian, K. and Pyrzynska, K., 2003. Spectrophotometric study of Cd(II), Pb(II), Hg(II) and Zn(II) complexes with 5,10,15,20-tetrakis(4-carboxylphenyl)porphyrin. Talanta, 60(4): 669-678.

Luther, G.W., Sundby, B., Lewis, B.L., Brendel, P.J. and Silverberg, N., 1997. Interactions of manganese with the nitrogen cycle: Alternative pathways to dinitrogen. Geochimica Et Cosmochimica Acta, 61(19): 4043-4052.

Ma, S. et al., 2008. Solid-state Au/Hg microelectrode for the investigation of Fe and Mn cycling in a freshwater wetland: Implications for methane production. Electroanalysis, 20(3): 233-239.

Okutani, T., Sasakura, M., Sakuragawa, A. and Takai, N., 1994. High-Performance Liquid-Chromatography of Metal Alpha,Beta,Gamma,Delta-Tetrakis(4-Carboxyphenyl)Porphine Complexes Following Preconcentration by Solvent-Extraction with Tributyl-Phosphate. Bunseki Kagaku, 43(10): 751-755.

Porta, V., Abollino, O., Mentasti, E. and Sarzanini, C., 1991. Determination of Ultra-Trace Levels of Metal-Ions in Sea-Water with Online Preconcentration and Electrothermal Atomic-Absorption Spectrometry. Journal of Analytical Atomic Spectrometry, 6(2): 119-122.

Post, J. E. (1999), Manganese oxide minerals: Crystal structures and economic and environmental significance, Proceedings of the National Academy of Sciences of the United States of America, 96(7), 3447-3454, doi:10.1073/pnas.96.7.3447.

Shamim, A. and Hambright, P., 1980. Exchange-Reactions of Transition-Metal Ions and Labile Cadmium Porphyrins. Journal of Inorganic & Nuclear Chemistry, 42(11): 1645-1647.

Shaw, T.J., Gieskes, J.M. and Jahnke, R.A., 1990. Early Diagenesis in Differing Depositional-Environments - the Response of Transition-Metals in Pore Water. Geochimica Et Cosmochimica Acta, 54(5): 1233-1246.

Sundby, B., Anderson, L. G., Hall, P. O., Iverfeldt, Å., Van Der Loeff, M. M. & Westerlund, S.F., 1986.. The effect of oxygen on release and uptake of cobalt, manganese, iron and phosphate at the sediment-water interface. Geochimica et Cosmochimica Acta, 50: 1281-1288.

Tabata, M., 1987. Kinetic Method for the Determination of Nanogram Amounts of Lead(Ii) Using Its Catalytic Effect on the Reaction of Manganese(II) with 5,10,15,20-Tetrakis(4-Sulphonatophenyl)Porphine. Analyst, 112(2): 141-144.

Takamatsu, T., Kawashima, M. and Koyama, M., 1985. The Role of Mn-2+-Rich Hydrous Manganese Oxide in the Accumulation of Arsenic in Lake-Sediments. Water Research, 19(8): 1029-1032.

Tanaka, M., 1983. Kinetics of Metalloporphyrin Formation with Particular Reference to the Metal-Ion Assisted Mechanism. Pure and Applied Chemistry, 55(1): 151-158.

Thamdrup, B., 2000. Bacterial manganese and iron reduction in aquatic sediments. Advances in Microbial Ecology, Vol 16, 16: 41-84.

Weiss, S., John, G.T., Klimant, I. and Heinzle, E., 2002. Modeling of mixing in 96-well microplates observed with fluorescence indicators. Biotechnology Progress, 18(4): 821-830.

Westerlund, S. F., Anderson, L. G., Hall, P. O., Iverfeldt, Å., Van Der Loeff, M. M. & Sundby, B.,1986. Benthic fluxes of cadmium, copper, nickel, zinc and lead in the coastal environment. Geochimica et Cosmochimica Acta, 50: 1289-1296

Xu, X.J., Zhang, H.S., Zhang, C.Y. and Cheng, J.K., 1991. Separation and Determination of Copper, Zinc, Palladium, Iron, and Manganese with Meso-Tetrakis(3-Bromo-4-Sulfophenyl)Porphine and Reversed-Phase Ion-Pair Liquid-Chromatography. Analytical Chemistry, 63(21): 2529-2532.

Zhang, H., Davison, W., Miller, S. and Tych, W., 1995. In-Situ High-Resolution Measurements of Fluxes of Ni, Cu, Fe, and Mn and Concentrations of Zn and Cd in Porewaters by Dgt. Geochimica Et Cosmochimica Acta, 59(20): 4181-4192.

Chapter 3:

A new planar optode for measuring 2D manganese distribution in marine sediments

Abstract

Manganese plays an important role in carbon, nitrogen, and sulfur cycling in marine environments. In this environment, the diverse set of chemical, physical, and biological components of its elemental cycling generate highly dynamic and potentially complicated 3-dimensional distribution patterns of the different species, turning the chemical characterization of this element into a major analytical challenge. For these reasons, in this chapter I explore alternative designs for a planar optode capable of measuring two-dimensional distributions of dissolved manganese (Mn II) in marine pore waters. Such multi-dimensional measurements may be used to further elucidate Mn cycling and associated biogeochemical processes in heterogeneous bioturbated marine deposits. The main concerns for designing this chemical sensor were to ensure measurements with minimal impact on the natural sedimentary structures of samples and with an appropriate dynamic detection range for typical environmental applications.

The planar optode sensing schemes explored in this work involved both chemical and numerical aspects. The reaction of Mn(II) with 4,4‘,4“,4“‘-(porphine-5,10,15, 20-tetrayl) tetrakis (benzenesulfonic acid) cadmium complex (Cd-TSSP), or a derivative of this compound, was used as the primary basis for optical sensing. The indicator was first characterized in free solution (Chapter 2), and then entrapped in D4 hydrogel or a blocked version (with inhibited functional group reactivity) of the same polymer, and its immobilized behavior evaluated. The numerical aspects in the present sensing schemes involved colorspace transformation and noise removal algorithms for improving conversion of electronic signals (e.g. digitized images) into chemical information.

After optimizing different possible sensing schemes, I successfully functionalized Cd-TSSP and immobilized it in a blocked version of D4 hydrogel. This sensing scheme showed suitable dynamic range, and tolerance to both interferences and changes in salinity for the acquisition of 2-D measurements of Mn(II) in marine pore-waters. The sensor membrane can depict the natural heterogeneity of dissolved Mn in bioperturbed marine sediments with minimal impact on natural sedimentary structures during its deployment. This sensor is envisioned as a complement to traditional 1-D methods for determining Mn(II), allowing us to increase our knowledge of biogeochemical cycling in in marine sedimentary deposits.

3.1 Introduction

As mentioned in previous chapters, manganese plays a key role in marine biogeochemical cycles. It is involved in numerous inorganic and organic reactions, where the transition between its different oxidation states in the water column and sedimentary deposits reflect interactions between both inorganic and biologically mediated reactions, as well as physical processes, including changes in phase and spatial redistribution for the different species. Additionally, macrofaunal activity in marine deposits has a major impact on sedimentary structures, generating and ventilating intricate burrowing systems (e.g. Figure 3.1). This highly dynamic cycle is one of the main challenges that analytical techniques used for quantifying dissolved and solid phases of manganese in marine pore water and sediments must overcome.

A wide spectrum of analytical techniques has been used for quantifying manganese species in marine environments, including X-ray fluorescence, atomic absorption spectrometry, ICP-MS, electroanalytical methods and spectrophotometry, with different dynamic ranges, accuracy levels, susceptibility to interferences or equipment costs, but all have the common restriction of representing intrusive one-dimensional measurements. This analytical limitation is particularly relevant in sedimentary environments where perturbation by macrobenthic animals substantially modify both reactive particle and solute distributions, as described by Aller (1982), and visually exposed by using two-dimensional (2-D) pH, dissolved ferrous iron and O_2 sensors and probes (Glud *et al*., 1996, 1999, 2001; Wenzhöfer and Glud, 2004; Precht *et al*., 2004; Hakonen et al., 2010; Zhu *et al*., 2006a, 2006b, 2012).

A diverse group of organisms that have manganese oxidizing or reducing capabilities, including bacteria and their spores (Johnston et al., 1988; Myers and Nealson, 1988; Bratina et

al., 1998; Francis et al., 2001; Francis et al., 2002; Villalobos et al., 2005; Miyata et al., 2007), fungi (Inferred from the presence of manganese peroxidase, Bonugli-Santos et al., 2010) and microalgae (Marshall, 1979), have been isolated from natural marine environments. The reported heterogeneous distribution of these organisms in sediments suggests that vertical manganese concentration profiles obtained using conventional techniques are far from representing the natural heterogeneity of perturbed marine coastal sediments, and far from showing how this deviation would impact our conceptual and quantitative modeling attempts.

Advances in 2-D measurements of manganese solid phases in sediment cores have been made using X-ray fluorescence (e.g. Jansen et al., 1998). However, problems related to artifacts from mass-balance and flux calculations used to convert intensities into element concentrations, and from element interactions, specimen inhomogeneity, variable water content, and irregular response to sediment surface irregularities reduces the value of this useful tool as a quantitative method (Croudace *et al*., 2006; Richter *et al*., 2006; Weltje *et al*., 2008).

Two dimensional distributions of metal concentrations in porewater have been measured using the diffusive equilibrium in thin films technique (DGT), where a hydrogel-based diffusive layer interacts with a Chelex resin to accumulate the analytes, which are measured using conventional techniques such as Proton-induced X-ray emission (PIXE) or laser ablation ICP-MS once the multilayered film is removed from sediments (Davison et al., 1994; Fones et al., 2002; Motelica-Hein et al., 2003). However, problems may arise during quantification of dissolved manganese in marine sedimentary environments using this technique because, among the transition metals, manganese has the weakest binding with the resin, and even if manganese binding was slightly more strongly than Ca^{2+} and Mg^{2+}, a competitive cation binding with Chelex has been reported with these cations, which are highly abundant in marine porewaters

(Tankéré-Muller et al., 2012); thus, 2-D spatial resolution for this measurements is highly dependent on the ”slicing” process.

As introduced in Chapter 1, the use of optical sensors represents an alternative for measuring 2-D distributional patterns of chemical species in marine deposits. Selecting supporting materials and indicator-immobilization methods are critical steps for the development of 2-D chemical sensors since both modulate the performance of the optode in terms of its optical response, dynamic range, quenching constants or acid dissociation constants, as well as diffusion of the target analyte within the polymer matrix.

Several methods of immobilization have been reported. They can be classified in three main categories: physical, electrostatic and covalent immobilization. The first refers to the physical entrapment of indicators in a polymer matrix, where the polymer pore size and/or indicator lipophilicity prevent leaking of indicators out of the matrix. Another type of physical immobilization is based on adsorption of the indicator just on the surface of the supporting material or its inclusion into the matrix by attachment onto particles. In electrostatic immobilization methods the indicator is retained by its Coulomb interactions with an oppositely charged supporting material, while in covalent immobilization methods, it is chemically bonded, either directly or through a molecular pendant (Oehme et al., 1998).

A wide variety of supporting matrices have been used for ion sensors, including glass, hydrophobic and hydrophilic polymer materials. The selection criteria must be related to the optical scheme, deployment environments, and the analyte's physical and chemical properties. Glass has been widely used as a supporting material because of its mechanical stability and optical properties (Oehme and Wolfbeis, 1997). However, its brittleness could be an undesirable

characteristic for deployment in marine sediments, and vertical diffusion would be a disadvantage for 2-D sensor development.

Hydrophobic polymer supports have been widely used in sensor fabrications. Unlike hydrophilic polymer supports, solutions containing the analyte do not reach the indicator; therefore, an ion exchange or coextraction mechanism is required to achieve measurements since the indicator is enclosed in the polymeric network. Additionally, not all the hydrophobic supports are suitable for ion measurements. Ion transport across either polystyrene and silicon membranes is too low, or even nonexistent, to allow the analyte to reach the indicator in the hydrophobic phase. Plasticized poly(vinyl chloride) using esters such as trioctyl phosphate or dioctyl phtalate coupled with ion transport mechanisms has been used successfully for ion measurement (e.g. Zhu et al., 2012). However, this approach is not suitable for all the chemical indicators used in ion sensing because some indicators become heterogeneously distributed in the supporting material by aggregate formation (Oehme and Wolfbeis, 1997).

Hydrophilic materials such as polysaccharides, polyacrylates, polyacrylamides, polyimines, polyglycols, polyvinyl alcohol and D4 hydrogels have been extensively used in optical-chemical sensing schemes. Their hydrophilicity is influenced by the efficiency of reactions between molecules (monomers) binding each other to form a polymer network and the mesh size constituted by the binding between polymer chains (the degree of polymerization and cross-linking respectively) (Oehme and Wolfbeis, 1997). In particular, hydrogel polymeric chains bind to each other covalently or physically to form a hydrophilic 3-D array capable of swelling up to 99% of the polymer dry weight and remain almost unreactive to proteins or biological cells (Buenger et al., 2012).

Even when hydrogels contain amide, amine and carboxylic acid groups that can bind with

heavy metal ions and dyes (e.g El-Hag Ali et al., 2003), many potential hydrophilic support materials are unsuitable for ion sensing because protons and hydroxyl anions compete with metal ions for binding with the polymers. Amino groups lose their chelating properties at low pH since they become positively charged by protonation. Carboxylic groups, the preponderant group in terms of metal ion binding, forms dimeric associations involving two hydrogen bonds at low pH, decreasing the swelling and ion binding properties of hydrogels (e.g. Aroua et al., 2007; El-Hag Ali et al., 2003). Extensive work has been done on "blocking" polymers, which decreases or even totally stops reactivity of hydrogel functional groups. Blocking becomes particularly useful to improve preservation during storage or when neutralizing highly reactive and toxic compounds such as isocyanates (e.g. Wicks Jr., 1975; Wicks and Wicks Jr.et al., 1999, 2001). In particular, if mechanical and optical properties of polymeric materials are required as part of immobilizing schemes, minimizing their interaction with active reaction sites of dyes or competition for the analyte, blocked materials become an interesting alternative as supportive material for 2-D ion sensing in marine sedimentary deposits.

Finally, selecting an appropriate chemical indicator for quantifying dissolved manganese in marine environments, as discussed in Chapter 2, is a fundamental step in developing new multidimensional sensors. The optically active complex formed by 5,10,15,20-tetrakis(4-sulfonatophenyl)porphyrin with Cd(II) (Cd-TSSP) has a suitable response for spectrophotometric quantification of dissolved manganese at natural ranges of pH, salinity, temperature and interference levels in marine pore waters (Soto-Neira *et al*., 2011), and is potentially amenable to incorporation into polymer substrates. In this study I explore immobilization of this complex in an unmodified/modified polyurethane hydrogel-based sensing foil, and test its analytical capabilities and spatial resolution to elucidate changes in two-dimensional measurements of

Mn(II) in heterogeneous marine sediments.

3.2 Experimental

The 2-D sensing scheme described in this chapter is a three component system, including a transparent supporting material (S), which holds the immobilizing agent (IA) that will entrap the selected chemical indicator (IN) (Figure 3.2). Six different variations of this general scheme were generated by combining different alternatives for IA and IN (Sch1 to Sch6, summarized in Table 3.1), with all of them using a 15 cm by 15 cm Mylar ® polyester film as supporting material.

A sequential description of the experimental approach includes 1) optimization of IA chemical concentration, oriented to improve the optical properties of the S-IA system before exploring its interaction with the indicator, 2) implementation of proposed sub-schemes, testing their chemical and physical response to the analyte, 3) calibration of the most suitable scheme, selected by its response to the analyte and optical properties, and 4) its deployment in natural samples to compare 2-D determinations against traditional chemical methods for Mn(II) quantification in marine pore waters, and to test the sensing capabilities of the scheme for Mn(II) measurements in marine bioperturbed sediments.

3.2.1 Equipment, reagents and standard solutions

As described in chapter 2, spectrophotometric measurements of manganese in solution were carried out using a BMG Labtech SpectroStar nano microplate and cuvette reader with

UV/VIS absorbance spectra. Settings, standards and sample preparation for quantifying dissolved manganese in solution used a formaldoxime-based method.

2-D spectrophotometric measurements for the sensing foils were performed using a Canon Scan LIDE 25 scanner equipped with a Contact Image Sensor (Canon Inc.) as light source and detector; excitation light was filtered by attaching a filtering foil with a peak of transmittance at 470 nm.

Two sets of Mn(II) working standard solutions with concentrations, salinity and pH required to test the sensor's response under marine conditions were used. The first set was made by using aliquots from 1.0 mM stock solutions of Mn(II) prepared using 8% hydroxylamine hydrochloride solution (Fisher) in artificial sea water (ASW, 35 salinity) and adjusting pH by adding HCl (trace metal grade) or NaOH as required to reach a desired pH value. The total $[H^+]$ scale of pH was used. The second set was prepared using aliquots of a 1000 ppm Mn(II) standard solution (FISHER, SM81-100) diluted in ASW and avoiding the use of hydroxylamine. This set was prepared fresh every time and kept under anoxic conditions during use (e.g. bubbling nitrogen gas into solutions and air-tight spectrophotometric cuvettes).

For sensing foil preparations, the Mylar ® polyester film (0.127 mm thickness) and the ether based polyurethane, D4 (part # 100028), were obtained from Ridout plastics (San Diego, CA) and Hydromed, respectively. 5,10,15,20-tetrakis(4-sulfonatophenyl)porphyrin (TSSP) was from Sigma (88074) and cadmium chloride from MP (152507). The amylene stabilized chloroform and 69% nitric acid used during the desulfonation and aryl nitration reaction were from Sigma (CAS 67-66-3) and J.T. Baker (9601-34). All the remaining reagents were from Sigma.

3.2.2 Spectrophotometric quantification of sensing foil response to Mn(II)

One-dimensional (1D) end point absorbance measurements of sensing foils were carried out using the plate reader in cuvette mode in 1-cm disposable cuvettes. A 1×2cm sensor piece was inserted into the cuvette and oriented both facing the light source for spectrophotometric characterization of the sensing foil, or parallel to it for detecting indicator leaks from the sensor; the reactive side was in contact with the selected solution (Figure 3.3). Two-dimensional measurements were performed by digitalizing the sensor image after the sensor was immersed and retrieved from the testing solution by using the modified scanner described above, fixing the sensors against the white screen.

Settings for the scanning process were controlled by using XSane (GNU licensed software) to obtain the unaltered signal from the optical sensor (RAW) and fixing the Gamma correction to 1 during acquisition of color channels (Red, Green, Blue) that form the data cube (commonly referred as RGB data). General post-processing scripts commonly used in commercial image acquisition devices for aesthetic purposes, such as automatic contrast and brightness adjustments, were disabled to keep the signal integrity. In addition, data interpolation during image storing was avoided by selecting uncompressed file formats (e.g. 8-bits, 16-bits and 32-bits TIFF).

Raw RGB data cubes from digitalized sensing foils were post-processed using Matlab (c) to obtain its translation into different color spaces (standardized RGB and HIS) using the formulation described by Gonzalez and Wood (1992) and Viscarra- Rossel et al. (2006) (equation 17 and 18, respectively), avoiding the use of pre-defined functions of this software to acquire control over the values of constants used during the color space transformations.

$$r = \frac{R}{R+G+B} \; ; g = \frac{G}{R+G+B} \; ; b = \frac{B}{R+G+B} \qquad \text{(eq. 17)}$$

where:

R, G and B: raw red, green and blue channels respectively.

r, g and b: standardized tri-stimuli signal.

$$H = cos^{-1}\left\{\frac{0.5[(R-G)+(R-B)]}{[(R-G)^2+(R-B)(G-B)]^{0.5}}\right\} \qquad \text{(eq. 18)}$$

$$I = \frac{1}{3}\{R+G+B\}$$

$$S = 1 - \frac{3}{(R+G+B)}[\min(R,G,B)]$$

where:

H, I and S: hue, intensity and saturation, respectively.

3.2.3. Sensing foil homogeneity test and electronic noise removal from digital information

Homogeneity tests were carried out on the images obtained during the tests of selected sensing schemes before checking interactions with the analyte in order to quantitatively detect optical irregularities in the produced sensing foils (e.g. by uneven distribution of IN and/or IA, dye micelles formation, drying patterns, etc.). These tests were accomplished using the Quad Tree test, proposed by Finkel and Bentley (1974), using the function *qtdecomp* from Matlab ®,

which iteratively sub-divides square regions of an image and tests whether a particular subregion meets a pre-defined homogeneity criterion. If a sub-region meets the criteria, it is not further subdivided; this results in identification of areas where the criteria are not met as areas with highly sub-divided regions. The homogeneity criteria used for our test was to consider sub-regions as homogeneous when the difference between local maximum and minimum value were lower than 0.1 in standardized images (equivalent to 10% difference between limit values), this test was performed using the I channel from the HIS color space transformation (equation 18).

Noise was removed from digital images by applying the anisotropic diffusion filter proposed by Perona and Malik (1990) (discrete form; equation 19). This filter was applied to the sensing foil images captured after reaction with the analyte since it removes the variability produced by electric noise during the image acquisition without compromising the optical-chemical signal in the sensor.

$$IM_S^{t+1} = IM_S^t + \frac{\lambda}{|\eta_S|}\sum_{p\varepsilon\eta_s} g\left(\nabla\, IM_{S,p}\right)\nabla\, IM_{S,p} \qquad \text{(eq. 19)}$$

Where:

IM_S^t: discretely sampled image.

t: iteration number.

s: position in a discrete, 2-D grid.

λ: diffusion rate (constant).

η_s: spatial neighborhood of pixel s.

$|\eta_s|$: number of neighbors (assigned value:4).

g: edge-stopping function.

3.2.4 Preparation and optimization of immobilizing agents

Two immobilizing agents were tested in combination with different entrapment techniques to generate the six immobilization sub-schemes (Table 3.1). The first immobilizing agent (IA1) was D4, an ether based polyurethane; it was used for Sch1, Sch2 and Sch3. The second was an alcohol blocked D4 (IA2), prepared by using KOH and ethanol as catalyst as described below; it was used for Sch4, Sch5 and Sch6.

The 0.1g/ml D4 Stock solution for IA1 was made by dissolving 15 g of D4 in 150 ml of an 98.3% solution of ethanol-MilliQ water with overnight stirring. Solutions with lower D4 content or ethanol percentage (from 0.025 g/ml to 0.4 g/ml in 97% ethanol) were prepared by diluting with 98.3% ethanol in MilliQ or/and just MilliQ water. Both stock and diluted solutions for IA2 were prepared in the same way described for IA1, but using 97% ethanol in MilliQ water as solvent, and the blocking reaction were carried out for each solution just before use.

The blocking process was aimed to extensively reduce the available -NCO and -OH groups in the immobilizing agent that might react with the analyte or the chemical indicator, as well as to reduce volume changes in the polymeric matrix due to water absorption. The selected method was to use the alcohol contained in the solution used to dissolve D4 as blocking agent, and to use potassium hydroxide in excess as a catalyst (Zengel et al., 1983; Wicks and Wicks Jr., 2001). The blocking reaction was carried out at 353.15° K and closely monitored to check when the CO_2 production stopped (assuming the blocking reaction had ended). Since the blocking reaction would be easily reversed by the remaining hydroxide at high temperatures, the potassium hydroxide residual was neutralized using 6M HCl. The salt produced in the

neutralization was removed by decantation, filtration and rinsing with Milli-Q water after the drying period. Additional tests were made on this material omitting the neutralization.

Optimization of the IA chemical concentration was carried out by preparing several sets of S-IA foils using different concentrations of IA1 and IA2. These foils were produced by evenly spreading 9.9 ml of solutions containing 0.025 g/ml, 0.05 g/ml, 0.1 g/ml, 0.2 g/ml and 0.4 g/ml of IA1 or IA2 on the surface of 15×15 cm Mylar ® polyester films, where the setup and drying time were the same for sensing foils, as described in 3.2.6, but omitting the use of indicator. Additional rinsing cycles with Milli-Q water were required after drying when IA2 was used.

Optical properties of each IA scheme were characterized by digitalizing four images for each S-IA foil, scanning them after the drying period, converting them to HIS color space using eq. 18 and forming 3-D matrices for each channel. The first two dimensions correspond to the height (n) and width (m) of the image, and the third represents the channels (k). The image replicates were combined to form three n by m by 4 matrices, where each of matrix contain a single channel. Calculations of 2-D average and 2-D standard deviation were carried out across the third dimension of these matrices (Figure 3.4). The resulting 2-D datasets from each channel were analyzed by grouping their data in a 1-D dataset and fitting Gaussian curves to them (equation 20). Higher values of Γ, the full width of the Gaussian curve at half maximum peak height (equation 21), implies wider variation during the recognition of the analyzed parameter in the digitalization processes. This variation may be produced by heterogeneous optical properties in the tested foil and/or electrical noise during image acquisition, while lower values for Γ represent narrower, less noisy digitalization processes and more homogeneous optical properties for the sensor under the selected method of acquisition.

$$f(x|\mu,\sigma) = \frac{1}{\sigma\sqrt{2\pi}} e^{-\frac{(x-\mu)^2}{2\sigma^2}} \quad \text{(eq. 20)}$$

where:

μ: mean or expectation;

σ: standard deviation.

$$\Gamma = 2\sqrt{2Ln(2)}\sigma \quad \text{(eq. 21)}$$

where:

Γ: full width of the Gaussian curve at half maximum peak height.

σ: standard deviation from Gaussian fitting.

3.2.5 Chemical indicator stock solution

Stock indicator solutions (IN) for testing different immobilization schemes were prepared by dissolving 36.4 mg of TSSP and 0.05 g of cadmium chloride in 2 ml of NaOH (0.001 M), checking the total consumption of free porphyrin during the metal complex formation reaction over time by spectrophotometry. Ten ml working indicator solutions for schemes Sch2 and Sch4 (IN1) were prepared by diluting 95 μl aliquot of IN to 10 ml using MilliQ water. Ten ml working indicator solutions for Sch3 and Sch5 (IN2) were prepared by diluting 95 μl aliquot of IN to 10 ml using 98% ethanol in MilliQ water. For Sch6, since an amine group binding at least one of the side chains is required for immobilizing a meso-substituted porphyrin using glutaraldehyde, a common desulfonation reaction followed by an aryl nitration reaction, as proposed by Kruper et al. (1988) and modified by Ladomenou et al. (2012), was carried out using amylene-stabilized

chloroform (Sigma, CAS 67-66-3) and 69% nitric acid (J.T. Baker, 9601-34). In contrast to the modified method, the final sulfonation step from the original procedure was retained to recover solubility in water, avoiding alterations in optical properties of the sensing foil by use of organic solvents. Metallation reaction with Cd(II) was carried out after nitration to complete the indicator solution for Sch6 (IN3).

3.2.6 Sensing foil preparation

For Sch1, 95 μl aliquots of IN were directly added to 9.9 ml diluted solution obtained from IA1, containing the D4 concentrations selected during the optimization of IA, to get a final indicator concentration of 0.173 mg/ml in a 97% ethanol-MilliQ water solution in each case. As for all the sensing foil variations used in this study, the resultant solutions were stirred until homogeneous, then evenly spread over S, mounted on a leveled glass surface and covered with a non-hermetically sealed glass tray, allowing the mixture to slowly evaporate in a semi enclosed area, in darkness if required (when indicator is present) and for at least 12 hours. Preparation of sensing foil sets for immobilization schemes Sch2, Sch3, Sch4 and Sch5 have the common initial step of homogeneously spreading 9.9 ml of IA on S, using the concentration selected during its optimization, and prepared from IA1 (Sch2 and Sch3) and from IA2 (Sch4, Sch5 and Sch6) stock solutions. Once the drying period was complete, 10 ml of IN1 was homogeneously spread on the surface of Sch2 and Sch4, while the same volume of IN2 was spread on Sch3 and Sch5. All sets were kept in darkness to avoid photo-oxidation. The remnant indicator solution on surface from Sch2 and Sch4 was removed after 1 hour by pipetting. All sensing foils were rinsed

several times with MilliQ water and allowed to dry at room temperature before measuring both homogeneity of the sensor foils and the amount of indicator immobilized.

Initial steps to prepare sensing foils for Sch6 were the same as for Sch4 and Sch5; however, the surface of Sch6 was treated with a 0.17 M glutaraldehyde solution (prepared at pH8 using 50 mM sodium phosphate) for 20 minutes after the IA2 drying period, Then the reaction was stopped by rinsing the sensing foils with PBS (50 mM sodium phosphate, 0.5 M sodium chloride at pH 7.4). Indicator was added to the foil by homogeneously spreading a 10 ml of IN3 on the dry surface of the immobilizer, and stopping the reaction after 90 minutes by rinsing the foil with PBS again.

3.2.7 Indicator entrapment, reactivity test and sensor foil calibrations

Reactivity tests for each sensing scheme proposed in 3.2.3 were carried out by adding 200 µl drops of Mn(II) standard solutions onto the surface of sensing foils, with concentrations between 0 and 150 µM Mn. This test provided a quick assessment of sensing foil chemical reaction with Mn(II), and it was also a useful technique for checking the proper response of sensing foils before deployment in the field or after an extended storage period.

Calibration curves were performed by immersing 1×1 cm square pieces of selected sensing foils (subtracted before the sensor deployment) in 20 ml glass scintillation vials containing Mn(II) standard solutions made in artificial seawater (s: 35, Section 3.2.1), using one sensor piece per vial, and measuring its optical properties as described in Section 3.2.2. After immersion for 30 min., the sensor foil strips were rinsed several times with Milli-Q water, and then dried for 1 hour in darkness.

Salinity, temperature, pH and response to chemical interference tests were performed using the same conditions and set ups described in Chapter 2 during the characterization of Cd-TSSP as a chemical indicator for Mn(II) in pore waters.

3.2.8 Natural samples

Coastal surface sediment used during incubation experiments for testing sensing foil deployments and sensor response to natural environments were collected from Smithtown Bay, NY, US using a 0.25 m^2 box-corer. Sub-sampling was carried out using transparent acrylic box cores (18 cm by 7.5 cm; height: 22 cm; sediment-water interface at ~12 cm from the bottom), previously fitted with foil place holders (transparent polyester sheets) attached to the internal sides of the box. These blank sheets facilitate insertion of the sensor foil along the lateral face of the core, minimizing the disruption of sedimentary structures during deployment (Figure 3.5). Box-cores were kept in darkness to avoid photo-oxidation or photosynthesis, and immersed (uncapped) in oxygenated bottom water collected in the same area to maintain oxic conditions in overlying waters while the gas tight seal at bottom allows the building up of sub-oxic and anoxic conditions in deeper sediments.

A comparison between 2-D measurements of Mn(II) carried out using selected sensing schemes against traditional 1-D determination methods for this analyte was accomplished using acrylic sheet (24×6.5 cm; thickness: 2 mm, insert Figure 3.6) as the sensor foil holder, attaching the foil to the acrylic along the edges using polytetrafluoroethylene tape (PTFE), keeping the reactive face contacting sediment, and inserting the holder-sensor in the center of the core. Once the pre-defined deployment time ended, three syringe cores were subsampled from areas

adjacent to the sensing foil before its removal. These syringe cores were sub-sampled every 0.5 centimeters for the top 3 cm, and at 1cm intervals for deeper sediments. Pore water extracted from each sub-sample was analyzed for Mn(II) using the formaldoxime method as described in Soto-Neira et al.(2011).

To test the capability of selected sensing schemes to resolve 2-D Mn(II) distributional patterns in bioperturbed sediments, individuals of *Yoldia limatula* (deposit-feeding protobranch clam from the family *Yoldiidae*) and *Nereis* sp. (polychaete worms from the family Nereidae) were released separately into selected boxcores, and after a short period of acclimation (~2 hours), Mn(II) sensing foils were deployed. X-ray images of the boxcores were taken during the deployment of the sensors foils to obtain more accurate information about sensor location, to locate animals, and to visualize the sedimentary structures generated during the burrowing.

All the sensing foils were deployed for 30 minutes in the sediments and rinsed multiple times with Milli-Q water after foil extraction. Mn(II) quantification using sensing foils was accomplished by performing 2-D spectrophotometric measurements as described in Section 3.2.2, converting intensity values from digitalized images into chemical concentrations *via* calibrating foils as proposed in section 3.2.7.

3.3 Results and discussion

3.3.1 Optimization of immobilizing agents

Chemical concentrations of immobilizing agents used in this study were optimized by preparing a set of S-IA foils as described in Section 3.2.4 and analyzing their digitized images (4 replicas per foil) to determine foil optical properties. The primary tests were the Gaussian plots of averaged hue, intensity and saturation channels obtained from processing digital images of S-IA foils containing 0.025 g/ml, 0.05 g/ml, 0.1 g/ml, 0.2 g/ml and 0.4 g/ml of IA1; these were calculated following the scheme illustrated in Figure 3.4. Results are depicted in Figure 3.7. No significant differences were found between foils containing equivalent concentrations of IA1 and IA2; however, this was highly depended on the efficiency of salt removal during the preparation of foils containing IA2.

Gaussian plots for H channels from S-IA1 foils with concentrations above 0.05 g/ml showed narrower distribution patterns, with Γ values of 24.83, 25.27 and 27.11 for 0.1g/ml, 0.2 g/ml and 0.4 g/ml respectively (equation 20), suggesting both more homogeneous IA distributions and higher stability for color detection during digitization processes for these foils (Figure 3.7, H panel). Nevertheless, the Gaussian distributions of I channels showed a consistent increase of their Γ values at higher IA1 concentrations, indicating a higher impact of diffracted light during the digitalization process at higher concentrations (Figure 3.7, I panel). In addition, the same plots for S channels depicted higher variability in this parameter for the two highest IA1 concentrations (Figure 3.7, S panel), supporting the hypothesis of diffracted light affecting the color recognition during digitization of foils containing 0.2 g/ml and 0.4 g/ml of IA1.

Qualitative examination of prepared foils suggested suitable degrees of transparency for all of them, which is a desirable property for deployment of optical sensors in marine sediments. However, S-IA foils containing 0.025 g/ml were susceptible to scratches and IA often peeled during manipulation, eliminating the use of these formulations.

Based on parameters analyzed above, the selected concentration for both IA was 0.1 g/ml. This concentration provides the combination of narrowest H, I and S distributions. While distributions of this parameter for foils containing 0.05 g/ml of IA were very close to those of foils containing the selected concentration, foils containing 0.1 g/ml provide extra mechanical strength, which is directly related to the foil preservation during deployment in marine sediments.

3.3.2 Immobilization and reactivity tests for proposed sensing schemes

Sensing foil prototypes for each of the six immobilization sub-schemes proposed in this study were prepared as detailed in section 3.2.4, using the IA concentration selected in section 3.3.1 (0.1 g/ml). After drying, foils were subject to both homogeneity and indicator entrapment tests, as well as chemical response to Mn(II) in ASW (per section 3.2.7). Figure 3.8 shows a regular unfiltered digitalized image of Sch 6 (A) and the result of its homogeneity test (B). As depicted in this figure, the Quad tree test (threshold: 0.1) did not find major irregularities in this foil, suggesting homogeneous distribution of the indicator, lack of micelles formed during the immobilization, and evenly distribution of immobilizing agent. This was the common result for sensing foils tested in this study; however, occasional issues during the drying step produced low quality sensing foils (e.g Figure 3.8 C and D). Low quality foils were discarded and were

replaced with new foils prepared following the same scheme. Uneven accumulation of indicator around the foil edges sometimes resulted from specific immobilization schemes (e.g. Sch 2, Sch 3 and Sch 6); in these cases the edges were trimmed (e.g., 5 mm boundary removed).

Indicator entrapment test results are summarized in Table 3.2. Spectrophotometric measurements oriented to detect releases of indicator from Sch 3 and Sch 6 during its immersion in ASW (salinity: 35; pH: 7.5) did not show detectable Cd-TSSP residuals in solution, while Sch 1 and Sch 2 showed low amounts of indicator released to the same immersion solution during the test (Figure 3.9). Residual traces of indicator were not detected in the immersion solution for these schemes after adding rinsing cycles with Milli-Q water following the drying period as a final step of its preparation; this suggested that detected residuals in the immersion solution correspond to indicator added in excess. On the other hand, Sch 4 and Sch 5 released extensive amounts of indicator once immersed in the ASW solution, with evident loss of sensing foil coloration as a result. The diminished capacity of IA2 to retain the indicator, in contrast with its unblocked form, was attributed to the lack of coordination centers in the blocked polymer, as a result of the reduced number of ligands available after blocking, which disabled the ability of this material to entrap metalloporphyrins unless an additional functionalized group binds both S and IA (e.g. Sch6). Therefore, Sch4 and Sch5 were rejected as possible immobilization schemes.

Chemical response to Mn(II) was checked for Sch1, Sch2, Sch3 and Sch6 as described in section 3.2.7, and results are summarized in Table 3.3. For Sch1, Sch2 and Sch3, 1-D spectrophotometric characterization of sensing foils confirmed the integrity of the immobilized Cd-TSSP complex, showing the expected absorbance peak at 469 nm (e.g. Figure 3.10); however, reactivity test for these sensing foils found that there was no (Sch1) or low (Sch2 and Sch3) response to Mn(II) after the sensors reacted for hours (Figure 3.11). The lack of response

to the analyte by these schemes could be interpreted as the result of two different processes. The first was the loss in motility of cadmium cation due to coordination with highly reactive groups available in the polyurethane based polymer (e.g. isocyanates); this would stop the transmetallation reaction required for insertion of Mn(II) in the porphyrin central ring. The second was alteration of the physical and chemical properties of the immobilizing agent due to ionic strength, which would slow down or even stop the motility of cadmium cations in the IA. Additional experiments were carried out to test the second hypothesis by including surfactants, or cationic/anionic additives during preparation (e.g. dextrose, cetyltrimethylammoniumbromide, sodium dodecylsulfate, ammonium tetrakis (4-chlorophenyl)borate, carboxymethyl cellulose). But even when some of these alteration resulted in measureable responses to Mn(II) in ASW, the use of additives to enhance cation motility in the immobilizing membrane was discarded because 1) internal diffusion in sensing foils decreased the spatial resolution for 2-D measurements, 2) distribution heterogeneity of additives increased, and 3) preservation issues were exacerbated for schemes containing additives such as dextrose (e.g. Figure 3.12). Even though carboxy methyl cellulose is used as an immobilizing agent in other studies, in the present work it was used as an additive to produce a composite immobilizing layer, resulting in better response to the cations in solution.

1-D spectrophotometric characterizations of chemical reactions between Sch 6 and Mn(II), as well as its response to both cationic interferences and salinity changes were performed by immersing sensor strips of Sch 6 (1×2 cm) in 1cm cuvettes, as described in section 3.2.2 and 3.2.7. Sch 6 displayed a quantifiable irreversible response to Mn(II) in ASW, showing a decrease in absorbance at 469 nm during the first 4 minutes of immersion, followed by a sigmoidal increase of the absorbance, reaching its maximum after 30 minutes of reaction (e.g. Figure 3.13).

The initial decrease in absorbance was interpreted as a result of ASW absorption into the immobilizing agent during the equilibration of Sch 6 with the solution, while the subsequent sigmoidal increase of absorbance corresponds to transmetallation reactions between the chemical indicator and Mn(II). The reaction time of 30 minutes required by Sch6 to reach the plateau in absorbance is double the time required by Cd-TSSP during Mn(II) determinations in solution (e.g. Ishii et al., 1982 and Soto Neira et al., 2011) . Nevertheless, this reduction in reactivity is in agreement with previous studies where aldehydes were used to immobilize porphyrins (White, 2001). It also represents a favorable practical characteristic for using this sensing scheme for marine sediments since this feature would provide a delay in response to Mn(II) and minimize artifacts from cross-contamination during insertion.

Response of Sch 6 formulations to cationic interferences such as the Fe(II) commonly present in porewater, salinity changes (Table 2.2, chapter 2), and pH (6-9) were carried out using 1-D spectrophotometric measurements (section 3.2.2). No quantitative effects were found at realistic representative concentrations. Because the metalloporphyrin central ring was not modified, the response of this indicator was expected to be similar to the one reported for Cd-TSSP in solution (Soto-Neira et al., 2011). A crucial final step in Sch 6 foil fabrication is rinsing the foil several times with Milli-Q water after the drying period in order to avoid any release of residual basic reagent into the contacting medium.

Sch 6 sensing foils shown to be stable for months, before and after its use, when stored at 4°C in dry and dark areas, where the temperature control reduce the chances of increased reaction rates by excessive heat, and reducing the light exposure avoids the photo-oxidation reaction.

3.3.3 Calibration of selected sensing scheme

Calibration curves for Sch 6 were constructed as detailed in section 3.2.7. After reaction, the exposed foil strips were arranged from low to high Mn(II) concentrations for digitization (Figure 3.14 A) and converted to HIS colorspace using equation 19. The I channel was used for calibration purposes (Figure 3.14 B). As shown in Figure 3.14 (C), the vertical averaging of each intensity column in the digitized image is inversely proportional to Mn(II) concentration. By averaging all the intensity values for each foil piece, we found a linear response in the 0 to 150 µM range, with a slope of -12646, and disturbance of 2048.3 and R^2 of 0.985 (Figure 3.15). Linearity was lost for solutions containing Mn(II) concentrations over 150 µM, but since intensity values kept decreasing (e.g. 200 µM, intensity: 0.149), the most likely interpretation of this change in trend was hardware limitations of the modified scanner used for this purposes.

The difference between dynamic ranges for Mn(II) quantification using TSSP in solution and the proposed immobilized method (3µM-47 µM and n.d-150 µM respectively) is explained by both the decreased reactivity of the immobilized indicator (White, 2001), and the difference in sensitivity between light detectors used by each method (spectrophotometer and digital scanner respectively).

The iterative electric noise removal based on the method of Perona and Malik (1990) (section 3.2.3) was used to reduce the standard deviation in measurements. Each iteration produced a new image calculated using equation 19. One hundred iterations were performed with

this method, analyzing the resulting images every 20 cycles. After 60 iterations the slope and disturbance values for calibration curves from the resulting images converged to -12420 and 2014, respectively (Figure 3.16A and 3.16B). While the standard deviation noticeably decreased after just 20 iterations (Figure 3.16 D), the highest R^2 (0.9653) was obtained after 80 iterations (Figure 3.16 C). This asymptotic value is not significantly different from the one obtained without noise removal techniques (0.964), implying that the anisotropic diffusive technique limits its effect to the noise in the images, keeping the chemical signal intact. The limit of detection before applying the anisotropic diffusive technique, calculated as 3σ, was 18.9 μM, and after applying the noise removal technique, was 8 μM (60 iterations). Therefore, 60 iterations was fixed as the optimal number of iterations because it is the lowest value at which slope, disturbance, and standard deviation converge to constants.

3.3.4 Deployment of selected sensing scheme in natural sediments

Sensing foils using Sch 6 were tested during incubations experiments as described in section 3.2.8. 2-D measurements of Mn(II) were carried out with this scheme and compared to a traditional spectrophotometric method. Figure 3.17 (A) depicts 2-D distributions of Mn(II) concentrations of the analyte expected to be undetectable near the oxygenated sediment-water interface, where Mn(II) is oxidized to manganese oxides and precipitates. A pronounced concentration peak of Mn(II) reaching over 100 μM, was found between 6 and 10 cm depth; This distribution, as well as the magnitude of its concentration are typical of Mn(II) profiles classically reported in the literature (see Chapter 1), and represent the use of manganese oxides as electron acceptors during organic matter remineralization. One dimensional profiles

generated by horizontally averaging 2-D measurements closely match 1-D Mn(II) profiles obtained by analyzing Mn(II) concentrations using formaldoxime in pore water from cores adjacent to the sensing foil (Figure 3.17 B). Matching between 2-D and 1-D datasets, even when they are obtained in close proximity, is highly dependent on the structural homogeneity of sedimentary environments where the sensor is deployed, as evidenced by the vertical asymmetrical distribution of Mn(II) below 12 cm depth in Figure 3.17 A. This vertical asymmetry below 12 cm depth can be interpreted as formation of local patches of organic matter remineralization due to the natural heterogeneity of sedimentary deposits.

Figure 3.18 (A) shows a close up X-ray image of a box-core lateral face, where burrows dug by *Nereis* can be seen, while Figure 3.18 (B) depicts distributions of Mn(II) obtained by deploying a Sch 6 sensing foil in the same location where these structures were visualized. The 2-D Mn(II) patterns agree with expected distributions, given that other studies using oxygen planar optodes in bioturbated sedimentary deposits have reported oxygen influx into deeper sediments through burrowing networks (e.g. Glud et al., 1996, 1999, 2001), consistent with oxidation as an explanation for lower Mn(II) concentrations following the track of these structures. However, the effect of mucus production by *Nereis*, and its deposition on the walls of burrowing structures, was not considered. This process could affect the gas and solute exchange between the burrow and surrounding sedimentary areas. A suggested method to evaluate the role of mucus in this processes is to compare organic compound measurements carried on samples from the burrow's water-sediment interface (e.g. aminoacids and/or carbohydrates), used as a proxy of mucus abundance, with planar optode information obtained before the organic sampling, correlating the flux magnitudes of oxygen and/or Mn(II) with the amount of mucus detected in the same area.

Multiple Sch 6 sensor foils were deployed in a box-core containing *Yoldia*, perpendicularly to the lateral face of the tank, as shown by x-ray images obtained after the insertion of sensor plates into sediments (Figure 3.19 A). As shown in Figure 3.19 (B), Mn(II) concentration was low to non-detectable as expected at the oxidized sediment water interface and near surface sediments. These low concentrations reached much deeper in sediments where *Yoldia* was present. X-ray images showed burrowed regions in lighter intensities (lower density, watery) where one of these structures can be recognized going close to the wall of the box-core from sensor foil 1 to foil 5. Sensor foils 1 to 4 provide quantitative and visual evidence of decreased Mn(II) concentrations where the lower density burrowed sediment is evident. Additionally, during multiple incubation experiments, gas-filled hollow spaces (created during introduction of sediment to mesocosms) were found during x-ray imaging. These structures can be seen in Figure 3.19 (A) and (B) (e.g. sensor foil 4, bottom), demonstrating that Sch 6 sensing schemes are capable of resolving highly heterogeneous patterns of Mn(II) concentrations in bioperturbed sediments. However, temporal scale of the measurements must be considered, while the 30 min. deployment is able to elucidate the effect of bioirrigation over the Mn(II) distributional patterns in sediments, this time window would not reach the required temporal resolution for sensing faster bioturbation processes (particle reworking, feeding, etc). Further work on reversible Mn(II) sensors is required for archiving the required temporal resolution for the above mentioned processes.

3.4 Conclusions

During this work, we explored the immobilization and use of Cd-TSSP as an optically active indicator for carrying out 2-D measurements of Mn(II) in marine sedimentary deposits. The six immobilization sub-schemes tested in this study shown different capabilities to both entrap the chemical indicator and/or react with the analyte as a result of using D4 or a blocked version of this hydrogel as immobilizing agent, and Cd-TSSP or a re-functionalized molecule as chemical indicator for Mn(II) in marine sediments. Schemes including unmodified D4 hydrogel as immobilizing agent showed low to no response to Mn(II); however, the inclusion of additives increased response of entrapped indicator to Mn(II). However, these approaches were rejected because internal diffusion in the resulting sensing foils reduced the spatial resolution of 2-D measurements. On the other hand, a blocked version of the hydrogel, used as an alternative immobilizing agent, was unable to entrap Cd-TSSP, and showed profuse release of indicator once immersed in ASW. Re-functionalizing the indicator allowed its immobilization by using an glutaraldehyde as crosslinker to the blocked immobilizing agent. This latter scheme showed a positive irreversible response to Mn(II) in marine conditions, and retained the same tolerance to interferences, pH and salinity as Cd-TSSP in solution. The resulting sensor foil was successfully deployed in natural sediments during incubation experiments, and allowed elucidation of heterogeneous 2-D distributional patterns of Mn(II) in bioperturbed sediments.

References

Aller, R. C. (1982), Carbonate Dissolution In Nearshore Terrigenous Muds - The Role Of Physical And Biological Reworking, Journal Of Geology, 90(1), 79-95.

Aroua, M. K., F. M. Zuki, And N. M. Sulaiman (2007), Removal Of Chromium Ions From Aqueous Solutions By Polymer-Enhanced Ultrafiltration, J. Hazard. Mater., 147(3), 752-758, Doi:10.1016/J.Jhazmat.2007.01.120.

Bonugli-Santos, R. C., L. R. Durrant, M. Da Silva, And L. D. Sette (2010), Production Of Laccase, Manganese Peroxidase And Lignin Peroxidase By Brazilian Marine-Derived Fungi, Enzyme And Microbial Technology, 46(1), 32-37, Doi:10.1016/J.Enzmictec.2009.07.014.

Bratina, B. J., B. S. Stevenson, W. J. Green, And T. M. Schmidt (1998), Manganese Reduction By Microbes From Oxic Regions Of The Lake Vanda (Antarctica) Water Column, Applied And Environmental Microbiology, 64(10), 3791-3797.

Buenger, D., F. Topuz, And J. Groll (2012), Hydrogels In Sensing Applications, Progress In Polymer Science, 37(12), 1678-1719, Doi:10.1016/J.Progpolymsci.2012.09.001.

.

Croudace, I. W., A. Rindby, And R. G. Rothwell (2006), Itrax: Description And Evaluation Of A New Multi-Function X-Ray Core Scanner, Geol. Soc. Spec. Publ., 267, 51-63, Doi:10.1144/Gsl.Sp.2006.267.01.04.

Davison, W., And H. Zhang (1994), In-Situ Speciation Measurements Of Trace Components In Natural-Waters Using Thin-Film Gels, Nature, 367(6463), 546-548.

El-Hag Ali, A., H. A. Shawky, H. A. Abd El Rehim, And E. A. Hegazy (2003), Synthesis And Characterization Of PVP/AAC Copolymer Hydrogel And Its Applications In The Removal Of Heavy Metals From Aqueous Solution, European Polymer Journal, 39(12), 2337-2344, Doi:Http://Dx.Doi.Org/10.1016/S0014-3057(03)00150-2.

Finkel, R And J.L. Bentley (1974). Quad Trees: A Data Structure For Retrieval On Composite Keys. Acta Informatica 4 (1): 1–9. Doi:10.1007/Bf00288933.

Fones, G. R., And J. W. Moffett (2002), In-Situ Cu Speciation Measurements In Boston Harbor Using DGT, Abstracts Of Papers American Chemical Society, 224(1-2), 18.

Francis, C. A., And B. M. Tebo (2001), Enzimatic Manganese(II) Oxidation By A Marine A-Proteobacterium, Appl Environ Microbiol, 67, 4024-4029.

Francis, C. A., K. L. Casciotti, And B. M. Tebo (2002), Localization Of Mn(Ii)-Oxidizing Activity And The Putative Multicopper Oxidase, Mnxg, To The Exosporium Of The Marine Bacillus Sp Strain Sg-1, Archives Of Microbiology, 178(6), 450-456, Doi:10.1007/S00203-002-0472-9.

Gonzalez, R. C., And R. E. Woods (1992), Digital Image Processing, 716 Pp., Addison-Wesley Longman Publishing Co., Inc.

Glud, R. N., I. Klimant, G. Holst, O. Kohls, V. Meyer, M. Kuhl, And J. K. Gundersen (1999), Adaptation, Test And In Situ Measurements With O_2 Microoptides On Benthic Landers, Deep-Sea Research Part I-Oceanographic Research Papers, 46(1), 171-183, Doi:10.1016/S0967-0637(98)00068-5.

Glud, R. N., N. B. Ramsing, J. K. Gundersen, And I. Klimant (1996), Planar Optrodes: A New Tool For Fine Scale Measurements Of Two-Dimensional O_2 Distribution In Benthic Communities, Marine Ecology Progress Series, 140(1-3), 217-226, Doi:10.3354/Meps140217.

Glud, R. N., A. Tengberg, M. Kühl, P. O. J. Hall, I. Klimant, And G. Holst (2001), An In Situ Instrument For Planar O_2 Optode Measurements At Benthic Interfaces, Limnology And Oceanography, 46(8), 2073-2080.

Hakonen, A., And S. Hulth (2010), A High-Performance Fluorosensor For pH Measurements Between 6 And 9, Talanta, 80(5), 1964-1969, Doi:10.1016/J.Talanta.2009.10.055.

Ishii, H., K. Satoh, Y. Satoh, And H. Koh (1982), Spectrophotometric And Analog Derivative Spectrophotometric Determination Of Ultramicro Amounts Of Cadmium With Cationic Porphyrins, Talanta, 29(7), 545-550, Doi:10.1016/0039-9140(82)80001-5.

Jansen, J. H. F., S. J. Van Der Gaast, B. Koster, And A. J. Vaars (1998), Cortex, A Shipboard Xrf-Scanner For Element Analyses In Split Sediment Cores, Marine Geology, 151(1-4), 143-153, Doi:10.1016/S0025-3227(98)00074-7.

Johnston, C. G., And G. W. Kipphut (1988), Microbially Mediated Mn(II) Oxidation In An Oligotrophic Arctic Lake, Applied And Environmental Microbiology, 54(6), 1440-1445.

Kruper, W. J., T. A. Chamberlin, And M. Kochanny (1989), Regiospecific Aryl Nitration Of Meso-Substituted Tetraarylporphyrins - A Simple Route To Bifunctional Porphyrins, J. Org. Chem., 54(11), 2753-2756, Doi:10.1021/Jo00272a057.

Ladomenou, K., T. Lazarides, M. K. Panda, G. Charalambidis, D. Daphnomili, And A. G. Coutsolelos (2012), Meso-Substituted Porphyrin Derivatives Via Palladium-Catalyzed Amination Showing Wide Range Visible Absorption: Synthesis And Photophysical Studies, Inorganic Chemistry, 51(20), 10548-10556, Doi:10.1021/Ic300714n.

Marshall, K.C. (1979), Chapter 5 Biogeochemistry Of Manganese Minerals, In Studies In Environmental Science, Edited By P. A. Trudinger And D. J. Swaine, Pp. 253-292, Elsevier, Doi:10.1016/S0166-1116(08)71061-6.

Miyata, N., Y. Tani, M. Sakata, And K. Iwahori (2007), Microbial Manganese Oxide Formation And Interaction With Toxic Metal Ions, Journal Of Bioscience And Bioengineering, 104(1), 1-8, Doi:10.1263/Jbb.104.1.

Motelica-Heino, M., And W. Davison (2003), Trace Metals Dynamics In Surface Sediments Investigated By DGT Micro-Scale Measurements, J. Phys. IV, 107, 899-902, Doi:10.1051/Jp4:20030443.

Myers, C. R., And K. H. Nealson (1988), Microbial Reduction Of Manganese Oxides - Interactions With Iron And Sulfur, Geochimica Et Cosmochimica Acta, 52(11), 2727-2732, Doi:10.1016/0016-7037(88)90041-5.

Oehme, I., And O. S. Wolfbeis (1997), Optical Sensors For Determination Of Heavy Metal Ions, Mikrochimica Acta, 126(3-4), 177-192, Doi:10.1007/Bf01242319.

Oehme, I., S. Prattes, O. S. Wolfbeis, And G. J. Mohr (1998), The Effect Of Polymeric Supports And Methods Of Immobilization On The Performance Of An Optical Copper(Ii)-Sensitive Membrane Based On The Colourimetric Reagent Zincon, Talanta, 47(3), 595-604, Doi:10.1016/S0039-9140(98)00084-8.

Perona, P., And J. Malik (1990), Scale-Space And Edge-Detection Using Anisotropic Diffusion, Ieee Trans. Pattern Anal. Mach. Intell., 12(7), 629-639, Doi:10.1109/34.56205.

Precht, E., U. Franke, L. Polerecky, And M. Huettel (2004), Oxygen Dynamics In Permeable Sediments With Wave-Driven Pore Water Exchange, Limnology And Oceanography, 49(3), 693-705.

Richter, T. O., S. Van Der Gaast, B. Koster, A. Vaars, R. Gieles, H. C. De Stigter, H. De Haas, And T. C. E. Van Weering (2006), The Avaatech Xrf Core Scanner: Technical Description And Applications To Ne Atlantic Sediments, Geol. Soc. Spec. Publ., 267, 39-50, Doi:10.1144/Gsl.Sp.2006.267.01.03.

Soto-Neira, J., Q. Zhu, And R. C. Aller (2011), A New Spectrophotometric Method To Quantify Dissolved Manganese In Marine Pore Waters, Mar Chem, 127(1-4), 56-63.

.

Tankere-Muller, S., W. Davison, And H. Zhang (2012), Effect Of Competitive Cation Binding On The Measurement Of Mn In Marine Waters And Sediments By Diffusive Gradients In Thin Films, Analytica Chimica Acta, 716, 138-144, Doi:10.1016/J.Aca.2011.12.028.

Villalobos, M., J. Bargar, And G. Sposito (2005), Mechanisms Of Pb(II) Sorption On A Biogenic Manganese Oxide, Environmental Science & Technology, 39(2), 569-576, Doi:10.1021/Es049434s.

Viscarra Rossel, R. A., B. Minasny, P. Roudier, And A. B. Mcbratney (2006), Colour Space Models For Soil Science, Geoderma, 133(3–4), 320-337, Doi:Http://Dx.Doi.Org/10.1016/J.Geoderma.2005.07.017.

Weltje, G. J., And R. Tjallingii (2008), Calibration Of Xrf Core Scanners For Quantitative Geochemical Logging Of Sediment Cores: Theory And Application, Earth And Planetary Science Letters, 274(3-4), 423-438, Doi:10.1016/J.Epsl.2008.07.054.

Wenzhofer, F., And R. N. Glud (2004), Small-Scale Spatial And Temporal Variability In Coastal Benthic O_2 Dynamics: Effects Of Fauna Activity, Limnology And Oceanography, 49(5), 1471-1481.

Wicks, D. A., And Z. W. Wicks Jr (1999), Blocked Isocyanates III: Part A. Mechanisms And Chemistry, Progress In Organic Coatings, 36(3), 148-172, Doi:Http://Dx.Doi.Org/10.1016/S0300-9440(99)00042-9.

Wicks, D. A., And Z. W. Wicks Jr (2001), Blocked Isocyanates III: Part B: Uses And Applications Of Blocked Isocyanates, Progress In Organic Coatings, 41(1–3), 1-83, Doi:Http://Dx.Doi.Org/10.1016/S0300-9440(00)00164-8.

Wicks Jr, Z. W. (1975), Blocked Isocyanates, Progress In Organic Coatings, 3(1), 73-99, Doi:Http://Dx.Doi.Org/10.1016/0300-9440(75)80002-6.

Zengel, H.G. and M. Bergfeld (1983), US patent 4,393,238.

Zhu, Q., And R. C. Aller (2012), Two-Dimensional Dissolved Ferrous Iron Distributions In Marine Sediments As Revealed By A Novel Planar Optical Sensor, Marine Chemistry, 136–137(0), 14-23, Doi:Http://Dx.Doi.Org/10.1016/J.Marchem.2012.04.002.

Zhu, Q., R. C. Aller, And Y. Fan (2006a), A New Ratiometric, Planar Fluorosensor For Measuring High Resolution, Two-Dimensional pCO_2 Distributions In Marine Sediments, Marine Chemistry, 101(1-2), 40-53, Doi:10.1016/J.Marchem.2006.01.002.

Zhu, Q., R. C. Aller, And Y. Fan (2006b), Two-Dimensional pH Distributions And Dynamics In Bioturbated Marine Sediments, Geochimica Et Cosmochimica Acta, 70(19), 4933-4949, Doi:10.1016/J.Gca.2006.07.033.

Chapter 4:

Flux measurements of Mn(II) in marine sediments:

classical 1-D versus multi-D approaches

Abstract

Total flux of dissolved manganese across the seawater-sediment interface is the result of the combinations of contributions from processes like molecular diffusion, advection, precipitation, bioturbation and bioirrigation, where the weighting coefficient for each process depends on the physical characteristics of the sedimentary deposit, and the type and number of organisms living in it. However, evaluation of the effects of bioturbation and bioirrigation on the manganese flux across the seawater-sediment interface is difficult due to significant heterogeneity and complex three dimensional reaction patterns in surface sediments caused by the activities of various bottom dwelling fauna.

Pore water concentration gradients are commonly used to estimate chemical fluxes across the water-sediment interface during both in situ measurements and laboratory incubation microcosms experiments. However, the traditional approaches for solute sampling and measurement such as regular electrodes, dialysis arrays (peepers), diffusive gradients in thin gel film, coring, sediment extruding, and pore water separation, could smear the spatial resolution, blur benthic organism effects, affect solute speciation (i.e. oxidation states) and even alter the seawater-sediment interface during transport process and/or tool deployment (Burdige, 2006).

In this study I explored the use of a novel planar optode for two-dimensional and three-dimensional determinations of Mn(II) distribution patterns in marine sediments, oriented to estimate manganese fluxes across the water-sediment interface during the development of hypoxia in a 12 hours incubation experiment . Estimations based on Mn(II) concentration changes in overlying water, using traditional UV-VIS and AAS methods, showed that after 12 hours of anoxic incubation, fluxes across the water-sediment interface under oxygen depleted conditions were ~ 2 μmol/cm^2·day. This value was in agreement with previously reported seasonal measurements for Long Island Sound, reflecting the effect oxygen depletion has on

increases in Mn(II) production in deeper sediments and fluxes across the water sediment interface. On the other hand, similar results (~ 1.5 µmol/cm^2·day) were obtained using 2-D sensing schemes. However, planar optodes also provided detailed information about 2D Mn(II) production, consumption, and transport patterns in the sediments.

The main goal of using this planar optode for flux estimations, besides its validation as a method for quantifying the total flux of Mn (II) across the water-sediment interface, was to provide multidimensional information about how manganese fluxes develop and migrate within marine sedimentary deposits during hypoxic events, and how macrofaunal activities modify these processes in terms of its spatial distribution and magnitudes.

4.1 Introduction

Manganese cycling in coastal areas is highly dynamic. It involves physical, chemical and biological components interacting with different species of this element to generate an intricate set of transport, transformation and accumulation events affecting both its dissolved and solid phases. In marine sedimentary deposits, manganese oxides reach the water-sediment interface by sedimentation from overlying water and/or by lateral transport across the bottom (Sundby et al., 1981), as well as by oxidation of reduced species of manganese produced in deeper sediments by diagenetic processes and directed toward the surface by diffusive transport (Lovely, 1991). Under certain conditions, the dissolved manganese supply from deeper sediments can turn over the manganese oxide pool found at the surface in 60-100 days (Aller, 1980). Under conditions of low oxygen in overlying waters, oxidation reactions may not occur and Mn(II) will be released into the overlying water as a consequence. This loss of manganese from sediments can even lead to exhaustion of the pool (Sundby and Silverberg, 1985; Aller, 1994).

Chemical transport across the sediment-water interface has been widely discussed in the literature, and various chemical transport processes affecting solutes on both sides of the interface have also been reported (e.g. Duursma and Smies, 1982; Krantzberg, 1985; Santschi et al, 1985). In the particular case of manganese, one of the goals of quantifying benthic fluxes is to obtain depth-integrated production or consumption rates at steady state conditions. Generally speaking, the total benthic flux can be estimated as the sum of Mn(II) ion diffusion, bioturbation, bioirrigation, pore water advection, and sediment resuspension or redeposition, as represented by equation 22.

$$F_{total} = F_{dif} + F_{adv} + F_{biot} + F_{irr} + F_{rsp} \quad \text{(eq. 22)}$$

Where

F_{total}: total benthic flux

F_{dif}: flux due to molecular diffusion

F_{biot}: flux due to bioturbation

F_{irr}: flux due to bioirrigation

F_{rsp}: flux due to resuspension or redeposition

Sundby and Silverberg (1985) proposed a schematic representation of the flux model described above, where marine sedimentary deposits and the overlying water column were sub-divided into 5 reservoirs, with 2 in the water column and 3 in sediments (Figure 4.1). Particulate manganese is produced in the first three reservoirs (surface waters, bottom water and oxic sub-surficial sediments), while dissolved manganese is produced only in the fourth reservoir (deeper, sub-oxic sediments), and burial into deeper sediments is represented by the fifth reservoir. A direct interpretation of this scheme is, at steady state, that a mass balance requires that the difference between the flux into and the flux out of each reservoir must be equivalent to precipitation or dissolution rates in that reservoir. Additionally, it is easy to imagine that during events involving hypoxia in bottom waters, the third and fourth reservoir would quickly merge to form a single dissolution zone, enhancing dissolved Mn(II) production and its release from sediments into bottom waters.

A traditional approach for direct estimation of fluxes across the water-sediment interface involves the isolation of a specific vertical section of surface sediment, with a fixed volume of its overlying water, and tracking the changes in concentration of the solute over time in the enclosed water. This incubation of sediment and overlying water can be carried out by both in situ using benthic chambers and by sediment microcosm incubation experiments in the laboratory. Tengberg et al. (1995) provided an extensive review on design and use of benthic chambers for in situ measurements of solute fluxes across the sediment-water interface, where one of the critical aspects to consider is to avoid overlying water stratification during measurements. This has been accomplished using several alternatives for stirring the water volume, with special considerations to prevent both particle resuspension and increases of turbulent flow close to the sediment water interface, which would disrupt or produce unnaturally thin diffusive boundary layers respectively (Jorgensen and Des Marais, 1990). However, even when advances have been made in terms of benthic chamber design and intercalibration between different available instruments, this technique provides a "single boundary" measurement of benthic fluxes, without information about how the fluxes are distributed or formed below the upper interface. Additionally, some issues arise when deployed in permeable and/or biopertubed sediments since changes in hydrodynamic conditions might influence macrofaunal activities (Tengberg et al., 2004), or reduce local pressure changes that control advective fluxes (Burdige, 2006).

Mn(II) flux determinations across the water-sediment interface have also been performed during incubation experiments in the laboratory (e.g. Aller, 1980; Kristensen et al., 2002). These studies involve estimation in a similar fashion to the benthic chambers described above, in terms of using a known volume of sediment and overlying water, as well as a fixed area for the water-sediment interface.

In this study, a novel multidimensional Mn(II) analytical technique used 2-D planar optical sensors in bioturbated marine sediments to determine two-dimensional fluxes of Mn(II) during changes in oxygenation conditions at the sediment-water interface. These changes were designed to mimic development of hypoxia. The net fluxes of Mn(II) across the seawater-sediment interface derived from multidimensional Mn(II) distribution patterns were compared with results obtained from classical 1-D methods based on spatially-averaged vertical concentration gradients. We defined internal physical boundaries in the sedimentary deposits to elucidate the effect of regionalized "whole" diffusive coefficients over both internal and water-sediment interface fluxes by coupling multidimensional chemical measurements to tomographic reconstructions of sedimentary properties. These simultaneous measures of structural patterns and compositional gradients allowed improved mesh generation for numerical estimates of 2-D fluxes in conditions of complex physical and redox reaction geometries.

In addition to flux measurements, Mn(II) and Fe(II) planar optodes were used simultaneously with CT-scan tomographic reconstructions during incubation experiments to elucidate the effect of the polychaete *Nereis* and the bivalve *Macoma* over 3-D distributional patterns of this chemical species. These measurements allowed to visualize the effect of bioirrigation produced by this two species over the geochemistry of sedimentary deposits, as well as, their interaction with the planar optodes during deployments.

4.2 Experiment

The general scheme used for contrasting traditional "single boundary" and 2-D derived flux estimations of Mn(II) across the water-sediment interface during the same incubation

experiment consisted on tracking the Mn(II) concentration changes in the overlaying water of four sealed cores containing natural sediments, previously kept under oxic conditions, and opening them sequentially along a 12 hours period to deploy a Mn(II) planar optode in them, discarding the core after the 2-D measurement (Table 4.1). While the scheme designed to characterize the effect of polychaete (*Nereis* sp.), and bivalve (*Macoma* sp.) over 3-D distributional patterns of Fe(II) and Mn(II) in bioperturbed sediment consisted in the simultaneous deployment of multiple planar optodes in sieved sediments containing individuals of the above mentioned species, characterizing the physical 3-D sedimentary structure by measuring the cores using a CT-Scan before and during the planar optode deployments.

Incubation experiments designed to study Mn(II) fluxes were conducted using muddy, organic rich, coastal surficial sediment samples collected from Smithtown Bay, NY, in the fall of 2013 using a Soutar style boxcorer (0.25 m^2). Sub-sampling was carried out by vertically inserting four cylindrical glass cores (radius=7 cm; height=30 cm) into the sediment through overlying water till the cores were about two thirds filled with sediment. The upper one third of the cores was filled with overlying water. After sealing the two ends of each core and transferring to the laboratory, the undisturbed sample cores were uncapped (but with tight bottom seal) and the overlying seawater was kept aerated (salinity = 27 - 28) in the dark at 15 ºC before use.

For experiments examining the effect of benthic organisms, homogenized marine sediment samples were prepared by using surface sediment (0-2 cm) from a coastal area close to Quebec, Canada. Sediment was gently sieved with 1-mm mesh (no added water) and mixed. The homogenized sediment was carefully transferred into two 11-cm radius round cores and water from the same site was added. The sediment cores were then incubated in the laboratory at 15 ºC

with continuously aerated overlying water for 4 days to allow it to establish well-defined Mn(II) and Fe(II) gradients.

4.2.1 Equipment and reagents

Spectrophotometric measurements of manganese in solution were made using a formaldoxime based method and were carried out using a BMG Labtech SpectroStar Nano plate reader with UV/VIS absorbance spectra and with a Graphite Furnace/Flame Perkin Elmer Atomic Absorption Spectrometer (AAS, Analyst 800) equipped with an automated motorized atomizer and a hollow cathode lamp for manganese. For the plate reader based UV/VIS method, BMG Labtech 96-well microplates were used (150 µL sample per well), while samples for AAS measurements were loaded into Teflon sample cups. For the AAS method each sample was injected three times (50 µL) per determination. Settings, standards and sample preparations for colorimetric and AAS measurements of dissolved manganese in solution are described in Chapter 2 and elsewhere (Soto-Neira et al., 2011).

Two-dimensional spectrophotometric measurements of Mn(II) planar optodes were carried out using a CanonScan LIDE 25 scanner equipped with a modified Contact Image Sensor (Canon Inc.) as light source and detector, with a peak of transmittance at ~469 nm, as described in section 3.2.2.

4.2.2 Mn(II) planar optodes

Optical planar sensing foils (14×5 cm), based on the immobilization of a cadmium metalloporphyrin (Cd-TSSP) onto the surface of a chemically blocked polyurethane hydrogel (D4), were prepared using a three layered scheme. The details of sensor optode fabrication are described in section 3.2.6 (Sch6).

Homogeneity tests were performed on each sensing foil by following the Quad tree procedure proposed in section 3.2.3 as a quality test. The sensor calibration was described in section 3.2.7 but in this study we used Mn(II) standard solutions of 0, 50, 100 and 150 µM prepared in artificial seawater (ASW; s=35; pH: 8)..

Settings and procedures to convert the electronic signal obtained by the digitizing process, as well as the Perona and Malik (1990) technique for noise removal (equation 19, # iterations = 60) were performed as proposed in section 3.2.2 and 3.2.2.

4.2.3 "Single boundary" Mn(II) flux measurements

'Single Boundary' Mn(II) flux estimations across the water-sediment interface have been performed during incubation experiments in the laboratory (e.g. Aller, 1980; Kristensen et al., 2002). In these studies, they use a known volume of sediment and overlying water (V), as well as a fixed area for the water-sediment interface (A). Aller (1980) carried out sequential extractions of overlying water at specific time intervals to track changes in solute concentration, estimating fluxes across the water-sediment interface using equations 23 and 24, where the first represents the cumulative mass of solute (M) released into overlying water from sediments at time t, and the

second represents the relationship between this quantity and the total flux across the water sediment interface. The first order rate constant (k) accounts for the solute loss by precipitation when the overlying water is oxic, when solute is redox sensitive (e.g. Mn(II)).

$$M = V(C - C_0) \quad \text{(eq. 23)}$$

where

M: cumulative mass of solute released into overlying water from sediments

V: volume of overlying water

C: solute concentration at time t in the overlying water

C_0: initial solute concentration (t=0) in the overlying water

$$\frac{\partial M}{\partial t} = (AF_{total} - kVC_0)e^{-kt} \quad \text{(eq. 24)}$$

where

A: water-sediment area

F_{total}: total flux

k: first order rate constant representing the precipitation kinetics of the solute

V: volume of overlying water

C_0: initial solute concentration (t=0) in the overlying water

t: flux time (progression of the experiment).

One of the assumptions of this approach is the flux F_{total} is constant and neither pore water concentration gradients nor solute concentration changes in overlying water during sampling affect the flux measurement.

In this study, the track of Mn(II) concentrations in overlying water were carried out by using three of the four cylindrical glass sediment cores described above. At the beginning of the experiment, the cores 'control','t1', and 't2' were sealed with caps with a non-intrusive stirring system inside and two valves on the cap for collecting the water samples from each core avoiding oxygen penetration (Figure 4.4 B). Six hundred microliters of overlying water were extracted from each of this three cores for Mn(II) determinations every 0.5 hrs during the first 6 hours of experiment, and then each 1 hour until the end, as scheduled in Table 4.1. The Mn(II) concentrations in the samples were analyzed by two independent methods, i.e. UV-VIS and AAS, as mentioned above.

One-dimensional flux estimations (F) were calculated using equation 25 for overlying water measurements. The volume of overlying water (V) and the surface sediment area (A) were obtained from our tomographic reconstruction (e.g. Figure 4.5). Since k (the rate constant for manganese precipitation) has an estimated value of 8×10^{-5} /min (295.15°K, pH 7.2-7.4), equation 24 can be simplified to equation 25 as proposed by Aller (1980).

$$F = \left(\frac{1}{A}\right)\frac{\partial\left(V(C-C_0)\right)}{\partial t} \qquad \text{(eq. 25)}$$

Where

V: volume of overlying water.

A: surface sediment area.

C: measured Mn(II) concentration at time t.

C_0: measured initial Mn(II) concentration (t=0).

4.2.4 2-D Mn(II) flux measurements

As mentioned above, 2-D flux estimations were calculated based on Mn(II) concentration gradients in pore water obtained by deploying Mn(II) planar optodes in the same cores used for 'single boundary' flux estimations, discarding the sediments after the planar optode deployment.

One sensing foil was backed by an acrylic sheet (2 mm thick) and deployed in the 't0'core, as depicted in Figure 4.4 (A) at the beginning of the experiment. Cores 't1' and 't2', previously capped and used for 'single boundary' flux estimations, were opened after 6 and 12 hours respectively (Table 4.1), and sensing foils were deployed for 30 min in each of them to obtain the two-dimensional Mn(II) distribution. In each case the core cap was removed under nitrogen and reclosed again during measurements. The remaining 'control' core was used just for 'single boundary' flux estimations.

For unperturbed fine grain sediments, total benthic Mn(II) fluxes are calculated from pore-water concentration gradients considering just molecular (or ion) diffusive transport, derived from Fick's first law of diffusion in one dimension (equation 26). This is the most basic and generally accepted method, which includes in its formulation difference in chemical concentration between two points, as well as the effective diffusion coefficient for porous media.

Since the diffusion coefficient and path length between the two considered points can be replaced by a mass transfer coefficient, this equation is valid at both sides of the interface (Thibodeaux, 1979).

$$F_D = -\frac{\varphi D_0}{\theta^2}\frac{\delta C}{\delta X} \qquad \text{(eq. 26)}$$

Where

F_D : 1-D flux diffusive flux

φ : porosity

D_0: molecular/ionic diffusion coefficient in free solution

θ: tortuosity

C : chemical concentration of the solute

X: diffusive path

By ignoring possible cross-coupling terms, the one-dimensional form of the Fick's first law of diffusion can be extended to its multidimensional Cartesian form, where the components of the flux in three dimensions for a solute will be given by equation 24 (Boudreau, 1996),.

$$F_{D,X} = -\varphi D'_x \frac{\delta C}{\delta X} \qquad \text{(eq. 27)}$$

$$F_{D,Y} = -\varphi D'_Y \frac{\delta C}{\delta Y}$$

$$F_{D,Z} = -\varphi D'_Z \frac{\delta C}{\delta Z}$$

Where:

D'_x, D'_y, and D'_z are the diffusivities in the x, y, and z-direction, respectively

φ : porosity

C : chemical concentration of the solute

X, Y, and Z: diffusive path in x, y and z direction, respectively.

However, determining the total flux across the water-sediment interface based only on molecular/ion diffusion may by subject to error, even when fluxes from other processes such as bioturbation, advection and/or resuspension are negligible. Traditional approaches consider direct contact between pore-water in sediments and overlying water, even when the presence of a laminar zone in the interface between both pools has been well documented, and commonly referred as the diffusive sublayer (e.g Jorgensen and Revsbech, 1985; Burdige, 2006). This sublayer may represent additional resistance to the transport of dissolved chemical species through the water-sediment interface (Figure 4.2). The formation of this layer is caused by velocity profiles created by friction between overlying waters and the boundary (e.g. Boudreau, 1996; Boudreau and Jorgensen, 2001).

In this study, flux determinations from two-dimensional Mn(II) concentration datasets were calculated using equation 27, where porosity (φ) was considered to equal 1.0 for the first 2 cm and 0.67 for deeper sediments, based on previous discrete measurements of density carried for Smithtown Bay sediments. Correction for relative changes in the bulk density were applied based on density difference, represented by intensity changes in X-ray images, calculated using tomographic reconstructions carried using a rotatory table and a digital x-ray screen (LTX-1717

digital flat panel) (Figure 4.5). Two-dimensional gradient calculations were carried out using Matlab ® internal functions.

Basic tomographic reconstructions of round cores were carried by mounting them on a rotating table, and sequentially capturing x-ray images of the cores during a 360 degrees rotation cycle (angular resolution of 5 degrees). Each 2-D x-ray image was stored as a matrix array, including the angle at which it was captured, and 3-D volumes of intensity were estimated by geo-referencing every x-ray image, defining the intersection between the base of the core with the rotation axis as origin, and calculating polar coordinates for each pixel using the angle of capture and the known dimensions of the core. Intensity values were standardized using overlying water values as reference (set to 1). Angular resolution of this reconstruction, as well as the low exposure time allowed by the digital x-ray screen didn't allow to generate high resolution reconstructions, however, this data was used just as a rough method to determine density changes in sediments.

The accuracy of neglecting Mn(II) precipitation in the overlying water for flux calculation purposes (equation 24 simplified to 25) was tested by simultaneously deploying two-dimensional sensor foils for Mn(II) and Fe(II) (Zhu et al., 2012). This test was carried by using a sediment core collected during the same sampling time as described above. Sensing foils were deployed in a similar fashion to the procedure depicted in Figure 4.4(A) by using Acrylic sheet as sensor holder, while fixing the Mn(II) sensing foil on one side of the holder and the Fe(II) sensing foil on the other. The methods used for core incubation, sensor deployment, 2-D distributions of Mn(II) and Fe(II), and flux calculation are the same as the individual 2-D Mn(II) flux measurement.

4.2.5 3-D Mn(II) and Fe(II) determinations and fluxes

Three-dimensional distributional patterns of Mn(II) and Fe(II) were reconstructed from multiple parallel two-dimensional measurements carried using planar optodes. Multiple sensors were deployed simultaneously in a 7-cm radius core containing natural sediments (3D core1) and two 11 cm radius round cores (3D core2 and 3D core3) containing incubated sieved sediments (e.g. Figure 4.6A). The 7-cm diameter core had no signs of macrofaunal activity, while polichaeta *Nereis* sp. and bivalve *Macoma* sp. were introduced into two 11 cm radius round cores (3D core2 and 3D core3), respectively, and allowed to settle for one day before sensor deployment. Overlying water in both cores was aerated to keep oxic conditions at surface.

CT-scan measurements were carried out for the 11 cm radius cores before and during the deployment of sensor foils (Figure 4.6B). Measurements made before deployment were used to elucidate sedimentary structures generated by the animals, and to permit targeting specific structures with the foils, while CT-scan data obtained during deployments was used to geolocate the sensors in the sedimentary deposit (e.g. Figure 4.7 A and B). Imaging treatment was made using proprietary software of the instrument, and later treatments using Matlab image toolbox were carried for visualization purposes. In addition, the density filtration carried by the proprietary software for CT-scan, which defines the burrow visualization, must be considered, assuming that visual representations generated using this technique are approximations modelled by subjective boundary definitions. For this reason, further studies are required to utilize this tool as a quantitative method.

4.3 Results and discussion

After 12 hours of anoxic incubation, the traditional one dimensional approach for determining Mn(II) fluxes across the water-sediment interface under oxygen depleted conditions gave fluxes of 2.2 ±1.7 μmol cm^{-2} day^{-1}, 1.9 ±0.5 μmol cm^{-2} day^{-1}, and 2.6 ±1.8 μmol cm^{-2} day^{-1} for the 'control', 't1' and 't2' cores, respectively, with increases of Mn(II) production with time. These values are consistent with previously reported seasonal for central Long Island Sound (e.g. Aller, 1980), and its order of magnitude contrast with much lower values reported for oxic sediments in coastal areas (e.g. Eaton, 1979), supporting the interpretation of hypoxia development as the driving process for Mn(II) flux enhancement across the water-sediment interface (Figure 4.8).

We would expect that manganese precipitation by oxygen would decrease after the initial period of hypoxia development, and that manganese precipitation as (for example) $MnCO_3$ and products of sulfate reduction could be ignored in this case. Dissolved manganese concentrations continuously increased (Figure 4.8) in the overlying water even after twelve hours.

Two-dimensional distribution patterns obtained from Mn(II) planar sensors for t0, t1, and t2 are shown in Figure 4.9. At t0, two sub-surface areas exhibited higher Mn(II) concentrations, and there was the expected decrease toward the water sediment interface, suggesting oxygen penetration at least in the first half centimeter from surface. Mn(II) was undetectable at the core bottom, which can be interpreted as precipitation by reaction with anaerobic metabolites produced during sulfate consumption. The sensor deployed after six hours of incubation (t1) shown a higher Mn(II) concentrations, particularly near the interface, suggesting the consumption of oxygen in both near surface sediments and overlying water and dissolution and

migration of Mn(II) upward. The low Mn(II) mid-depth region in t1 may be due to bioturbation. However, the formation of sub-regions of Mn(II) production by microbial reduction of manganese oxides is more like to account for this distributional pattern. Residual oxygen supplied by bioturbation is rejected as the cause for the lower middepth manganese since oxygen is expected to be depleted after six hours of hypoxia development.

The sensor foil deployed after 12 hours ('t2') shown the highest Mn(II) concentrations, with an almost homogeneous distribution below the surface. As expected, hypoxia enhanced manganese reduction reactions, and molecular diffusive processes would generate a homogeneous distribution of the analyte in the incubated sediments. Additionally, the Mn(II) signal in the sensing area exposed to overlying water shown increases of Mn(II) concentrations, and its non-homogeneous distribution was attributed to circulation patterns generated during the sensor deployment.

The size of the fluxes estimated for the sediment water interface using this two dimensional sensing scheme and equation 24 were in the same range as provided by the one dimensional method , with 0.68±1.31 μmol/cm^2 day, 1.66±1.08 μmol/cm^2 day and 2.19±1.58 μmol/cm^2 day for t0, t1 and t2, respectively (Figure 4.10). However, the two dimensional gradient calculations provided additional information about where in the sedimentary deposit Mn(II) builds up, and how the formation of regions with higher flux below the surface modifies the supply of Mn(II) to the upper section of sediment (Figure 4.10 and 4.11).

At t0, the two-dimensional distribution patterns of flux showed two sub-surface peaks (Figures 4.10). The first was a near-surface isolated area (right, below water-sediment interface) and is interpreted as molecular diffusion from deeper sediments. The much lower fluxes found at the left of this sub-region are probably affected by oxygen penetration into the first centimeter of

sediment. On the other hand, the second sub- region found at t0, located as a horizontal band crossing the image at mid-depth represents both production and molecular diffusive transport of Mn(II) in sub-oxic sediments. Low concentration gradients at the bottom left of the core reduce the average value calculated during the conversion of two dimensional gradients to its one dimensional equivalent.

Mn(II) fluxes calculated from the sensing foil deployed after 6 hours (t1) showed major flux areas located in deeper sediments than at t0. This could be interpreted as a result of new patches of manganese reduction, and molecular diffusion produced by the gradient generated between higher concentrations at mid-depth and deeper lower concentration areas. A special feature was the flux peak area located just below the water-sediment interface (Figure 4.10, t1, left), suggesting the presence of a diffusive boundary layer in the right hand side of the core. Since t1 Mn(II) concentrations are high near the water sediment interface (Figure 4.10), the presence of this single area of higher fluxes in one side of the sensor implies the Mn(II) release in the adjacent areas of the interface has been reduced or blocked, which is a characteristic of interfaces where a significant diffusive boundary layer is present. This interpretation is supported by the fluxes calculated from t2 (deployed after 12 hours), since this sensor depicted a homogeneous horizontal band of high fluxes matching the location of the water sediment interface, which could be a result of an artifact generated by the diffusive boundary layer, where the Mn(II) gradient in the water-sediment interface is increased by slowing down the Mn(II) flux into overlying water due to possible concentration of the analyte below and in the diffusive boundary layer, but slowly released to the overlaying water.

In addition, further research must be conducted to elucidate the effect of core diameters over the preservation of the diffusive boundary layer. Circulation patterns in overlying waters

generated by stirring systems could unevenly disrupt the diffusive boundary layer, producing artifacts during flux estimations using both ‘single boundary’and/or planar optode approaches.

The average of the two-dimensional flux calculations in each horizontal layer provides a one-dimensional representation of fluxes along the vertical dimension of the sediments (Figure 4.11). This figure not only depicts how fluxes migrate to the water-sediment interface, as discussed above, but also visualizes the horizontal variability of these calculations. By comparing the values of t0 (blue), t1 (red), and t2(black), we can visualize the effect of developing hypoxia in overlying waters over the Mn(II) removal from sediments, as discussed in section 4.1. Nevertheless, the twelve hours of this experiment were not enough to produce exhaustion of the manganese pool in sediments.

Additional flux calculations were carried out for multiple sensors deployed during incubation experiments using bioturbated sediments (chapter 3, Figure 3.19). As depicted in Figure 3.19(A), the sedimentary deposit is highly perturbed by *Yoldia* sp., so discrete density measurements would not allow accurate flux measurements using the two-dimensional Mn(II) dataset from the sensors deployed in this experiment. However, instead we calculated two-dimensional concentration gradients shown in Figure 4.12 which can be used as an indirect representation of two-dimensional flux determinations. These gradients were highly heterogeneous on a small scale, in contrast to with the fluxes shown in other incubation experiments (e.g. Figure 4.10). Sensor 4 in this set was the only sensor to show a distinctive area where higher fluxes were located. The interpretation for this experiment was that bioirrigation over the main portion of the incubated sediments was tending to cause very patchy distributions. Oxygen penetration and Mn(II) ion diffusion through bioirrigated sediments could produce this heterogeneous distribution of gradients by decreasing the chemical gradients and enhancing

transport. In this particular incubation experiment, the lack of a deeper sub-oxic reservoir of Mn(II) reduced the total flux of this element into shallower sediments even when the water-sediment interface effective area was increased by macrofaunal activities.

Two-dimensional distribution patterns of Mn(II) and Fe(II) obtained from simultaneous deployment of Mn(II) and Fe(II) sensing foils are shown in Figure 4.13, where vertical distribution of the two elements is opposite to that expected from traditional diagenetic sequences (Fe(II) typically appears under more anoxic conditions than Mn(II)). This distribution pattern could be obtained by intrusion of oxygen into the deeper portions of the sedimentary deposits, oxidizing Fe(II) at a much faster rate than Mn(II), but giving enough time for manganese to be transported by diffusion to both shallower and deeper sediments, or by non-biologically mediated reactions as mineral formation. Additionally, the lack of Fe(II) in the overlying water, in contrast with the Mn(II) detected above the sediment surface, would support the interpretation of oxygen penetration into sediments as the source of this irregular pattern since Fe(II) would be precipitated mush faster than Mn(II).

Three-dimensional Mn(II) distributions were obtained by simultaneously deploying multiple sensors in 3D core1 as depicted in Figure 4.14. The distributional patterns showed concentrations lower than 20 µM at surface, increasing with depth, reaching values over 160 µM in at the bottom of the sensing depth (6 cm). The general distribution of Mn(II) in this reconstructed volume matches the expected values for sediments overlaid with well oxygenated waters; nevertheless, the lack of decreasing values at the bottom suggest sensors were not deployed deep enough to fully characterize the depth where manganese concentrations are reduced during precipitation reactions.

An special feature of the reconstructed Mn(II) volume was the concavity exposed by lower concentrations (from shallower to the sides of the core in Figure 4.14 to deeper in the middle of the core). This feature was interpreted as an artifact of the overlying water circulation pattern, which could enhance oxygen penetration at the center due to the small radius of the core. Additionally, the lack of a three-dimensional density dataset for this core won't allow us to estimate three dimensional fluxes of Mn(II) even when though chemical gradients are available.

Three-dimensional reconstructions of Mn(II) distributional patterns were not possible for 3D core2 and 3D core3 since very low concentrations of Mn(II) were detected. Nevertheless, Fe(II) sensors successfully provided two dimensional distributional patterns of Fe(II) (3D core2, Figure 4.15A and 3D core3, 4.16B).

Two-dimensional Fe(II) distributional patterns showed the effect of bioturbation by showing changes in concentration from sensor to sensor, featuring areas of low Fe(II) concentrations surrounded by higher concentrations (Figure 4.15A), as expected for sediments burrowed by a polychaete such as *Nereis*. Nevertheless, the calculated two-dimensional gradients depicted the same trend in all the sensors deployed in this core (Figure 4.15B), with higher values following the water-sediment interface. The lack of density data to calibrate tomographic reconstructions does not allow the estimation of total fluxes; nevertheless, for sieved sediments is expected the two-dimensional gradients of Fe(II) would provide an estimation of relative distribution of fluxes.

Figure 4.16 (A) depicts the location of the sensor foil deployed to visualize the effect of sedimentary structures generated by *Macoma* sp. on Fe(II) distributional patterns. In this reconstruction, the syphons and valves of the animal can be clearly seen, matching very closely to the features represented in the two dimensional distribution patterns of Fe(II) depicted in

Figure 4.16(B) for the same location. This was interpreted as evidence of oxygen penetration into deeper sediments through the burrows created by the syphons. Additionally, the two dimensional concentration gradients (Figure 4.16C), calculated from the dataset shown in Figure 4.16(B), closely followed the location of both animals detected with the tomographic reconstruction (Figure 4.16 A). The high gradient of Fe(II) round the biogenic structures and in the burrow wall implies a high flux of Fe(II) into overlying water through the burrow.

4.4 Conclusions

Results from 2D Mn(II) sensors showed that when overlying water was well oxygenated there was a complex set of Mn(II) gradients within bioturbated deposits. As oxygen in overlying water decreased, as occurs during a hypoxia event, internal gradients dissipated. Anoxic incubation experiments also showed that the net vertical flux of Mn(II) across the upper sediment water interface was comparable when measured using traditional 1-D and our new 2-D method despite complex sub-surficial reaction patterns in the marine sediments. However, the use of two dimensional Mn(II) planar optodes allowed visualization of the formation of heterogeneously distributed fluxes in deeper sediments when overlying water was oxic, and and to see migration of the zone of highest flux toward the water-sediment interface as anoxic conditions develop over surface sediments.

Results from both 1-D and 2-D methods for Mn(II) flux determinations also suggested that during development of anoxic conditions in overlying waters, fluxes across the water sediment interface produced by concentration gradients in this boundary are slowed down during early stages of anoxia, but after hours of increased Mn(II) production in deeper sediments, the

fluxes may increase rapidly, possibly due to physical disruptions of the diffuse boundary layer. However, this could be one of the possible patterns to follow during development of anoxia in sediments, and further studies are required.

In sieved sediments to which benthic fauna had been added, estimates of relative flux derived from two-dimensional gradients of pore water concentrations allowed us to visualize heterogeneous flux patterns generated by bioirrigation, showing how oxygen intrusion and enhanced molecular diffusion could increase total fluxes of Mn(II) into overlying waters.

In conclusion, a novel planar optode with capabilities to determine two-dimensional and 3-dimensional distributional patterns of Mn(II) in marine sediments provides a valuable alternative for measurement of benthic fluxes of this analyte. As well, it provides important information about both the formation of sub-surficial fluxes, and the effect macrofaunal activity over these processes.

References

Aller, R. C. (1980), Quantifying Solute Distributions In The Bioturbated Zone Of Marine-Sediments By Defining An Average Micro-Environment, Geochimica Et Cosmochimica Acta, 44(12), 1955-1965, Doi:10.1016/0016-7037(80)90195-7.

Aller, R. C. (1994), The Sedimentary Mn Cycle In Long-Island Sound - Its Role As Intermediate Oxidant And The Influence Of Bioturbation, O2, And C(Org) Flux On Diagenetic Reaction Balances, Journal Of Marine Research, 52(2), 259-295, Doi:10.1357/0022240943077091.

Boudreau, B. P. (1996), The Diffusive Tortuosity Of Fine-Grained Unlithified Sediments, Geochimica Et Cosmochimica Acta, 60(16), 3139-3142, Doi:10.1016/0016-7037(96)00158-5.

Boudreau, B. P., And B. B. Jorgensen (2001), The Benthic Boundary Layer : Transport Processes And Biogeochemistry: Transport Processes And Biogeochemistry, Oxford University Press, USA.

Burdige, D. J. (2006), Geochemistry Of Marine Sediments, Princeton University Press.

Duursma, E.K. And Smies, M. 1982. Sediment And Transfer At And In The Bottom Interfacial Layer. Pollutant Transfer And Transport In The Sea. Ed. G. Kullenberg. Boca Raton : Crc Press, 1982. P. 101-139.

Eaton, A. (1979), Impact Of Anoxia On Mn Fluxes In The Chesapeake Bay, Geochimica Et Cosmochimica Acta, 43(3), 429-432, Doi:10.1016/0016-7037(79)90208-4.

Jorgensen, B. B., And D. J. D. Marais (1990), The Diffusive Boundary-Layer Of Sediments - Oxygen Microgradients Over A Microbial Mat, Limnology And Oceanography, 35(6), 1343-1355.

Jorgensen, B. B., And N. P. Revsbech (1985), Diffusive Boundary-Layers And The Oxygen-Uptake Of Sediments And Detritus, Limnology And Oceanography, 30(1), 111-122.

Krantzberg, G. (1985), The Influence Of Bioturbation On Physical, Chemical And Biological Parameters In Aquatic Environments - A Review, Environmental Pollution Series A-Ecological And Biological, 39(2), 99-122, Doi:10.1016/0143-1471(85)90009-1.

Kristiansen, K. D., E. Kristensen, And E. M. H. Jensen (2002), The Influence Of Water Column Hypoxia On The Behaviour Of Manganese And Iron In Sandy Coastal Marine Sediment, Estuarine, Coastal And Shelf Science, 55(4), 645-654.

Lovley, D. R. (1991), Dissimilatory Fe(III) And Mn(IV) Reduction, Microbiological Reviews, 55(2), 259-287.

Santschi, P. H. (1985), The Merl Mesocosm Approach For Studying Sediment-Water Interactions And Ecotoxicology, Environmental Technology Letters, 6(8), 335-350.

Sundby, B., And N. Silverberg (1981), Pathways Of Manganese In An Open Estuarine System, Geochimica Et Cosmochimica Acta, 45(3), 293-307, Doi:10.1016/0016-7037(81)90240-4.

Sundby, B., And N. Silverberg (1985), Manganese Fluxes In The Benthic Boundary Layer, Limnol Oceanogr, 30, 372-381.

Tengberg, A., et al. (1995), Benthic Chamber And Profiling Landers In Oceanography — A Review Of Design, Technical Solutions And Functioning, Progress In Oceanography, 35(3), 253-294, Doi:Http://Dx.Doi.Org/10.1016/0079-6611(95)00009-6.

Tengberg, A., H. Stahl, G. Gust, V. Muller, U. Arning, H. Andersson, And P. O. J. Hall (2004), Intercalibration Of Benthic Flux Chambers I. Accuracy Of Flux Measurements And Influence Of Chamber Hydrodynamics, Progress In Oceanography, 60(1), 1-28, Doi:10.1016/J.Pocean.2003.12.001.

Thibodeaux, L. J. (1979), Chemodynamics Environmental Movement Of Chemicals In Air Water And Soil, 501 pp.

Zhu, Q., And R. C. Aller (2012), Two-Dimensional Dissolved Ferrous Iron Distributions In Marine Sediments As Revealed By A Novel Planar Optical Sensor, Marine Chemistry, 136–137(0), 14-23, Doi:Http://Dx.Doi.Org/10.1016/J.Marchem.2012.04.002.

Chapter 5:

Conclusions and perspectives

Summary of major findings

The nature of manganese cycling in coastal areas is highly dynamic. It involves physical, chemical and biological components interacting with different species of this element to generate an intricate set of transport, accumulation, and chemical transformation events affecting both its dissolved and solid phases. A wide spectra of inorganic and biologically mediated reactions in which the different species of manganese are involved, as well as a range of physical processes which drive the transport and accumulation of these species in marine environments.

In this work, progress in quantification methods of dissolved manganese in marine sedimentary deposits was accomplished by developing new spectrophotometric techniques based on transmetallation reaction between 4,4‘,4“,4“‘-(Porphirine-5,10,15,20-tetrayl)tetrakis (benzenesulfonic acid) cadmium complex (Cd-TSPP) and Mn(II) for determining chemical concentrations of dissolved Mn(II) in pore water from marine sediments. This method showed a good analytical response to Mn(II) under characteristic values of pH, temperature, salinity, and interference levels in marine sedimentary environments. In this technique, the second derivative method for analysis of absorbance spectra was implemented, allowing improved peak identification and analytical calibration and providing a reliable method for Mn(II) determinations up to 37.5 µM Mn(II) for 200 µL samples, with detection limits of 0.4 and 0.3 µM Mn (II) using end-point absorbance and second derivative approach, respectively.

Even though there is a wide variety of analytical approaches for determining Mn(II) in marine environments, with different levels of precision, operational cost, and sample volume requirements (see chapter 1), the advantages of the UV-VIS method developed in this dissertation over, for example, the traditional formaldoxime method are the procedure simplicity,

the high selectivity, good precision and accuracy, the high throughput sample analysis, and low volume (<200 μL) sample consumption. The method can also be readily utilized to simultaneously determine multiple samples (up to 96 or 386) when the analysis is performed using a plate reader spectrometer.

The method developed in this work for Mn(II) determinations provides the foundation for new technologies based on low cost colorimetric methods and affordable instrumentation. In particular, the properties of Cd-TSPP make it a very attractive alternative for use in developing optical sensing schemes for in situ measurements, profilers, microsensors, and planar optodes in marine environments. Testing the analytical properties of Cd-TSSP as a chemical indicator for Mn(II) determinations in marine environments was necessary for the development of an irreversible planar optode with capabilities to determine two-dimensional distributional patterns of Mn(II) in sedimentary deposits.

Multiple possible sensing schemes for an irreversible planar optode based on the colorimetric reaction of Mn(II) with immobilized Cd-TSSP or its derivative, involving both chemical and numerical aspects, were explored. After optimizing different possible schemes, a functionalized Cd-TSSP immobilized in a blocked version of D4 hydrogel was selected as the most suitable sensor design. This sensing scheme showed suitable dynamic range, tolerance to interferences, with no effect of salinity changes over measurements, to perform 2-D measurements of Mn(II) in marine sediments.

During the sensor development, including the design of both one- and two-dimensional methods for determining Mn(II) in marine environments, it was found that the use of numerical analysis is fundamental for acquisition and evaluation of chemical data. For absorbance methods, utilizing the second derivative approach, involving the use of Gaussian characterizations of

spectral data, represented a significant improvement for Mn(II) determinations in pore water in the presence of high concentrations of interfering cations. While for the 2-D planar optical sensor development, color space transformations, homogeneity tests for the sensing foils (e.g. *Quad tree* method), and noise removal algorithms such as the Perona and Malik methods were critical steps for improving conversion of electronic signals (e.g. digitized images) into chemical information.

The irreversible planar optode for Mn(II) sensing developed in chapter 3 was successfully applied to in-situ mapping of 2-dimensional Mn(II) distribution patterns with high spatial resolutions in bioturbated marine sediments and depicting the natural heterogeneity of dissolved Mn(II) in bioperturbed marine sediments with minimal impact on natural sedimentary structures during its deployment. Traditional one-dimensional methods for determination of Mn(II) lack both the spatial resolution and the non-intrusive sampling required to elucidate the natural heterogeneity of bioperturbed sediments, where macrofaunal activities as burrowing and feeding would generate highly intricate three-dimensional sedimentary structures. The novel planar optode is envisioned as a significant advance for spatial and temporal in-situ quantification of Mn(II) in complex marine sedimentary deposits, allowing us to directly discern the 2-D Mn(II) distribution patterns associated to the biogenic sediment structures and benthic organism activities, and enhance our understanding of manganese biogeochemical cycling in marine deposits. Another advantage of the irreversible Mn(II) optical sensor is its easy and convenient in-situ application. Because the sensor optode foil can be readily inserted into sediment along with the support of plastic sheet and the chemical reaction of sensor with Mn(II) is irreversible, it's not necessary to bring complicated and bulky camera systems to the field for in-situ 2-D Mn(II) measurements in shallow water environments (<1 m) such as wetland, marshes, coastal

mudbank etc. The sensor optodes can be directly inserted into the sediment for 30 min; the color developed sensor foil withdrawn, rinsed with water and brought back to laboratory for scanning.

In chapter 4, the Mn(II) planar optode was tested as an alternative method to determine benthic fluxes of dissolved Mn(II) at both the water-sediment interface and in sub-surface sediments during anoxic incubation experiments designed to mimic the development of hypoxic conditions in overlying water. Two-dimensional flux distributional patterns were calculated using a multidimensional Cartesian expression of Fick's first law and compared with traditional flux measurements based on tracking the changes of Mn(II) concentrations in the overlying water of incubated sediments. Results from both the traditional one- and novel two-dimensional flux measurements were in agreement with previously reported seasonal measurements for the sampling region in central Long Island Sound. Planar optodes provided additional information about dissolved manganese production and migration in deeper sediments, and how the formation of regions with higher fluxes below the surface modify the supply of Mn(II) to the upper section of sediment. In addition, planar sensors allow visualization of the effect of the diffusive boundary layer on the flux calculations based on pore water concentration gradients.

Additional relative flux calculations were carried out for bioturbated sediments during incubation experiments by simultaneously deploying multiple parallel Mn(II) planar optodes.. Given the lack of detailed information for porosity and density, relative distributions of Mn(II) fluxes were represented by two-dimensional concentration gradients. Resulting data showed the effect of sedimentary processes such as bioirrigation on patterns of Mn(II) fluxes, revealing highly heterogeneous distributions for high gradient regions in the bioturbated subsurface zone, as well as decreased magnitudes for both Mn(II) concentrations and net fluxes across burrow walls due to oxygen penetration into deeper sediments. Additionally, this set up allowed to

generate three dimensional reconstruction of chemical concentrations of Mn(II) in sedimentary deposits, providing an expansion of our analytical capabilities to characterize chemical environments during benthic studies.

In conclusion, novel spectrophotometric techniques for one-, two-, and three-dimensional determination of Mn(II) in marine sedimentary deposits have been developed in this study, and they represent new approaches for the study of manganese cycling in marine environments. The one-dimensional method provides a simple and fast alternative for determining Mn(II) in pore water, with capabilities to determine literally hundreds of samples simultaneously, while the planar optode successfully elucidates two-dimensional distribution patterns of Mn(II) in highly heterogeneous bioperturbed sediments, and provides an alternative method for Mn(II) flux estimations across both the water-sediment interface and deeper sediments.

Future work

As introduced in chapter 1, imaging techniques ranging from submarine optical systems, oriented to characterize macrofaunal activities and sedimentary structures, to planar optode technologies used for chemical characterization of sedimentary deposits have been widely employed in benthic studies. In the work of this dissertation, the development of Mn(II) irreversible planar optode expands the analytic options for multidimensional chemical measurements in marine sedimentary deposits, visualizing benthic processes previously described solely by conceptual models based on classical intrusive one-dimensional methods of chemical determinations. Nevertheless, our capabilities for determine multidimensional chemical distribution of key elements in marine geochemical cycles is not the only limitation to fully

characterize marine sedimentary deposits, and the chemical processes occurring in it. As stated in chapter 1, physical and biological processes interact with different chemical species, generating intricate and highly dynamic elemental cycling in benthic systems. For this reason, the challenge is to develop techniques to expand the multidimensional analysis of benthic system to all, chemical, physical and biological aspects of this environments. On this matter, development of instruments for in situ multidimensional characterization of physical structures in marine sedimentary deposits, with capabilities to estimate parameters as density or porosity, would be fundamental to take full advantage of the chemical multidimensional information provided by planar optode technology.

Another aspect to consider as future work in benthic studies using planar optodes is the development of new methodologies and instrumentation for its deployment during in situ measurements. Developing new autonomous benthic landers with capabilities to carry in situ experiments using multiple analytical techniques, complementing the information provided by planar optodes would become fundamental to expand the variety of environments and aspects of benthic biogeochemical cycling approached by using thi sensors.

The use of 2D X-ray imaging and tomographic reconstruction based on CT-scanning during deployments of Mn(II) planar optodes provided valuable information about sedimentary structures generated by macrofaunal activities, as well as, the exact position of animals during experiments. Additionally, this sources of information provided precise geo-referencing for the sensor position during the deployments in marine sediments. However, limitations and accuracy issues arose during the analysis of tomographic data due to the medical orientation of the proprietary software used by the CT-scan. These issues were partially overcome by using visualization and filtering techniques incorporated in the image toolbox of MATLAB. Therefore,

developing software designed specifically to reconstruct sedimentary structures is necessary. So, in order provide quantitative information about three-dimensional sedimentary structure, and being able to match this information with multidimensional chemical information provided by planar optodes, additional work must be done improving tomographic reconstructions of bioperturbed sedimentary environments, enhancing the use of these sensors for three-dimensional flux determinations.

In terms of future work with Mn(II) planar optodes, the capabilities to elucidate intricate distributional patterns of the analyte in bioperturbed sediments, and its use for estimating two-dimensional flux distributions in both the water-sediment interface and sub-surface sediments, suggest there is extensive work to be carried out using this sensing scheme to quantify specie-specific macrofaunal effects on Mn(II) distributions and fluxes in a diverse set of benthic environments. Additionally, shortening the time of deployment required by Mn(II) sensors , for increasing the temporal resolution of measurements, as well as , the development of reversible sensors for this analyte would represent future areas to be explore.

The spatial scale required for addressing scientific questions related to specie-specific effects of animal activities over chemical environments in marine sedimentary deposits using the sensing scheme proposed in this work would be directly related to the size of sedimentary structure to be analyzed. For organisms as *Nereis* or *Macoma*, sensors with size in the decimeter scale would be appropriate to characterize the chemical environment, while new techniques and advances in instrumentation would be required for carrying deployments of bigger sensors into deeper sediments. Additionally, must be kept on mind this sensor is designed to characterize specific environments, instead of surveying extensive coastal regions. To accomplish the last, a probabilistic analysis must be carried by deploying multiple sensors in representative areas.

In summary, the techniques for one- and two-dimensional Mn(II) determinations in marine pore waters developed in this work expand our analytical capabilities to study biogeochemical cycles in marine deposites, allowing us to elucidate the intricate spatial distributional patterns of both Mn(II) concentrations and fluxes in bioperturbed sediments, providing new insights into Mn(II) biogeochemical processes that was previously undocumented or studied just in a theoretical way. But, more research in terms of tomographic reconstruction of sediments needs to be done for the 3-D Mn(II) flux measurements and model development.

Figures

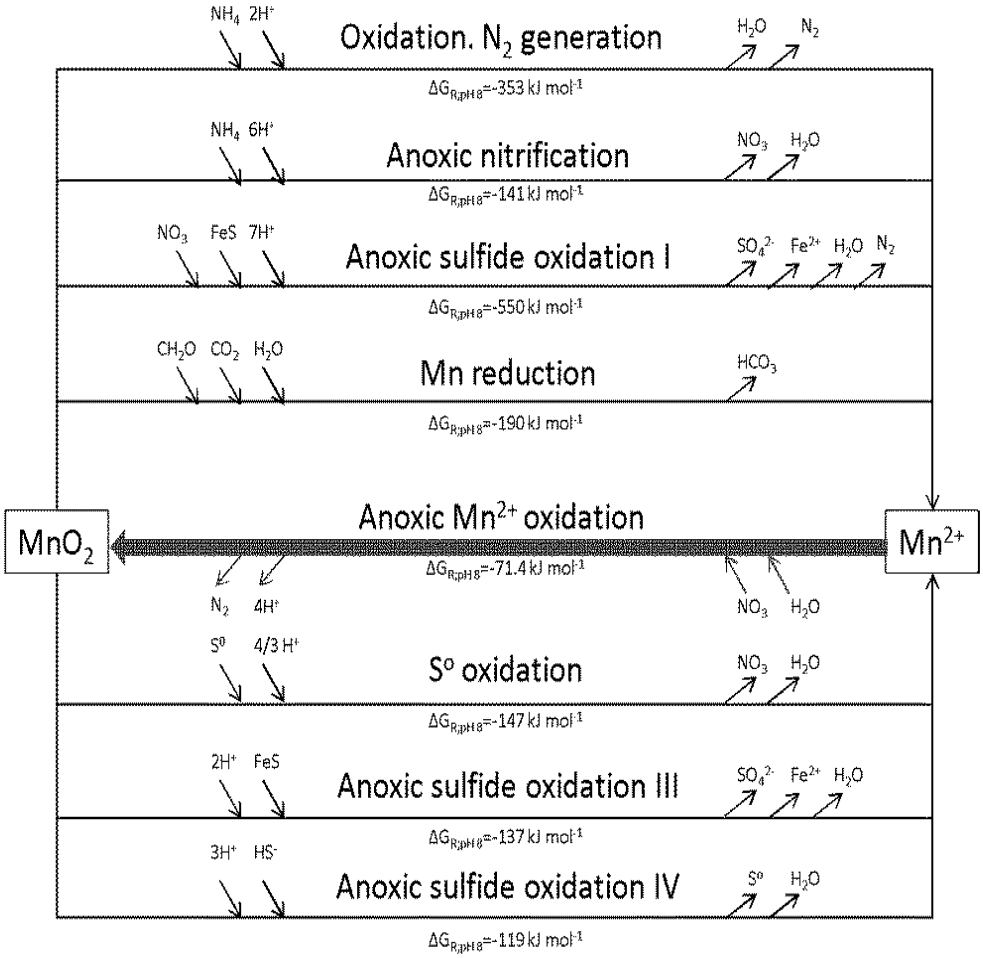

Figure 1.1

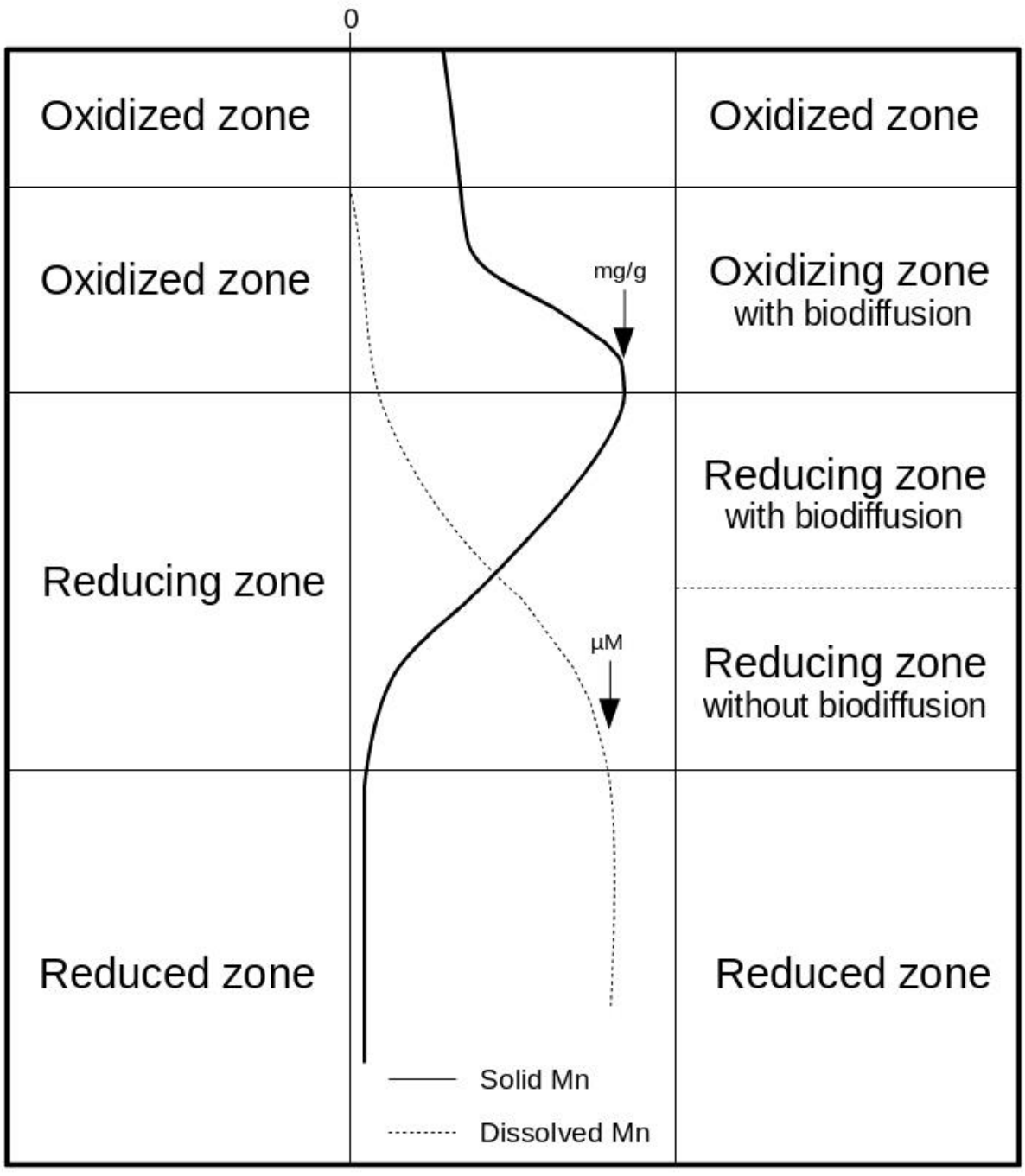

Extracted from Gratton et al.,1990

Figure 1.2

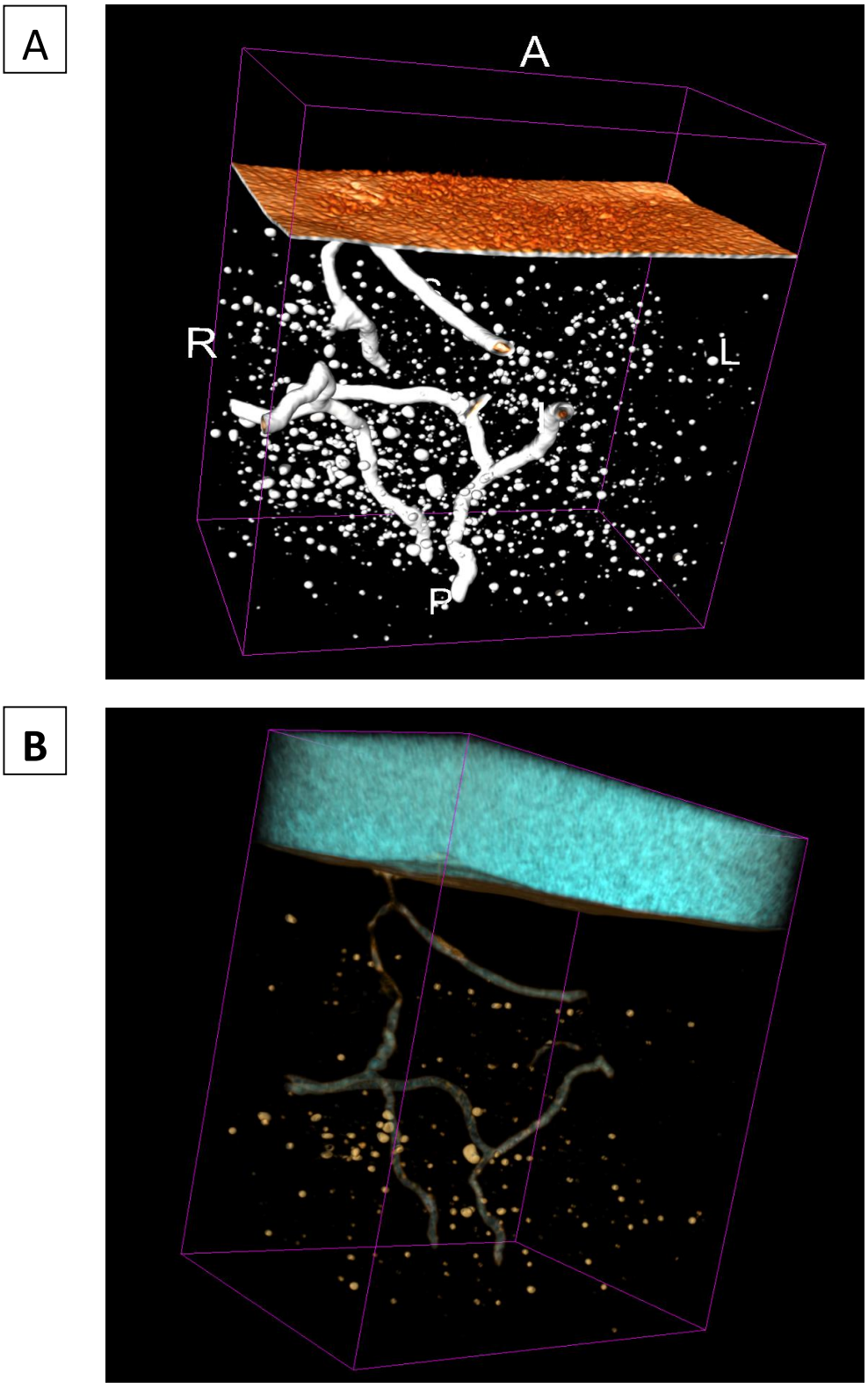

Figure 1.3

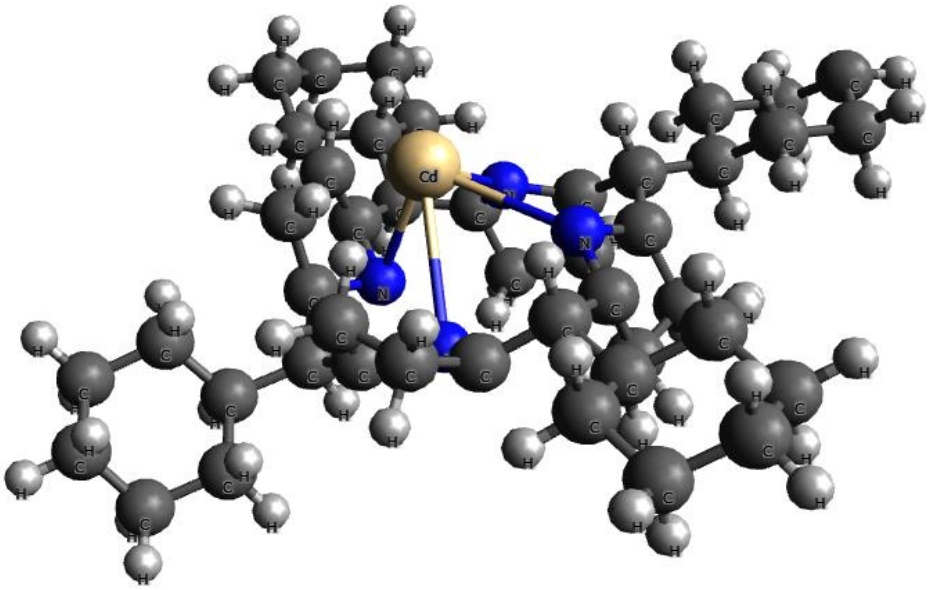

Figure 2.1

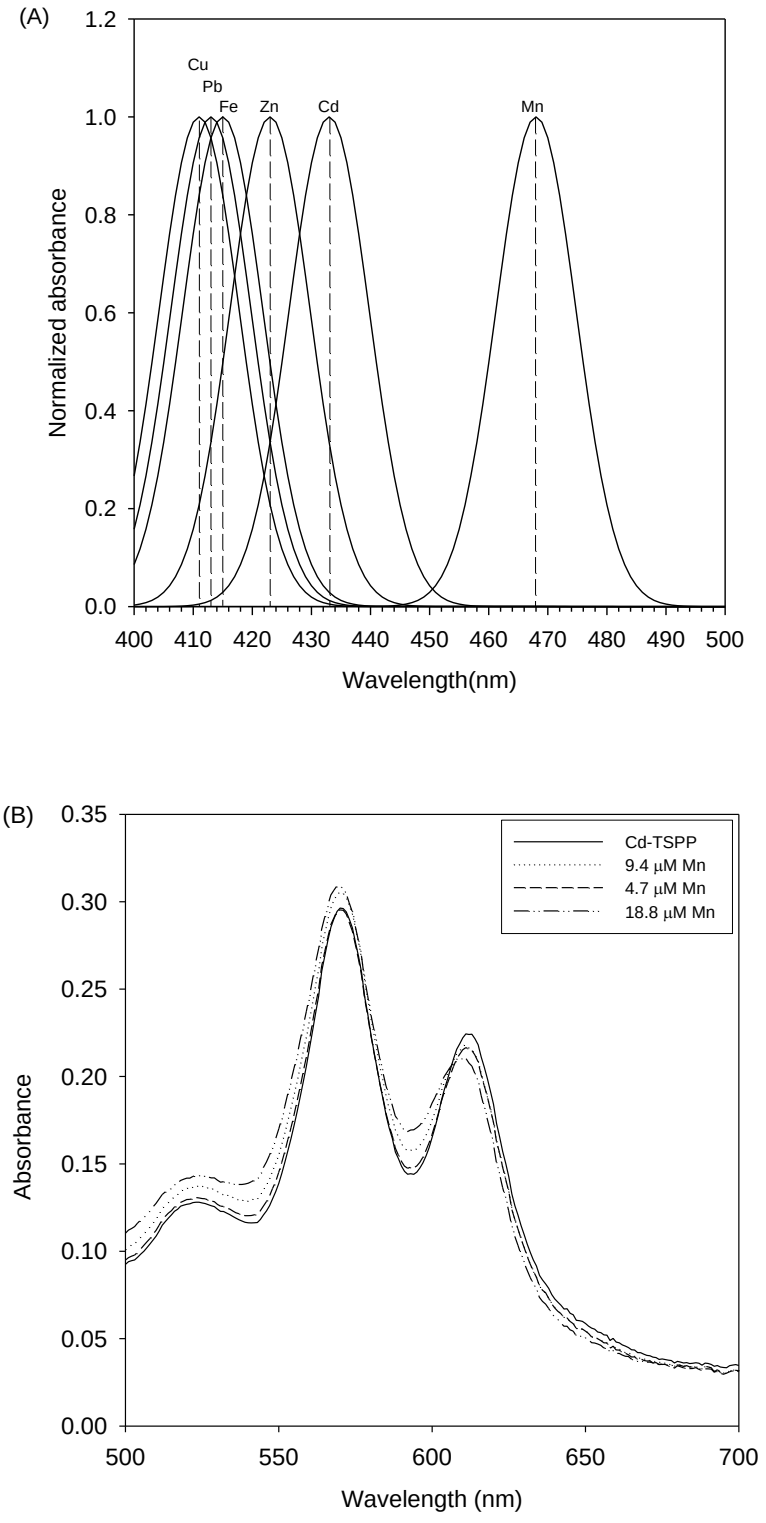
(A)
Cu
Pb
Fe
Zn
Cd
Mn
Normalized absorbance
Wavelength(nm)
(B)
Cd-TSPP
9.4 μM Mn
4.7 μM Mn
18.8 μM Mn
Absorbance
Wavelength (nm)

Figure 2.2

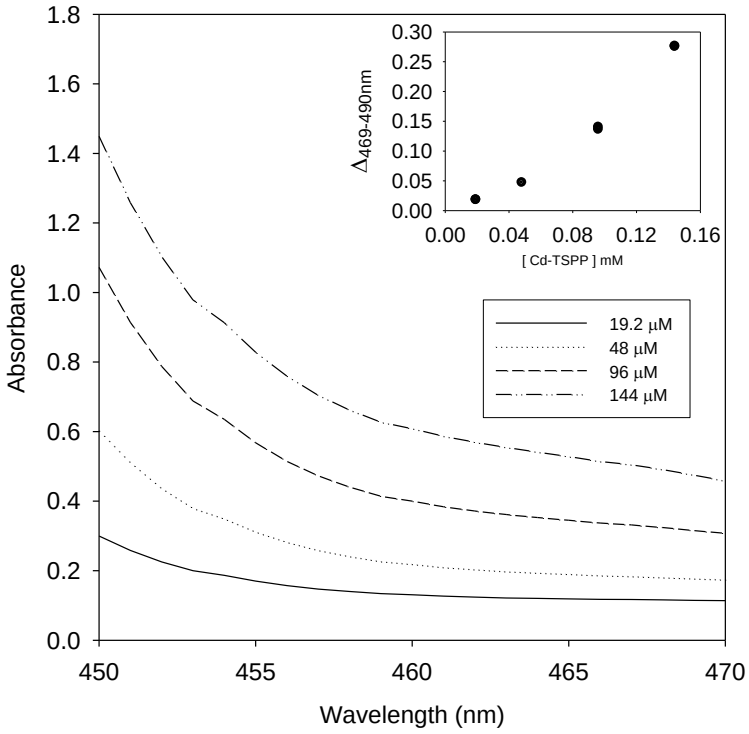
Absorbance
Wavelength (nm)
1.8
1.6
1.4
1.2
1.0
0.8
0.6
0.4
0.2
0.0
450
455
460
465
470
19.2 μM
48 μM
96 μM
144 μM
Δ469-490nm
[Cd-TSPP] mM
0.30
0.25
0.20
0.15
0.10
0.05
0.00
0.00
0.04
0.08
0.12
0.16

Figure 2.3

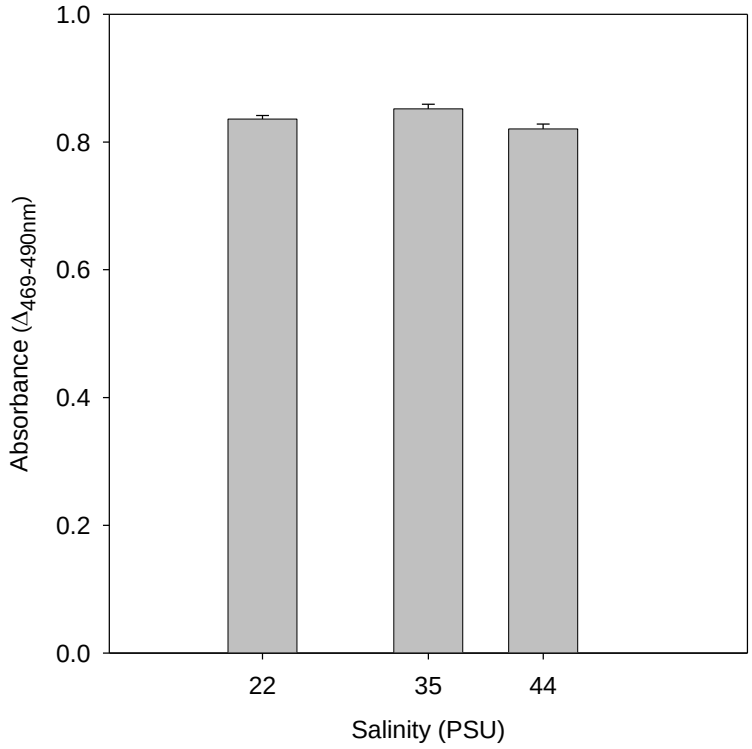

Figure 2.4

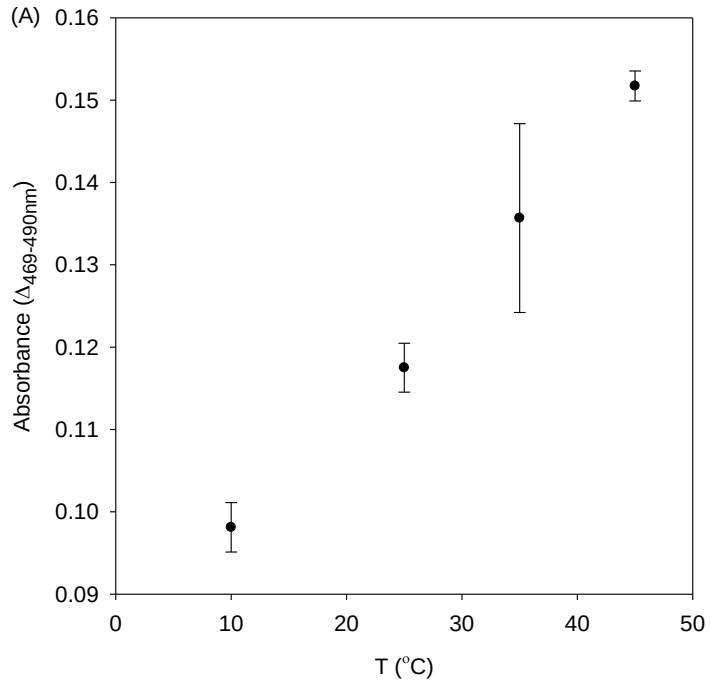
(A)
0.16
0.15
0.14
0.13
0.12
0.11
0.10
0.09
Absorbance ($\Delta_{469-490nm}$)
0
10
20
30
40
50
T (^{o}C)

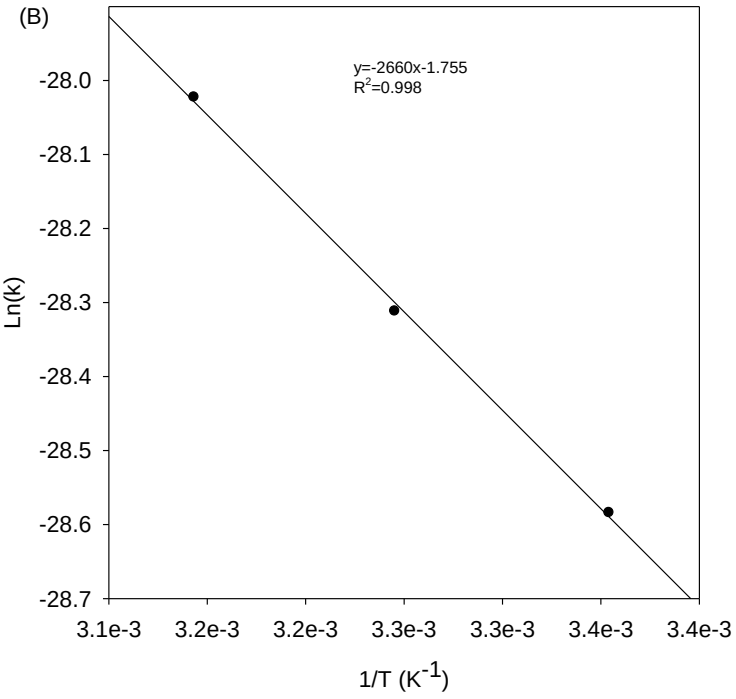
(B)
y=-2660x-1.755
R^2=0.998
-28.0
-28.1
-28.2
-28.3
-28.4
-28.5
-28.6
-28.7
Ln(k)
3.1e-3
3.2e-3
3.2e-3
3.3e-3
3.3e-3
3.4e-3
3.4e-3
1/T (K^{-1})

Figure 2.5

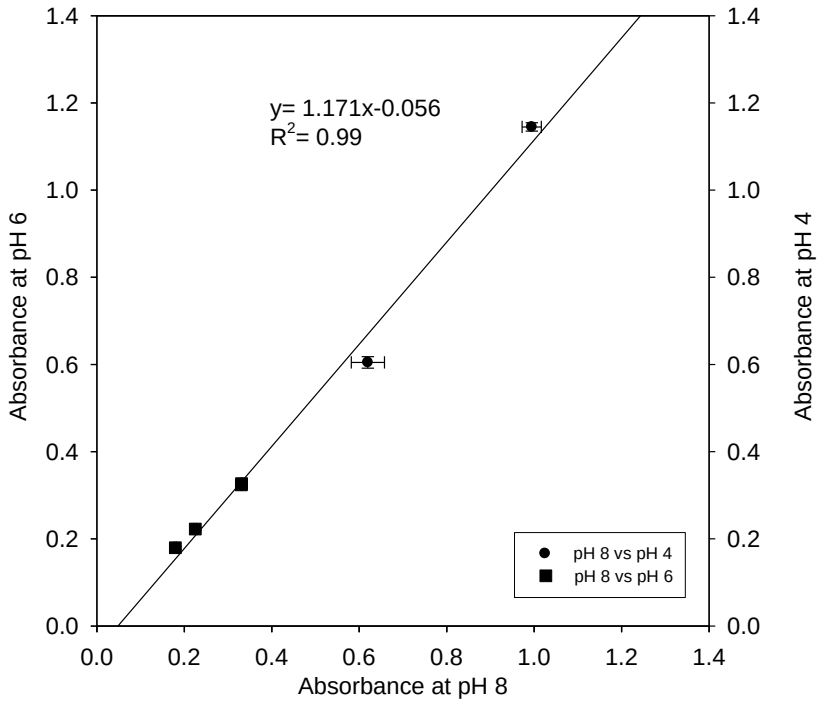
y= 1.171x-0.056
R2= 0.99
pH 8 vs pH 4
pH 8 vs pH 6
Absorbance at pH 6
Absorbance at pH 4
Absorbance at pH 8
0.0
0.2
0.4
0.6
0.8
1.0
1.2
1.4

Figure 2.6

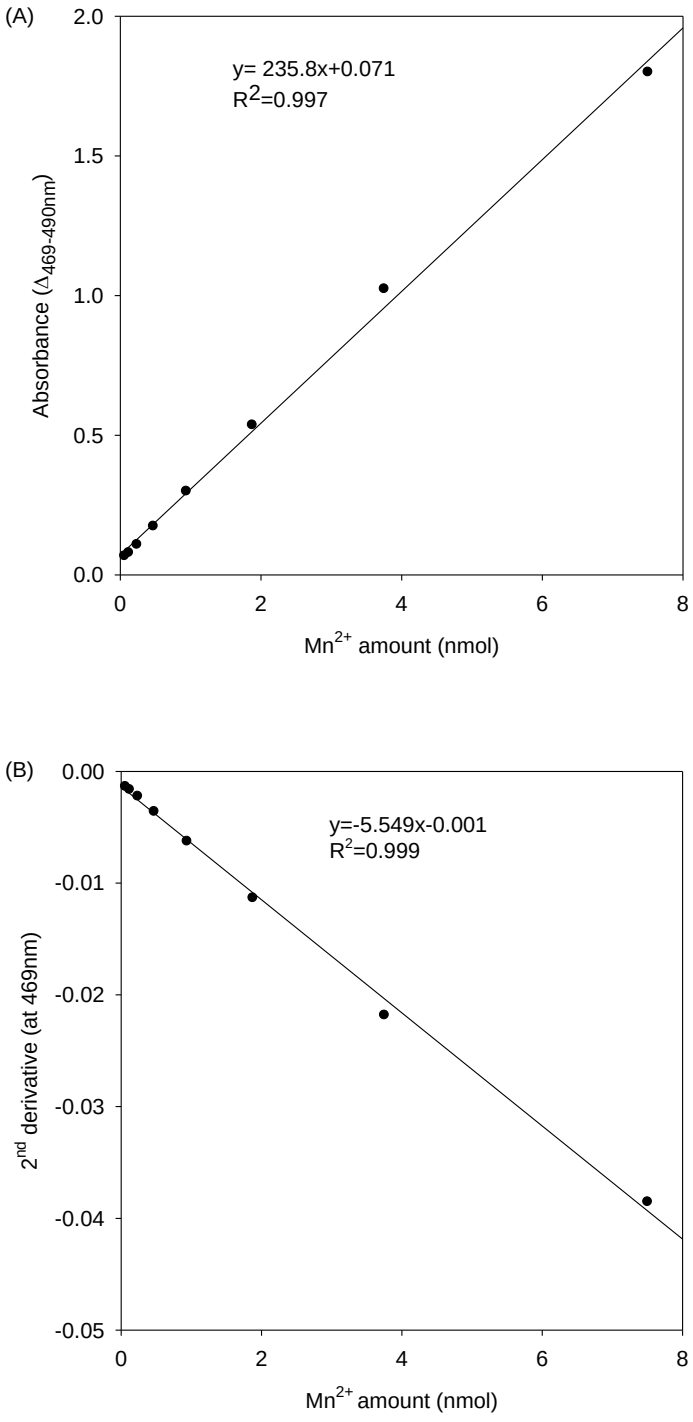
(A)
y= 235.8x+0.071
R2=0.997
Absorbance (Δ469-490nm)
Mn2+ amount (nmol)
(B)
y=-5.549x-0.001
R2=0.999
2nd derivative (at 469nm)
Mn2+ amount (nmol)

Figure 2.7

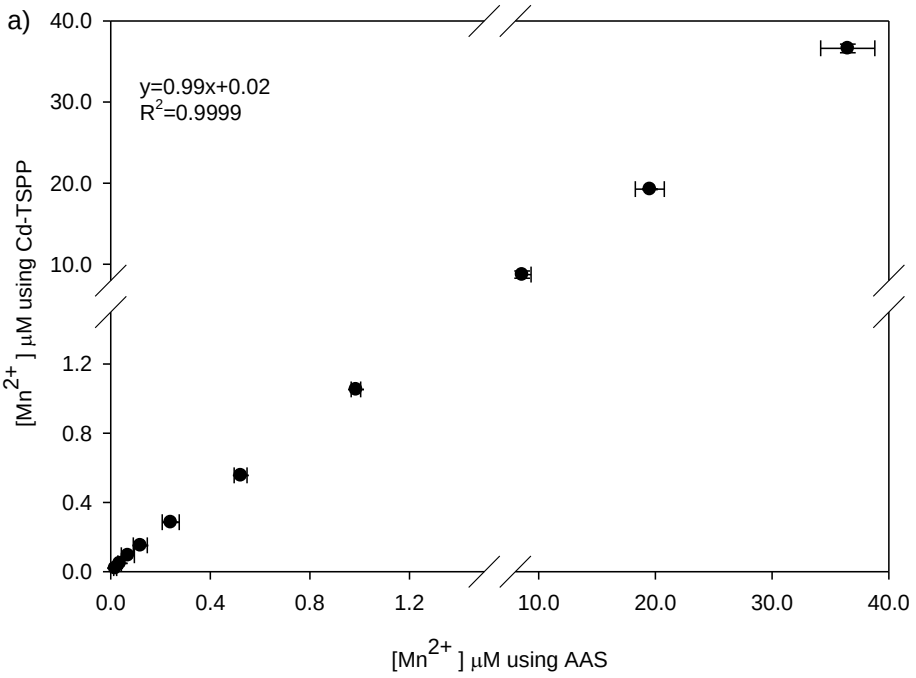
a)
y=0.99x+0.02
R2=0.9999
[Mn2+] µM using Cd-TSPP
[Mn2+] µM using AAS
0.0
0.4
0.8
1.2
10.0
20.0
30.0
40.0

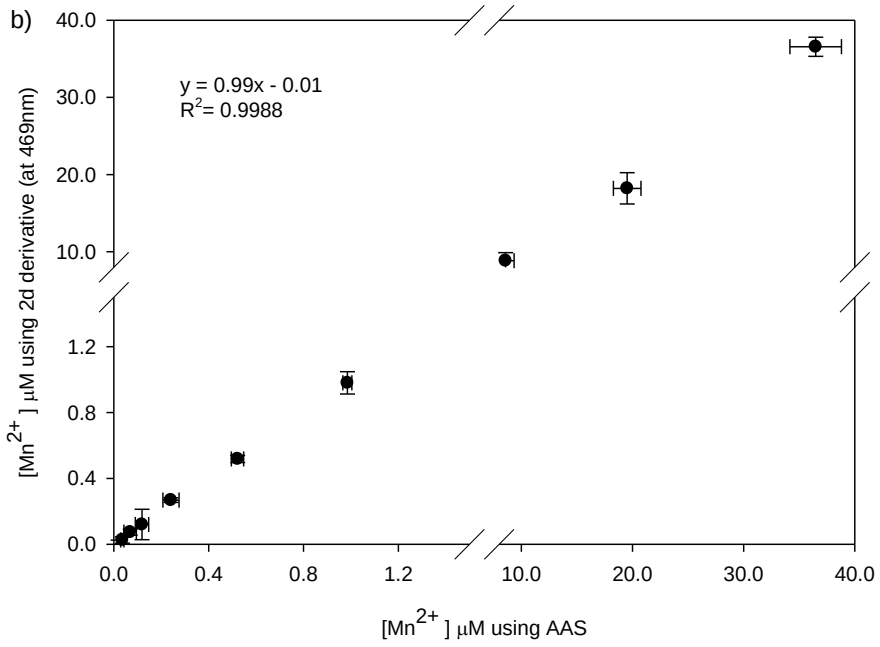
b)
y = 0.99x - 0.01
R2= 0.9988
[Mn2+] µM using 2d derivative (at 469nm)
[Mn2+] µM using AAS
0.0
0.4
0.8
1.2
10.0
20.0
30.0
40.0

Figure 2.8

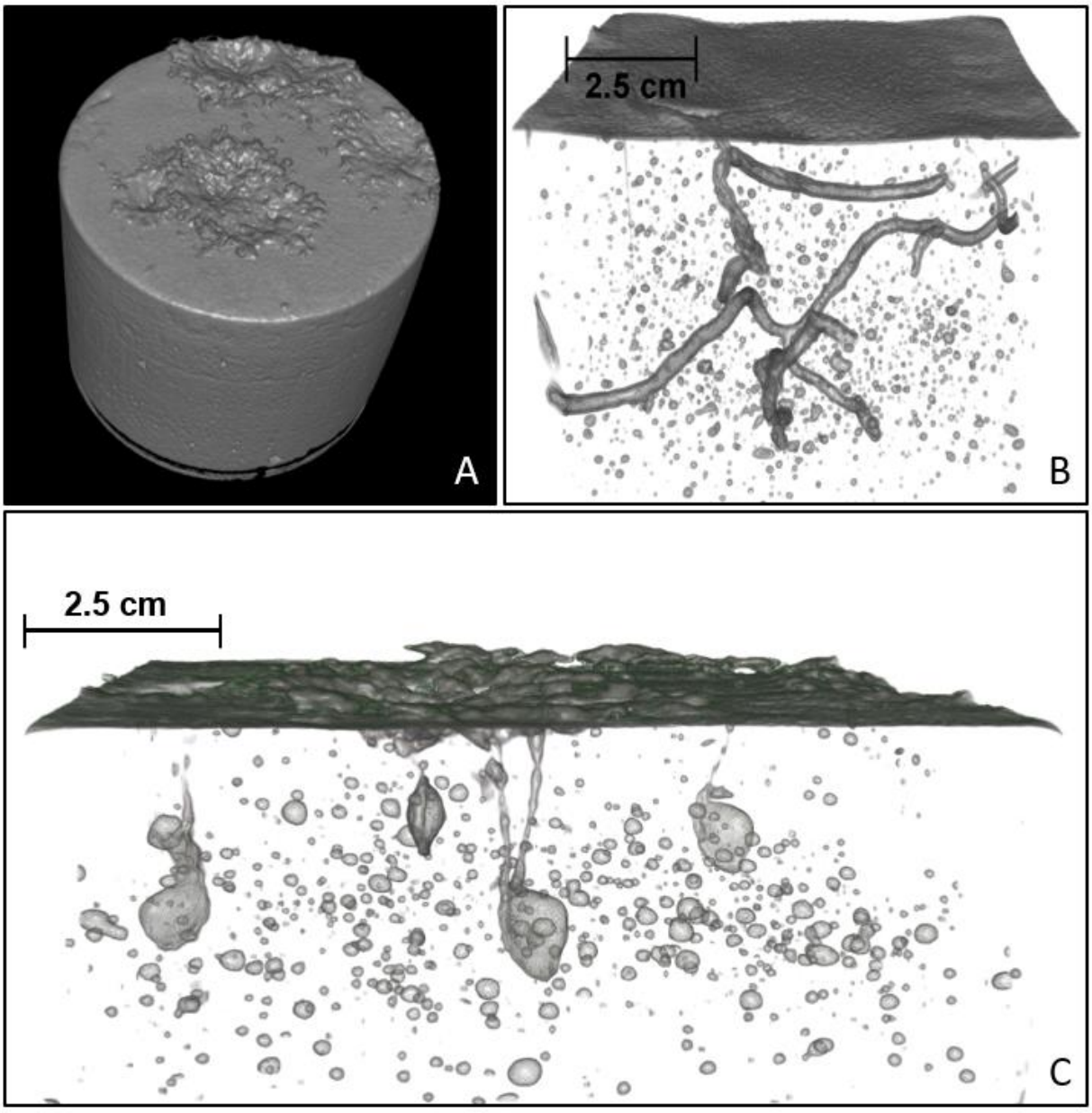

Figure 3.1

support material+immobilizing agent+indicator
immobilizing agent
(urethane based polymer; D4 or blocked D4)
transparent supporting sheet
(Milar(R) polyester film

Figure 3.2

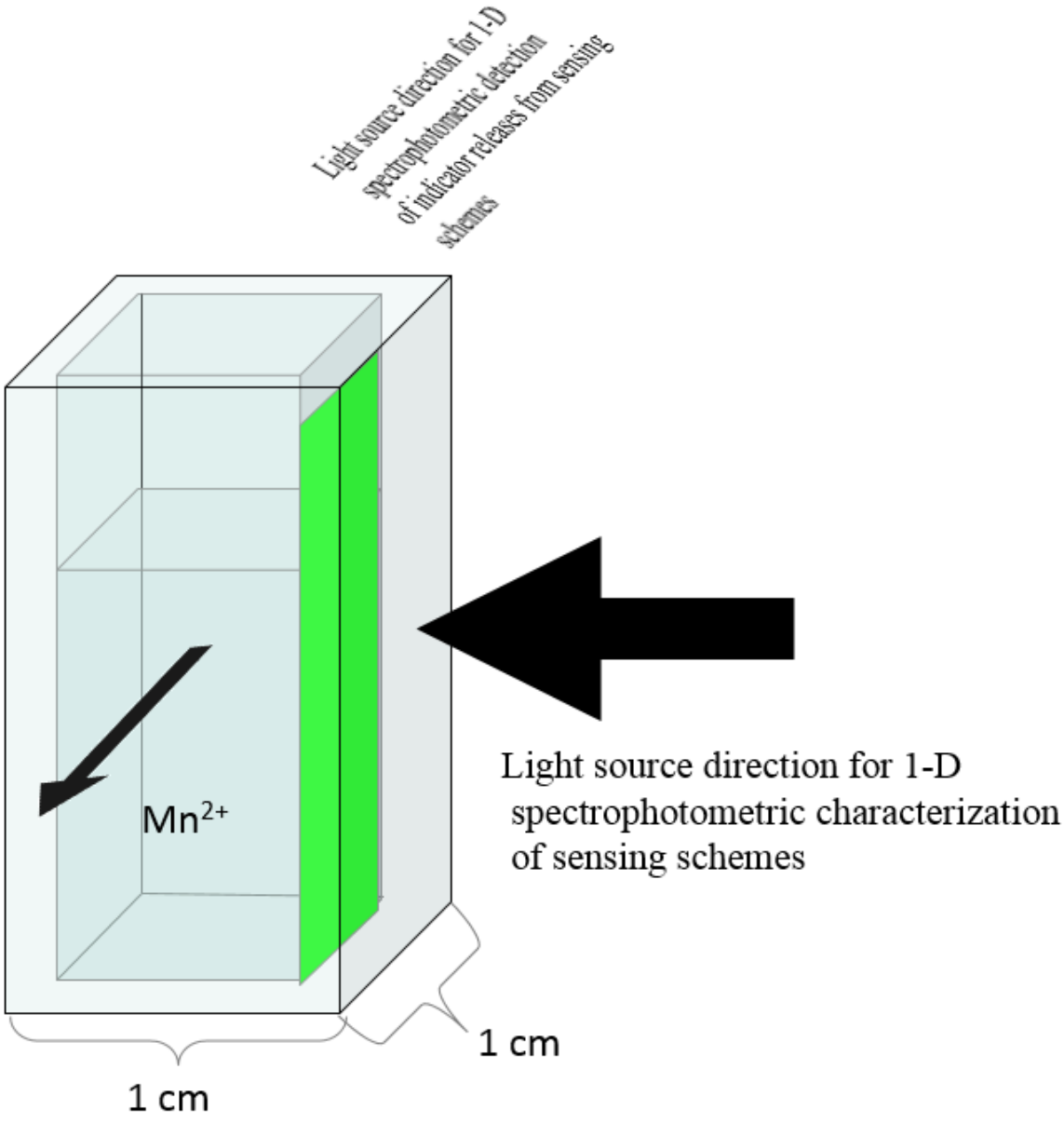
Light source direction for 1-D spectrophotometric detection of indicator releases from sensing schemes
Mn2+
Light source direction for 1-D spectrophotometric characterization of sensing schemes
1 cm
1 cm

Figure 3.3

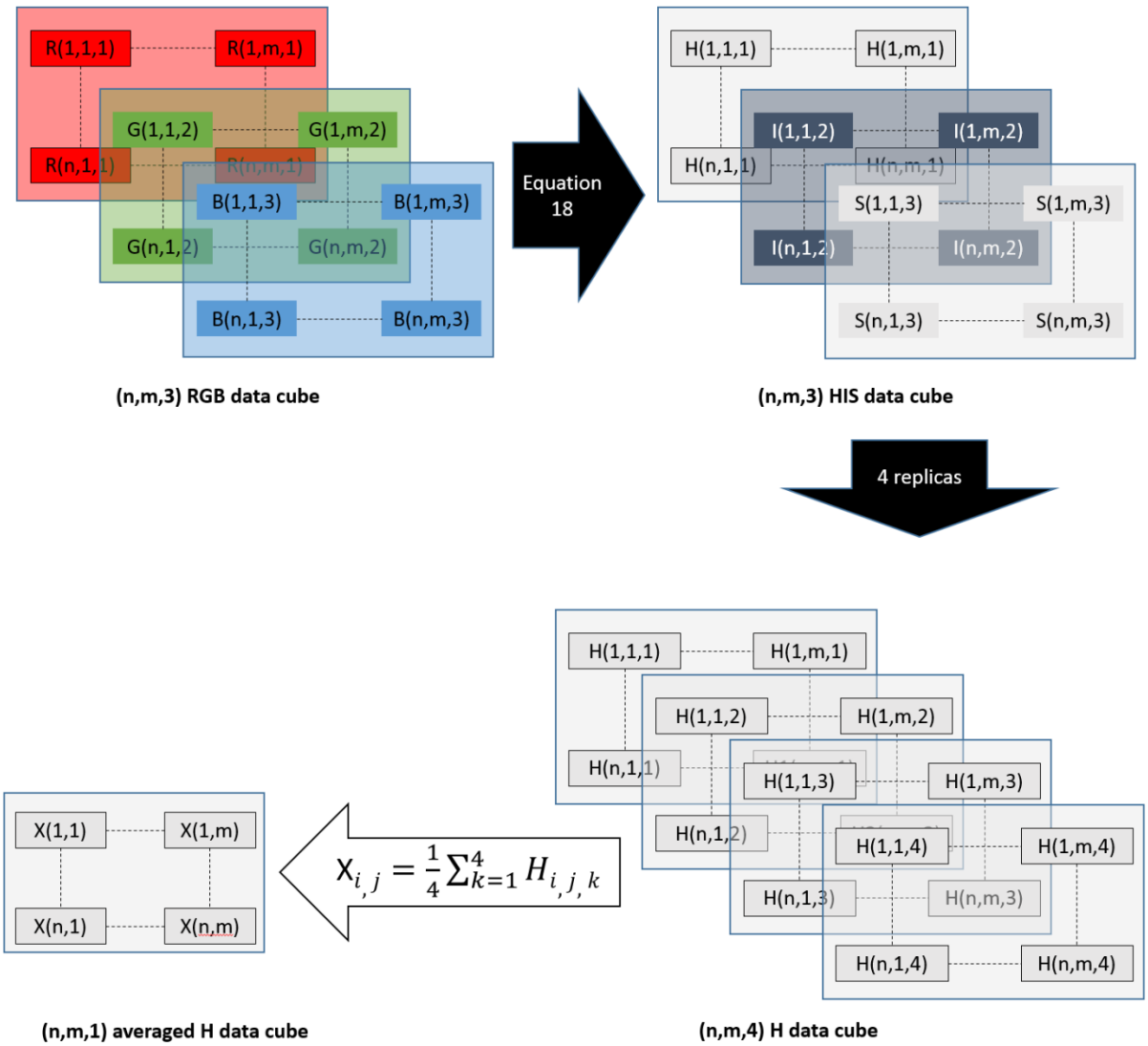
R(1,1,1)
R(1,m,1)
G(1,1,2)
G(1,m,2)
R(n,1,1)
R(n,m,1)
B(1,1,3)
B(1,m,3)
G(n,1,2)
G(n,m,2)
B(n,1,3)
B(n,m,3)
Equation 18
H(1,1,1)
H(1,m,1)
I(1,1,2)
I(1,m,2)
H(n,1,1)
H(n,m,1)
S(1,1,3)
S(1,m,3)
I(n,1,2)
I(n,m,2)
S(n,1,3)
S(n,m,3)
(n,m,3) RGB data cube
(n,m,3) HIS data cube
4 replicas
H(1,1,1)
H(1,m,1)
H(1,1,2)
H(1,m,2)
H(n,1,1)
H(1,1,3)
H(1,m,3)
H(n,1,2)
H(1,1,4)
H(1,m,4)
H(n,1,3)
H(n,m,3)
H(n,1,4)
H(n,m,4)
X(1,1)
X(1,m)
X(n,1)
X(n,m)
$x_{i,j} = \frac{1}{4}\sum_{k=1}^{4} H_{i,j,k}$
(n,m,1) averaged H data cube
(n,m,4) H data cube

Figure 3.4

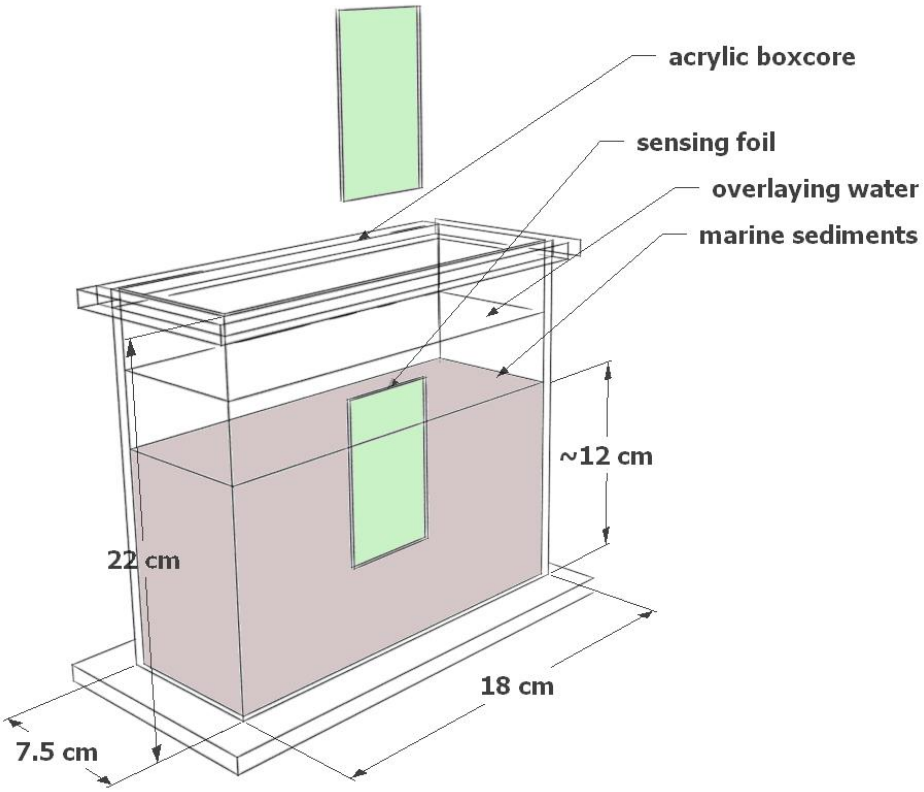
acrylic boxcore
sensing foil
overlaying water
marine sediments
~12 cm
22 cm
18 cm
7.5 cm

Figure 3.5

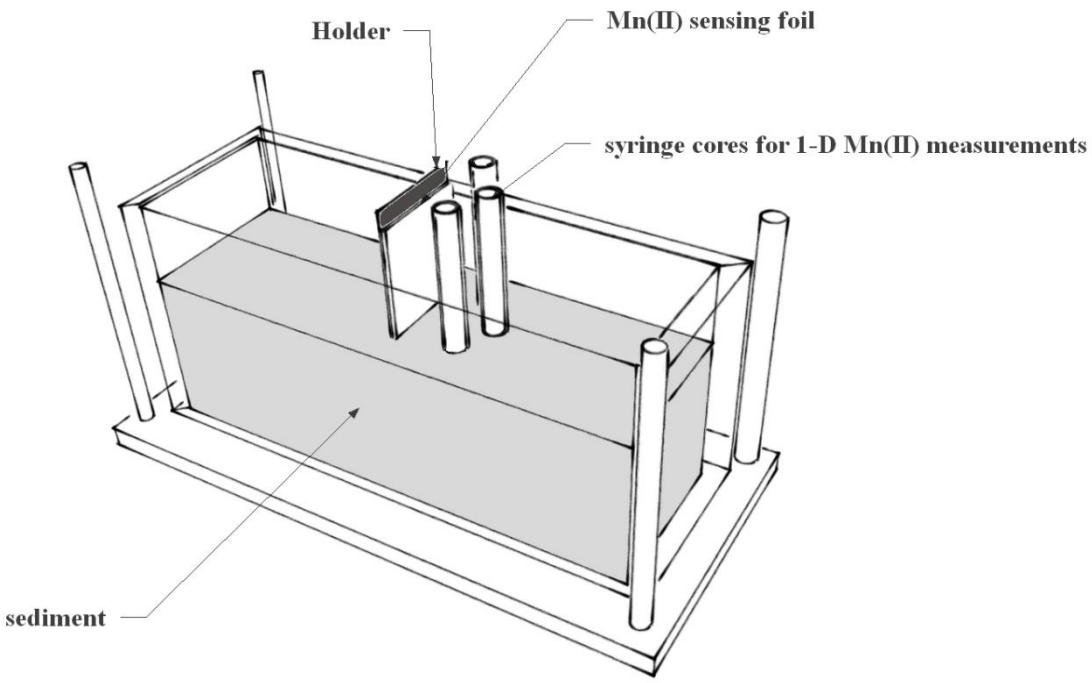
Holder
Mn(II) sensing foil
syringe cores for 1-D Mn(II) measurements
sediment

Figure 3.6

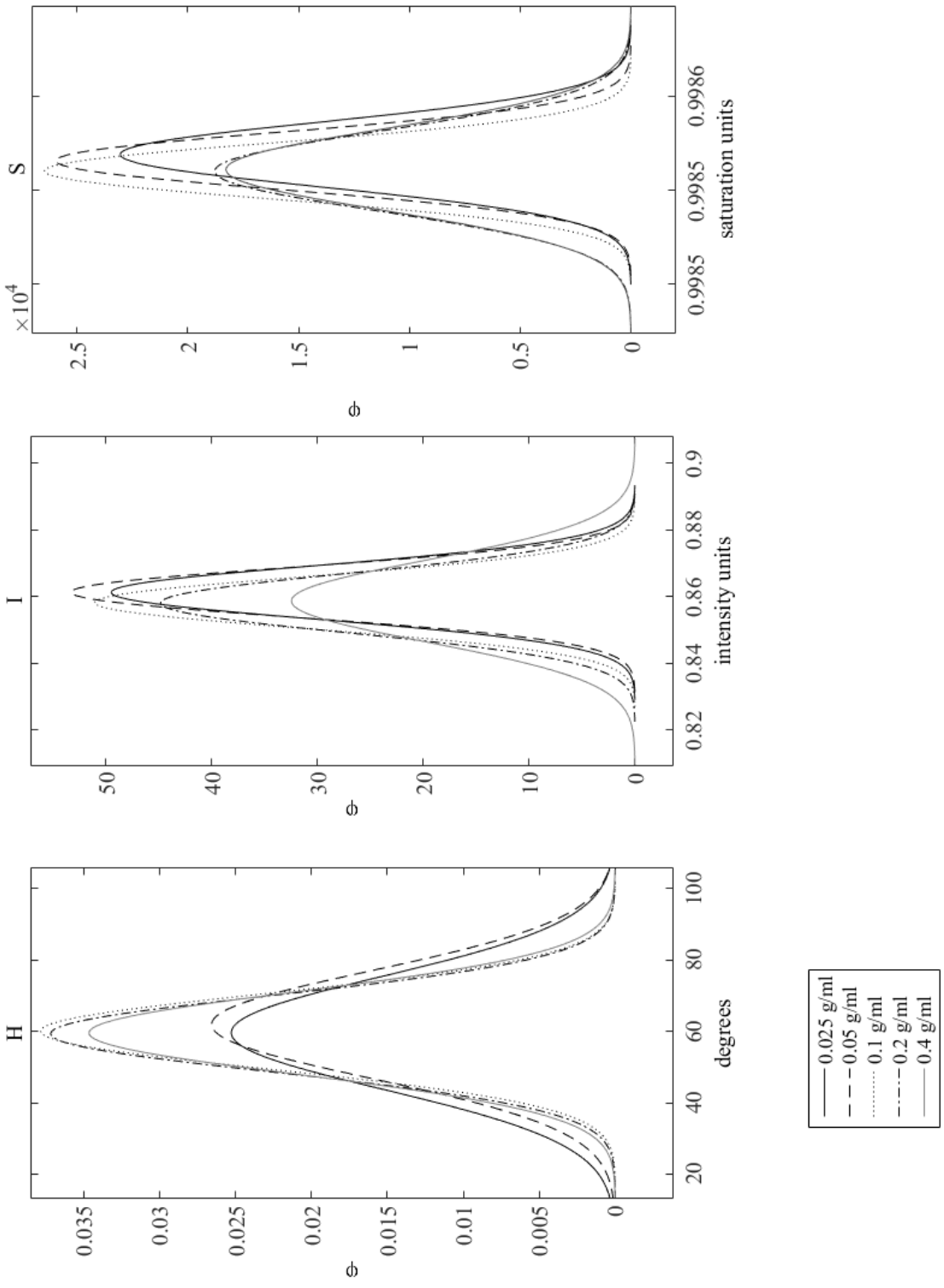
H
degrees
20
40
60
80
100
0.035
0.03
0.025
0.02
0.015
0.01
0.005
0
ϕ
I
intensity units
0.82
0.84
0.86
0.88
0.9
50
40
30
20
10
0
ϕ
S
saturation units
×10^4
0.9985
0.9985
0.9986
2.5
2
1.5
1
0.5
0
ϕ
0.025 g/ml
0.05 g/ml
0.1 g/ml
0.2 g/ml
0.4 g/ml

Figure 3.7

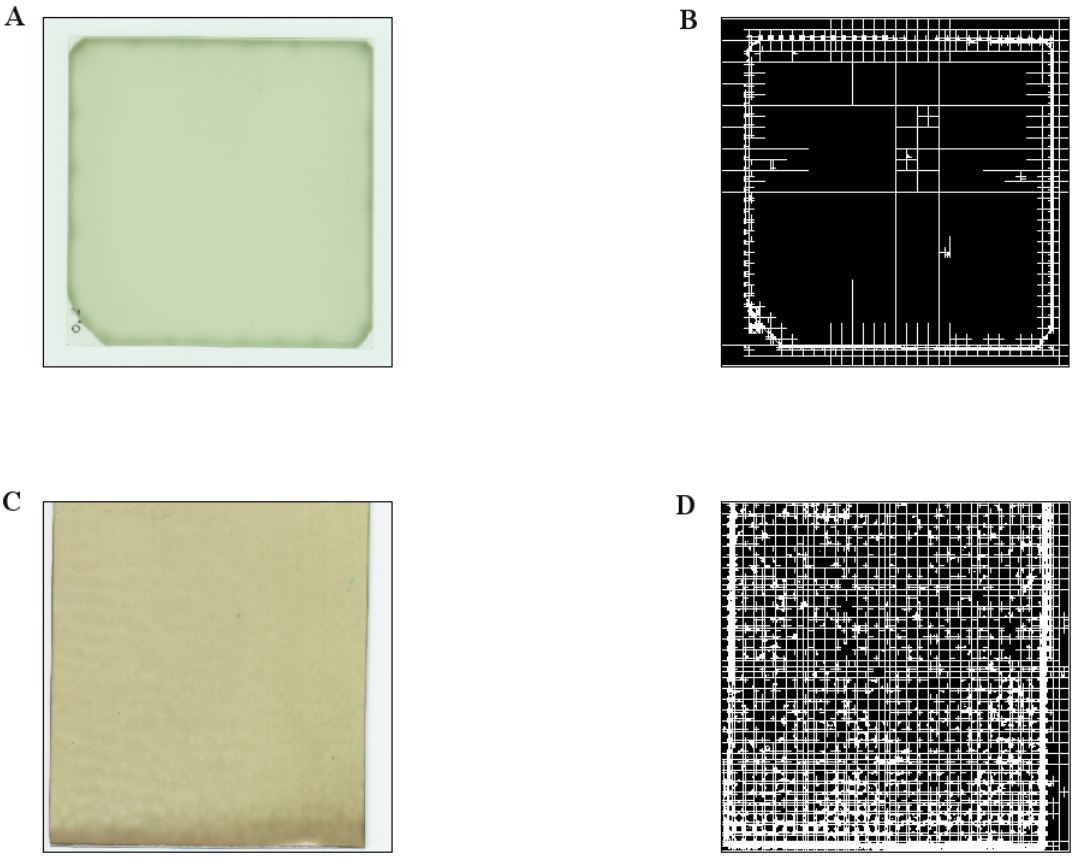

Figure 3.8

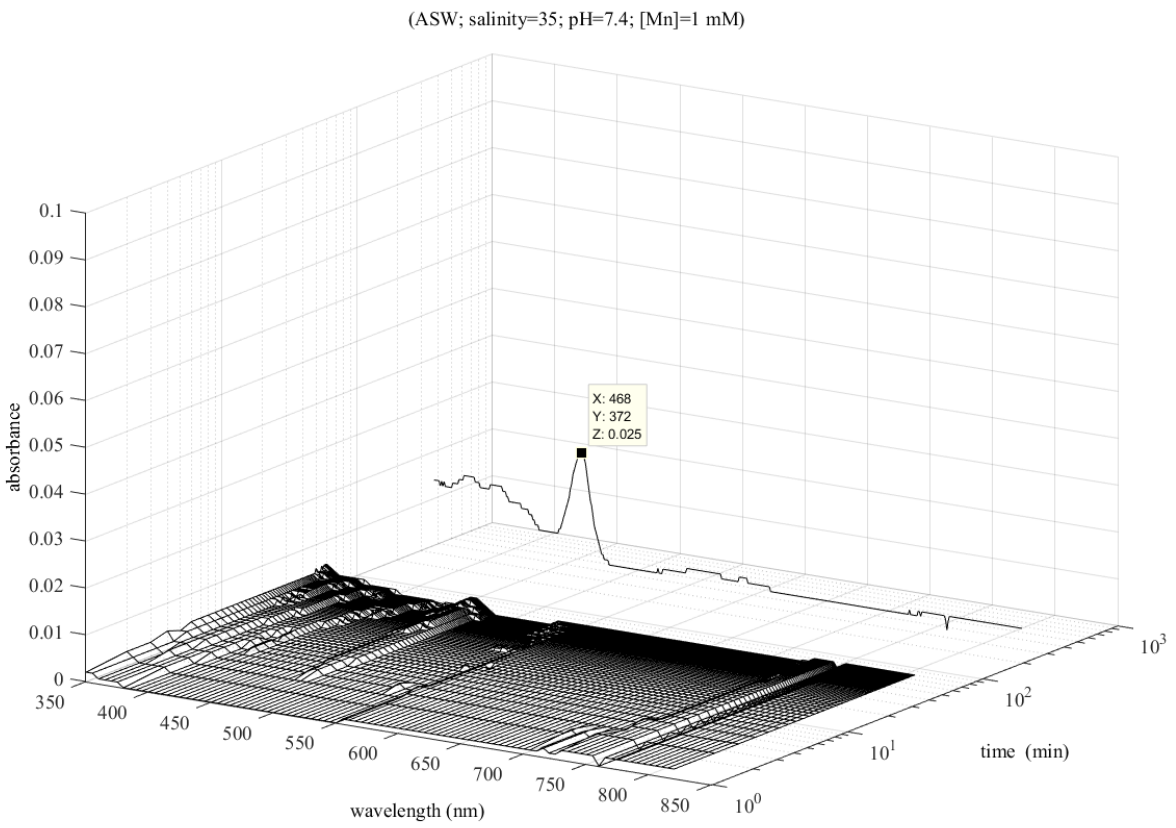
(ASW; salinity=35; pH=7.4; [Mn]=1 mM)
absorbance
0.1
0.09
0.08
0.07
0.06
0.05
0.04
0.03
0.02
0.01
0
X: 468
Y: 372
Z: 0.025
350
400
450
500
550
600
650
700
750
800
850
wavelength (nm)
10^0
10^1
10^2
10^3
time (min)

Figure 3.9

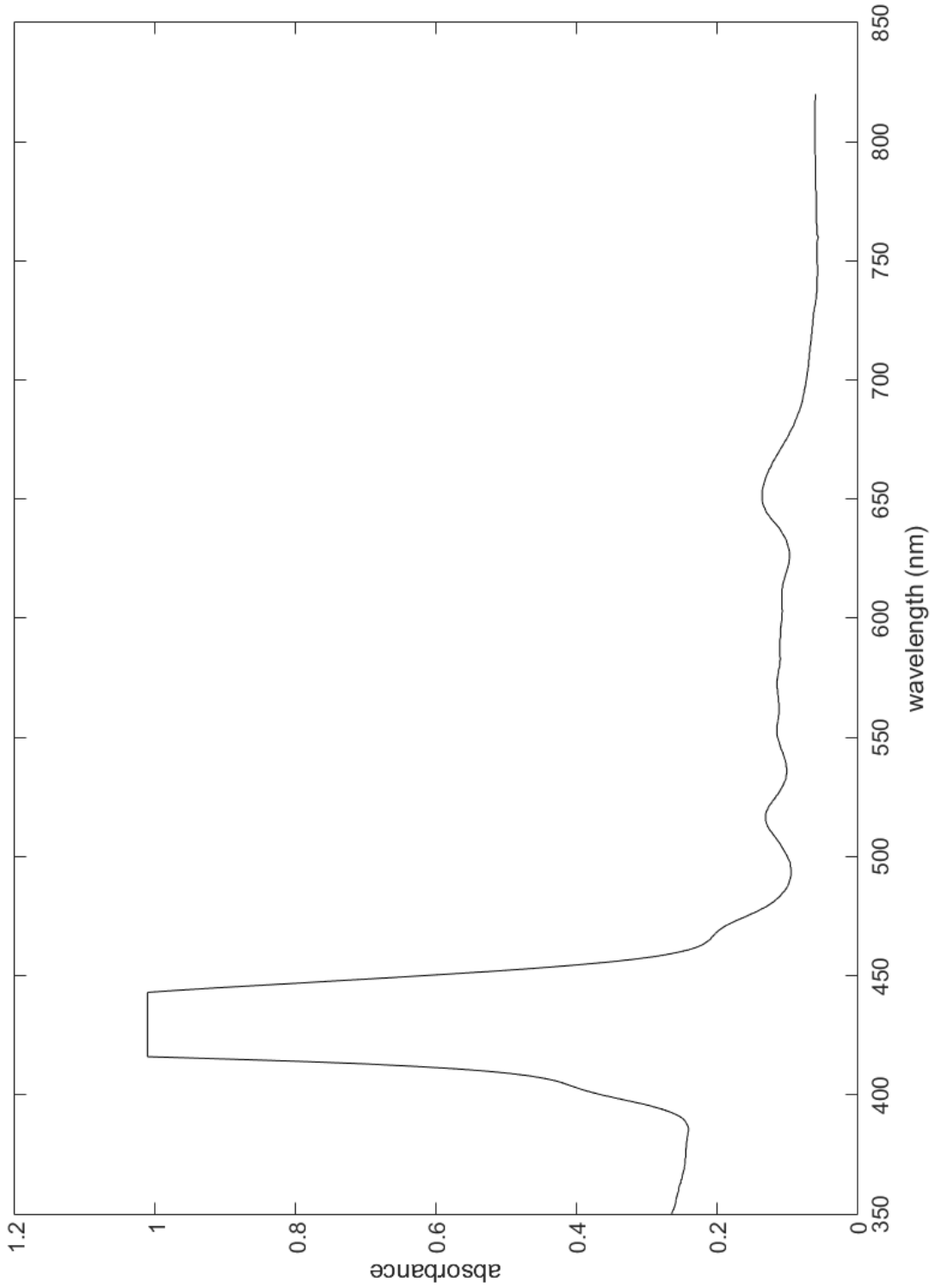
absorbance
wavelength (nm)
1.2
1
0.8
0.6
0.4
0.2
0
350
400
450
500
550
600
650
700
750
800
850

Figure 3.10

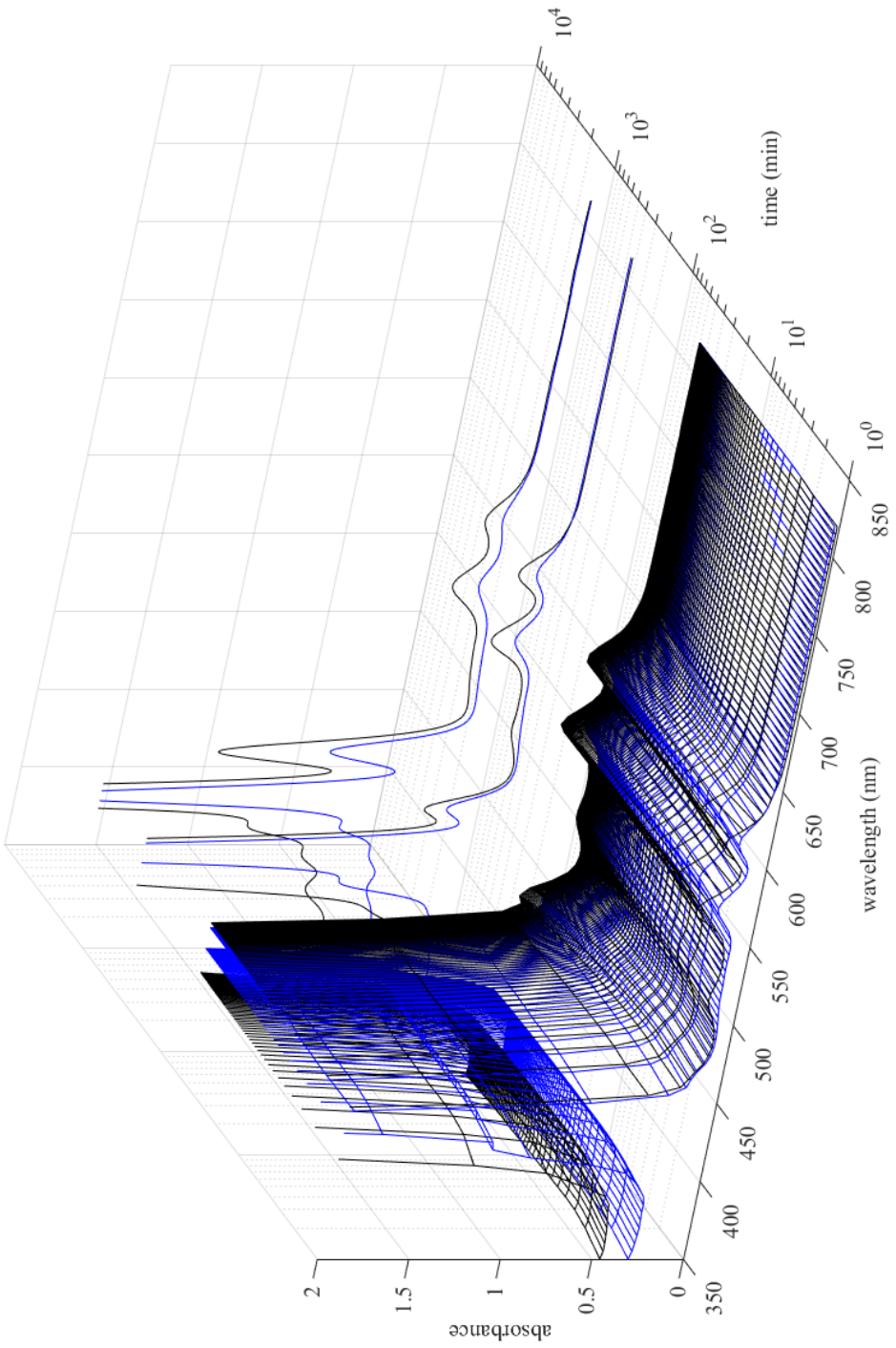
absorbance
2
1.5
1
0.5
0
350
400
450
500
550
600
650
700
750
800
850
wavelength (nm)
10^0
10^1
10^2
10^3
10^4
time (min)

Figure 3.11

A) dextrose

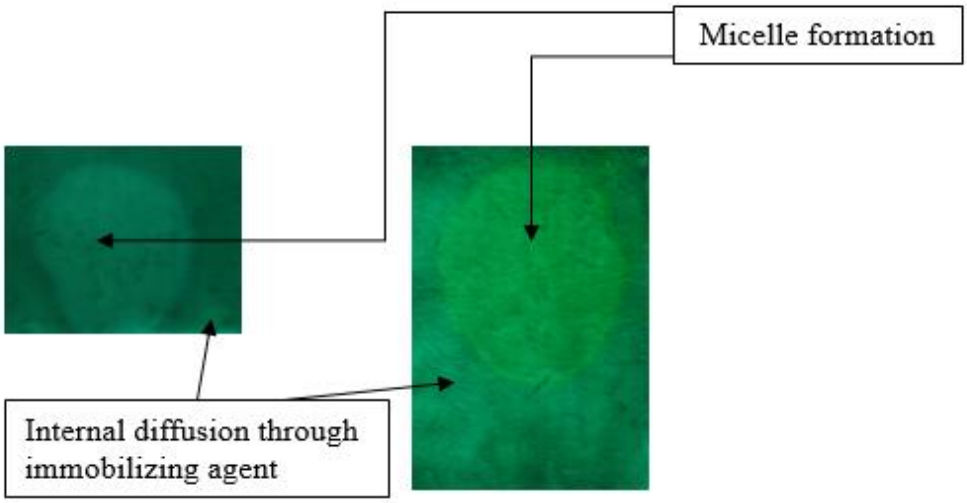

B) Carboxymethyl cellulose

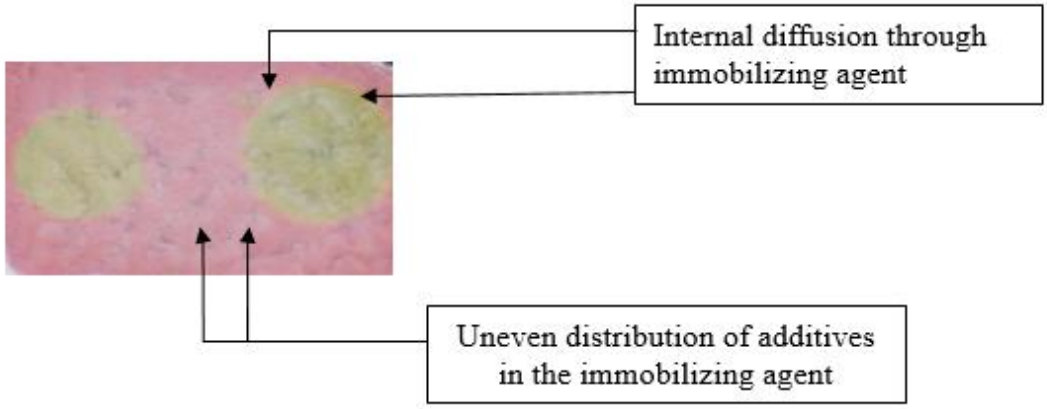

Figure 3.12

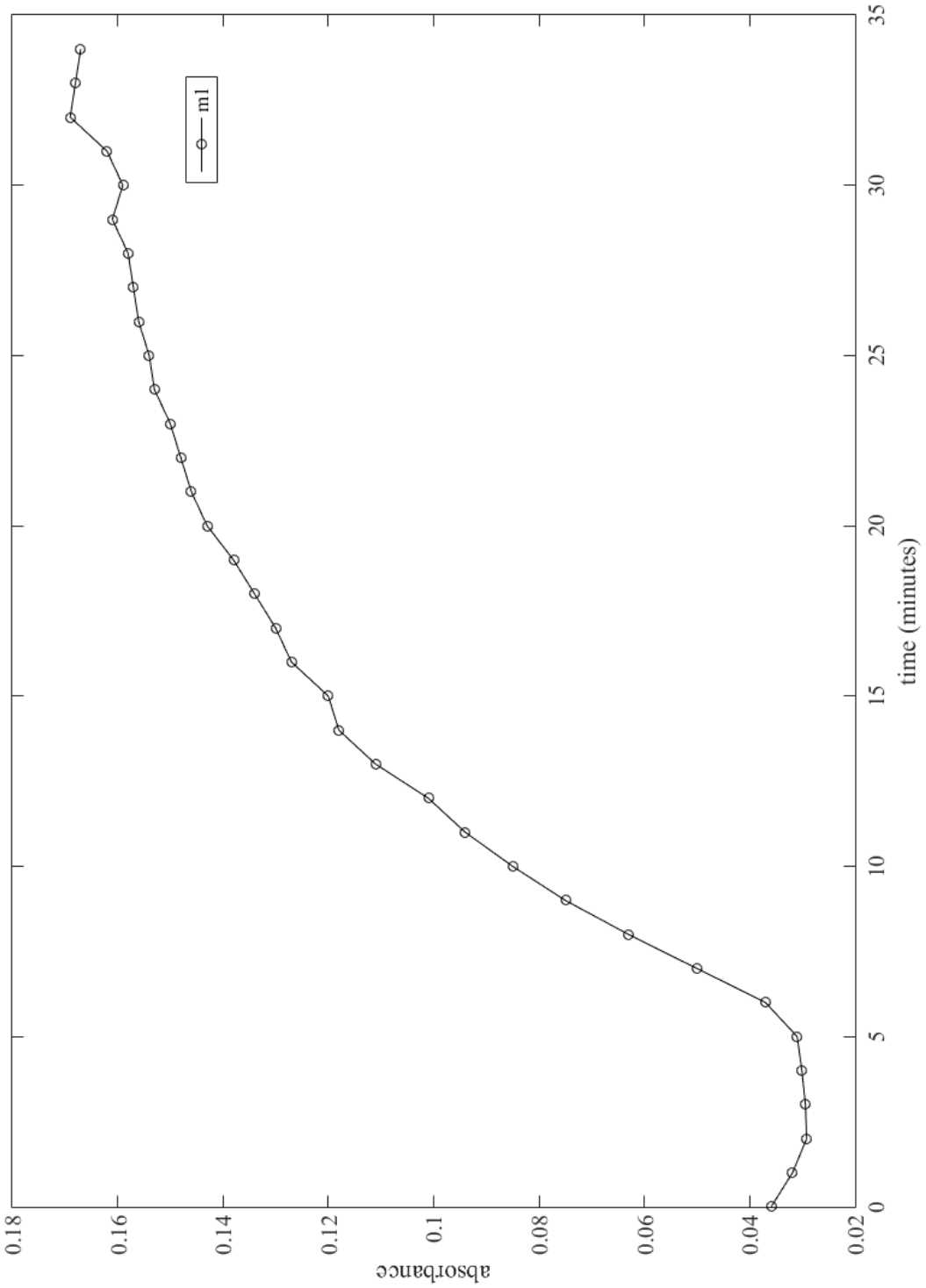
m1
absorbance
time (minutes)
0.18
0.16
0.14
0.12
0.1
0.08
0.06
0.04
0.02
0
5
10
15
20
25
30
35

Figure 3.13

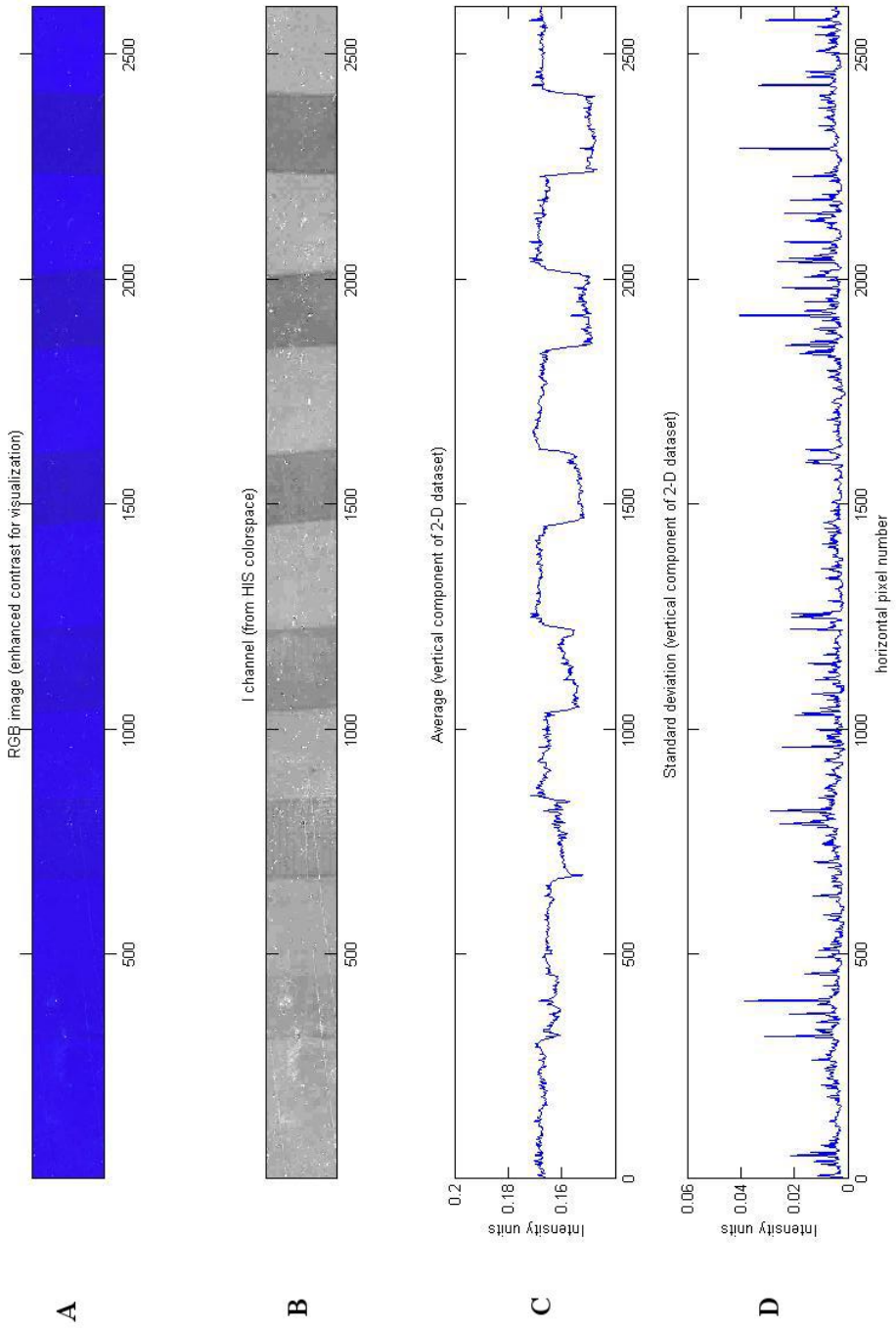
A
RGB image (enhanced contrast for visualization)
500
1000
1500
2000
2500
B
I channel (from HIS colorspace)
500
1000
1500
2000
2500
C
Average (vertical component of 2-D dataset)
0.2
0.18
0.16
Intensity units
0
500
1000
1500
2000
2500
D
Standard deviation (vertical component of 2-D dataset)
0.06
0.04
0.02
Intensity units
0
500
1000
1500
2000
2500
horizontal pixel number

Figure 3.14

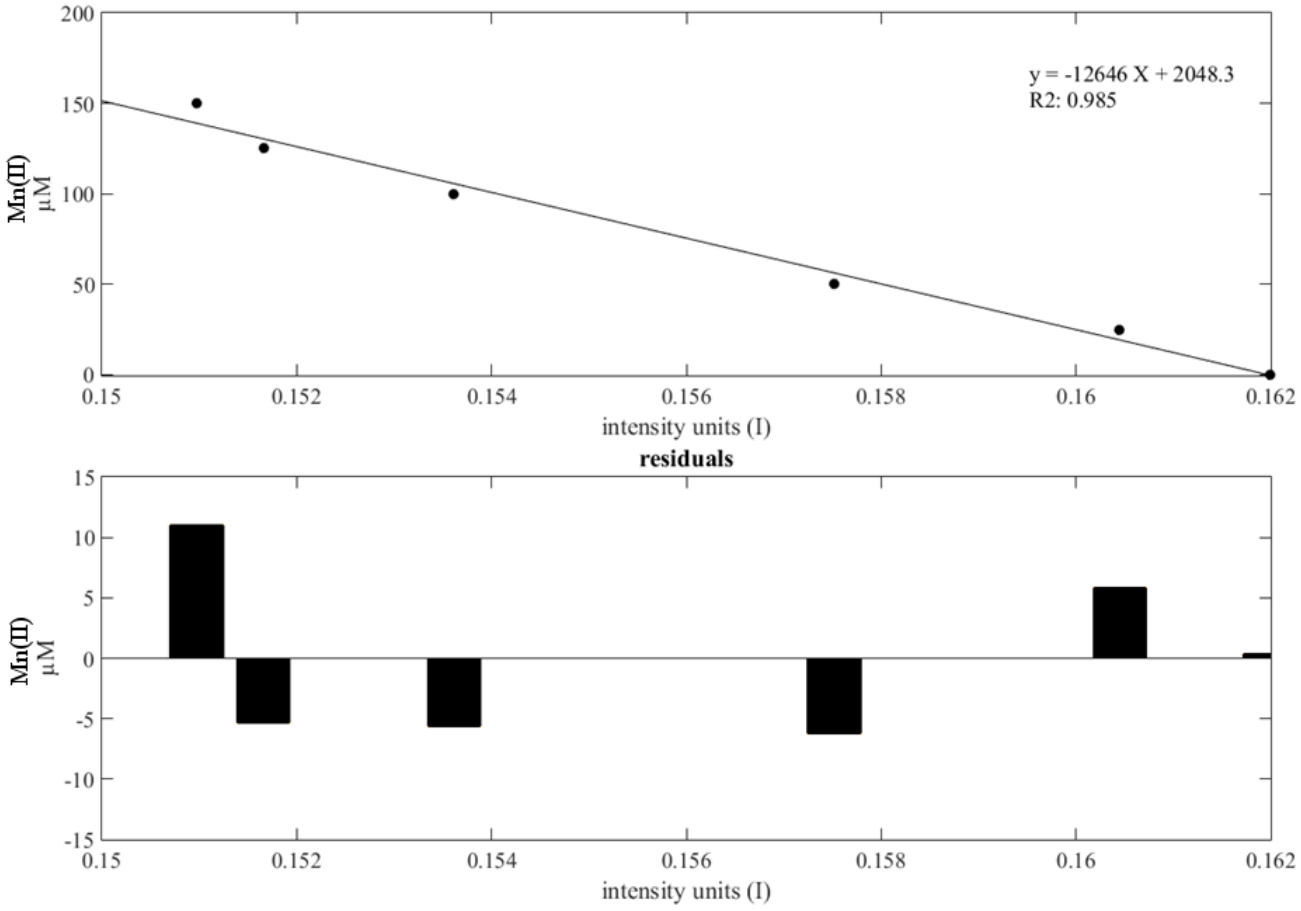
y = -12646 X + 2048.3
R2: 0.985
Mn(II)
µM
intensity units (I)
residuals
Mn(II)
µM
intensity units (I)

Figure 3.15

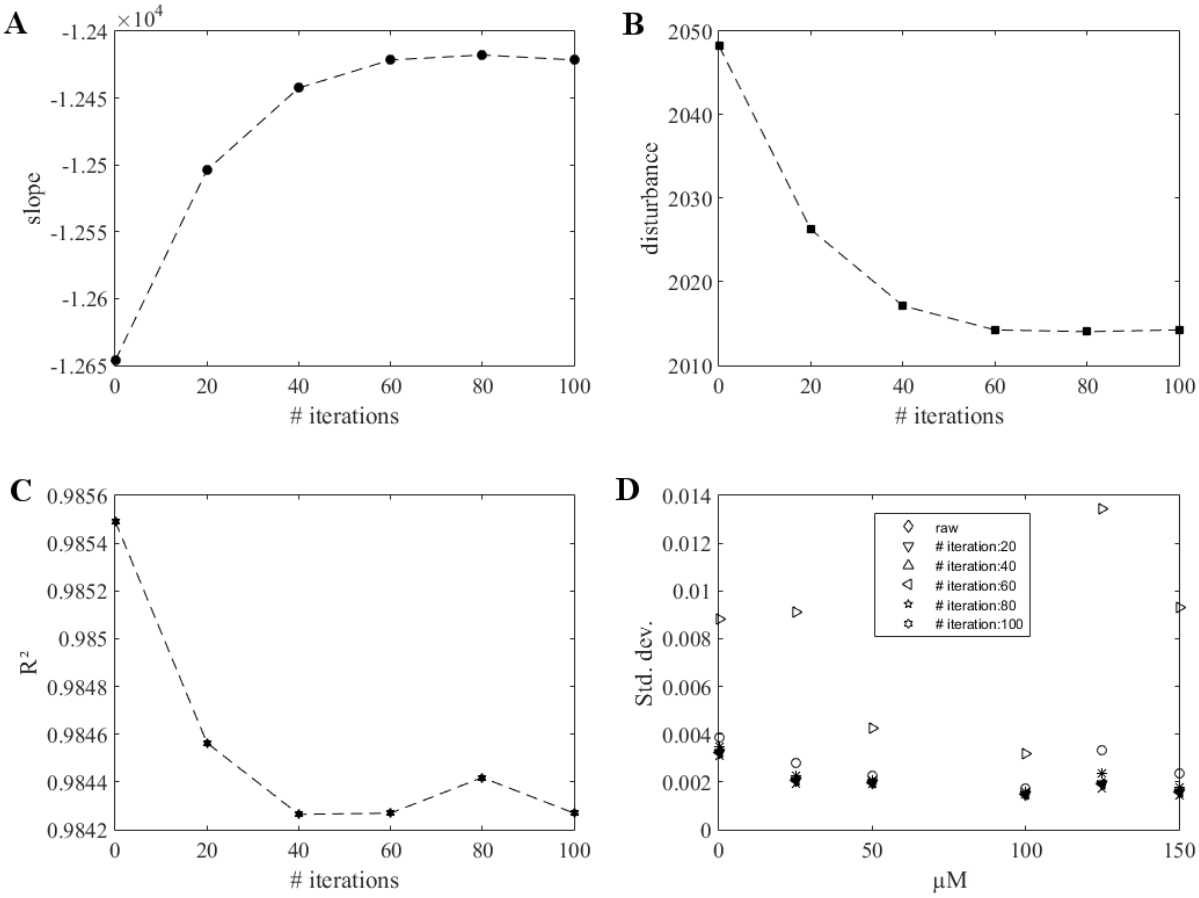
A
×10^4
-1.24
-1.245
-1.25
-1.255
-1.26
-1.265
slope
0
20
40
60
80
100
iterations
B
2050
2040
2030
2020
2010
disturbance
0
20
40
60
80
100
iterations
C
0.9856
0.9854
0.9852
0.985
0.9848
0.9846
0.9844
0.9842
R²
0
20
40
60
80
100
iterations
D
0.014
0.012
0.01
0.008
0.006
0.004
0.002
0
Std. dev.
raw
iteration:20
iteration:40
iteration:60
iteration:80
iteration:100
0
50
100
150
µM

Figure 3.16

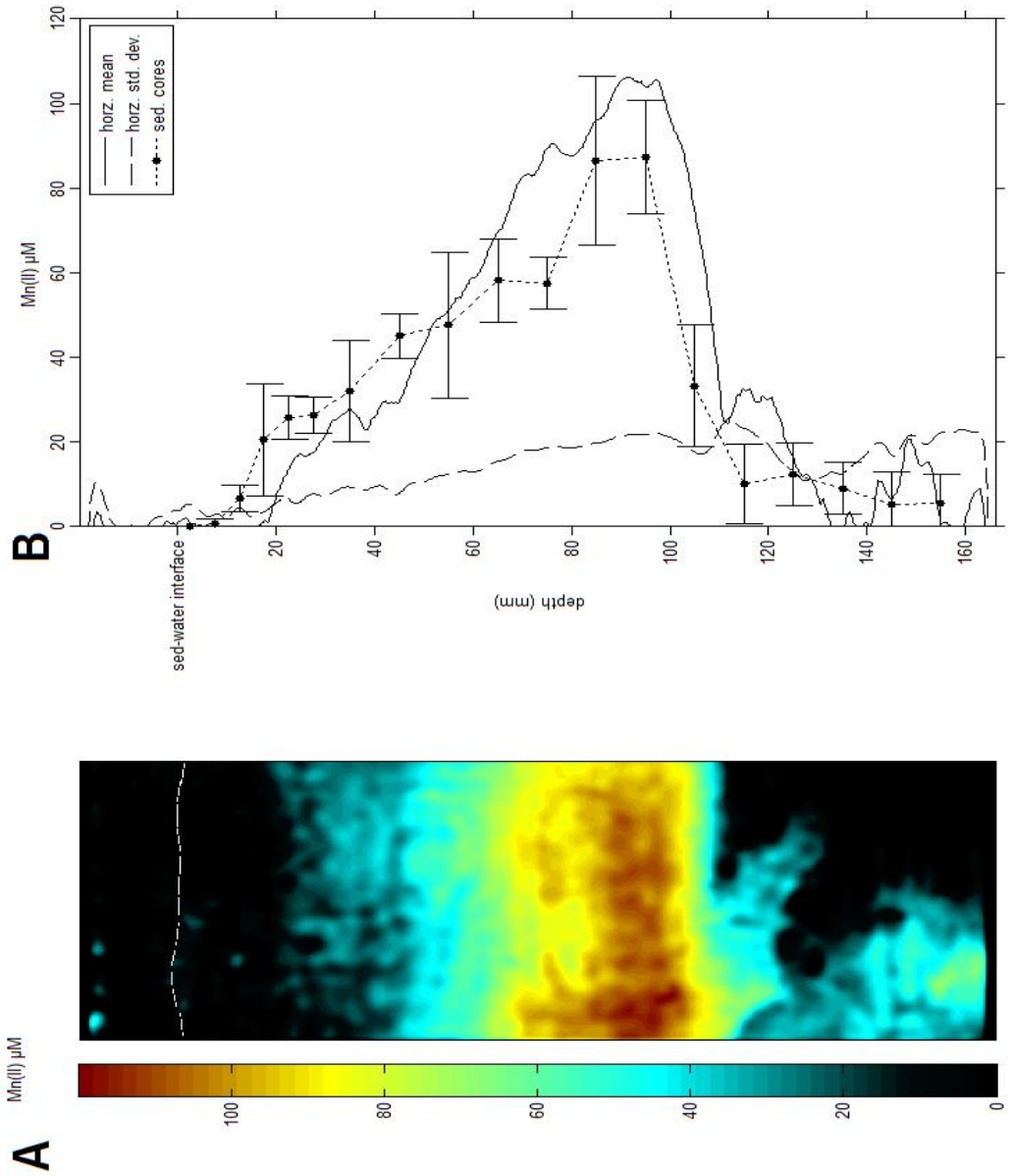
A
Mn(II) µM
100
80
60
40
20
0
B
Mn(II) µM
horz. mean
horz. std. dev.
sed. cores
sed-water interface
depth (mm)
0
20
40
60
80
100
120
140
160

Figure 3.17

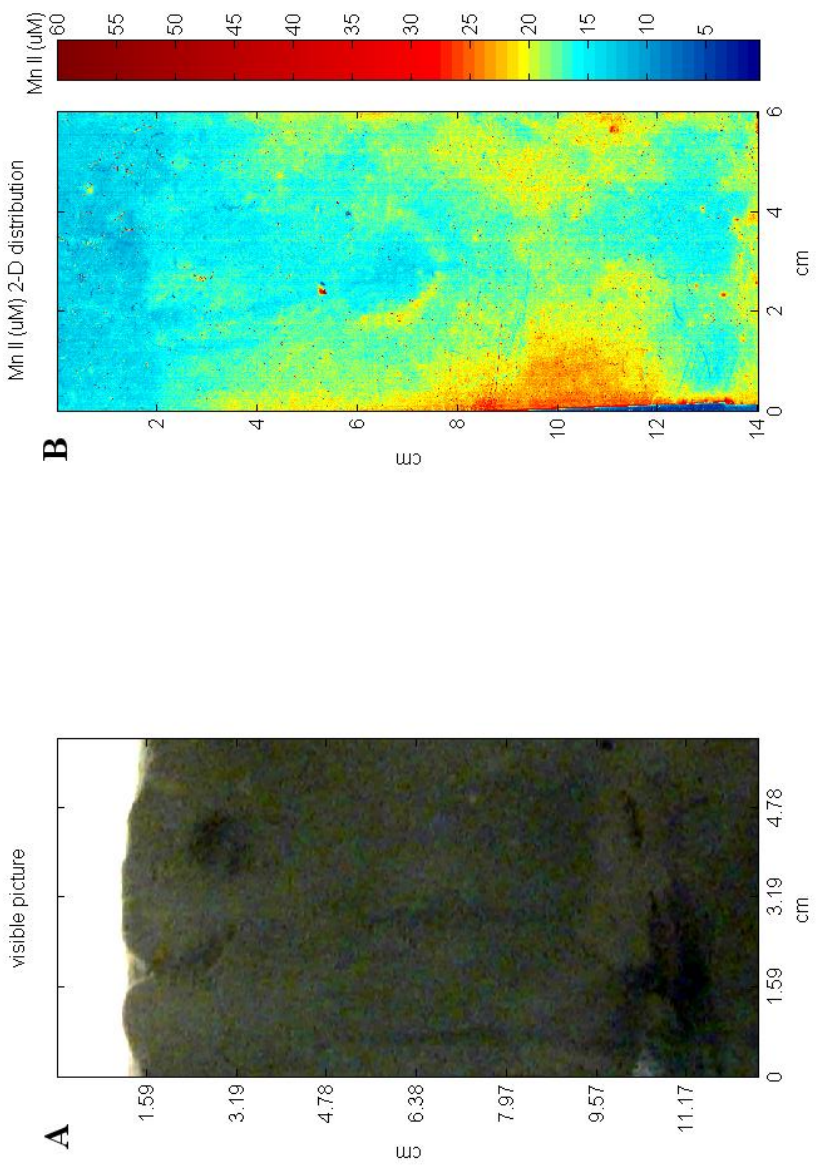
Mn II (uM)
60
55
50
45
40
35
30
25
20
15
10
5
Mn II (uM) 2-D distribution
B
cm
2
4
6
8
10
12
14
0
2
4
6
cm
visible picture
A
cm
1.59
3.19
4.78
6.38
7.97
9.57
11.17
0
1.59
3.19
4.78
cm

Figure 3.18

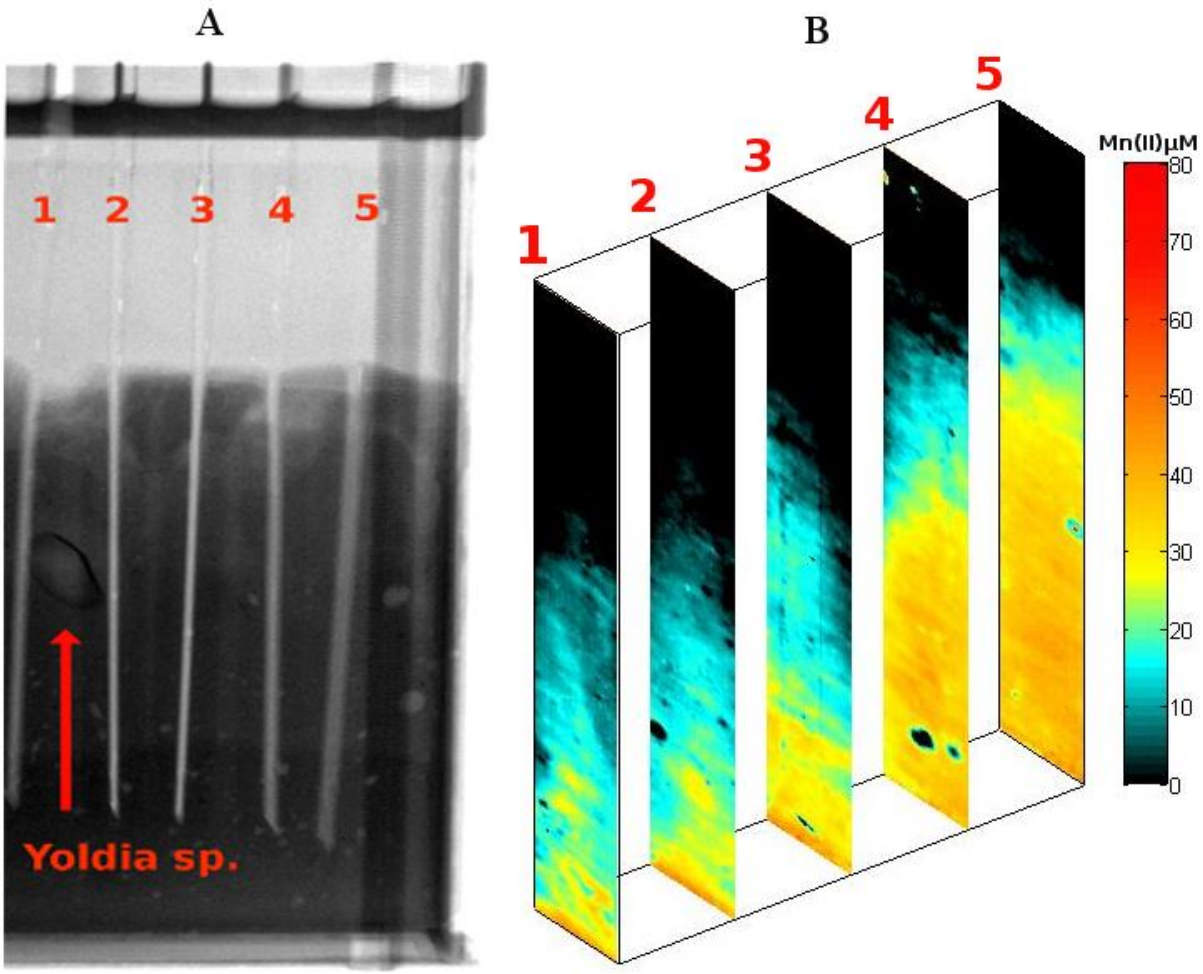

Figure 3.19

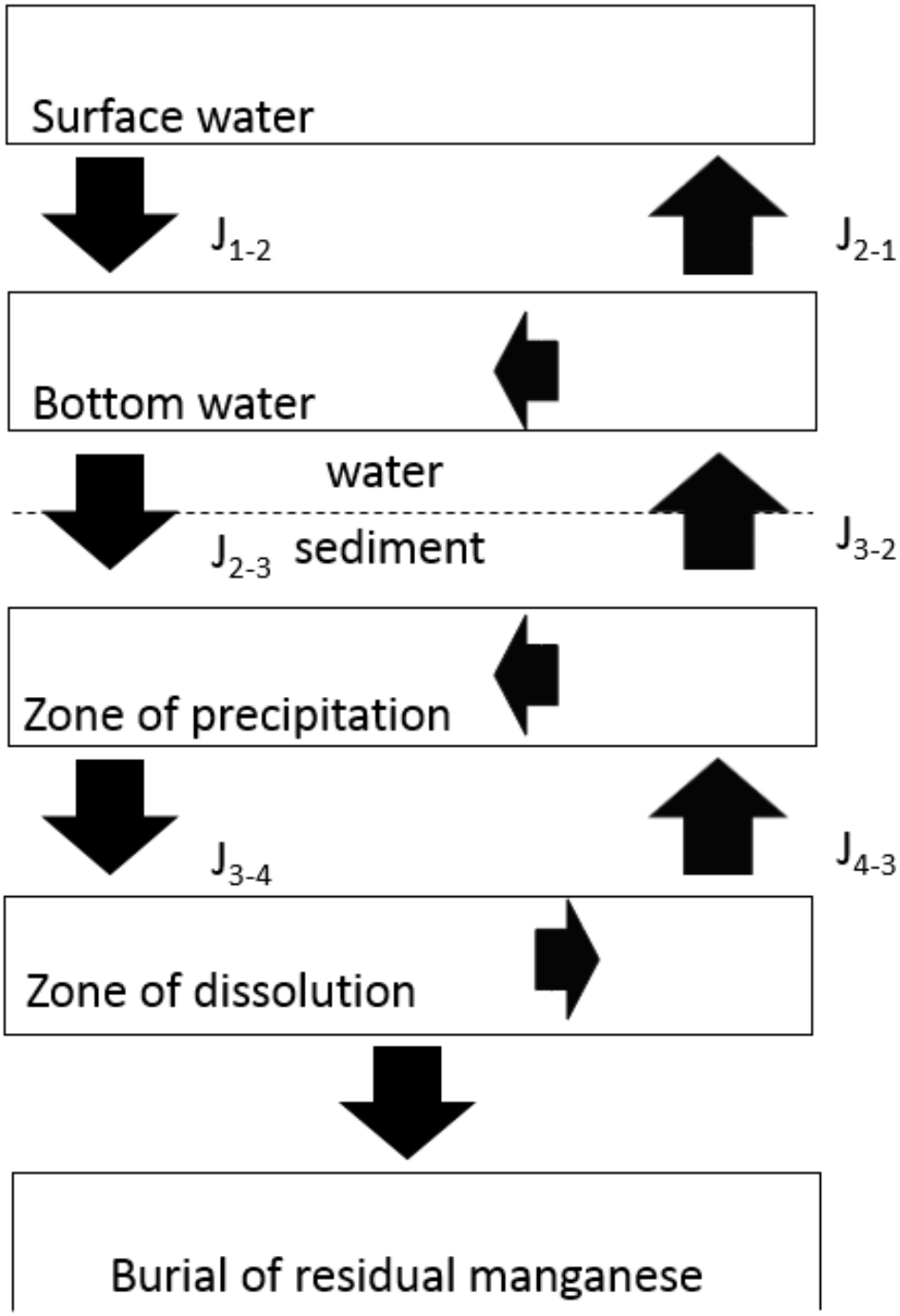
Surface water
J_{1-2}
J_{2-1}
Bottom water
water
J_{2-3} sediment
J_{3-2}
Zone of precipitation
J_{3-4}
J_{4-3}
Zone of dissolution
Burial of residual manganese

Figure 4.1

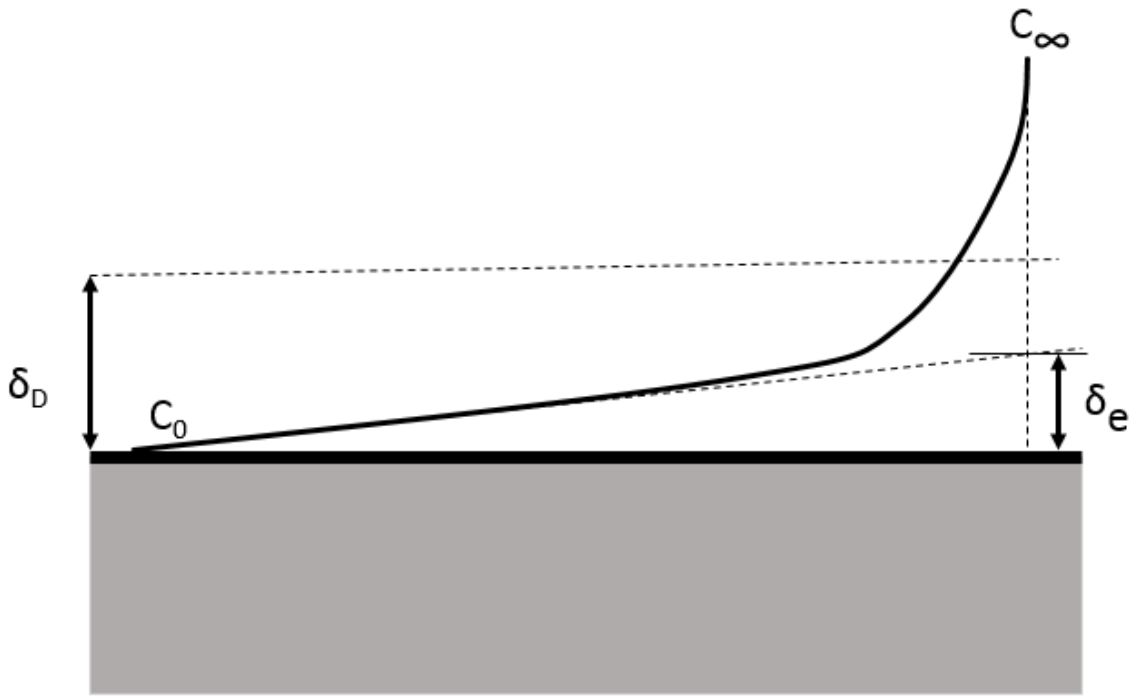

Figure 4.2

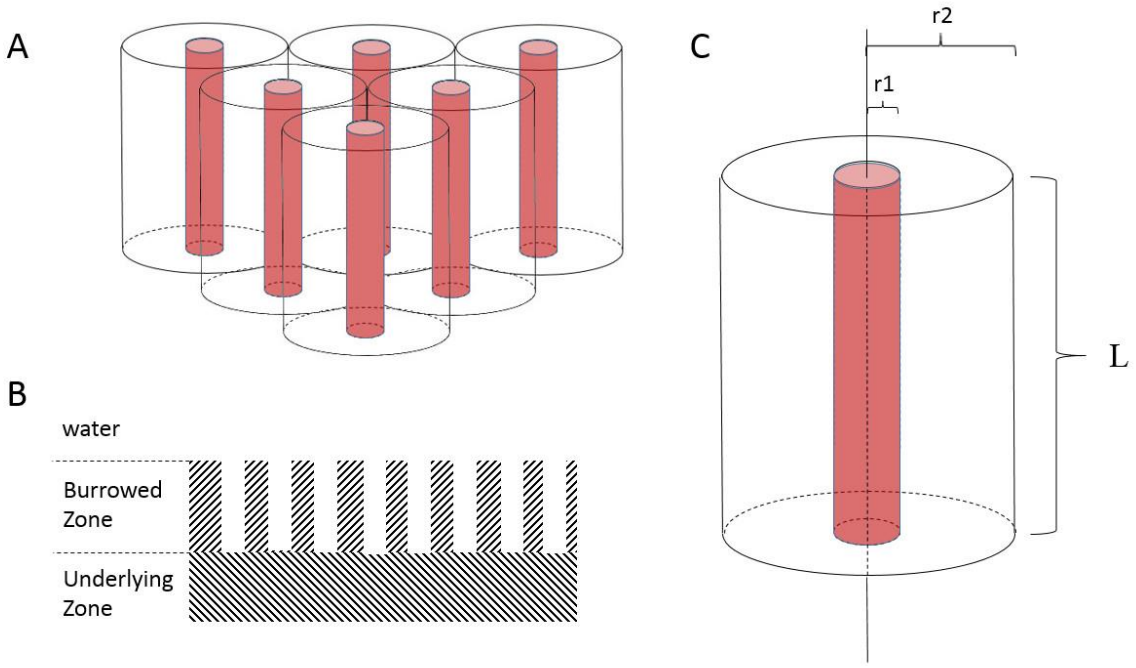

Figure 4.3

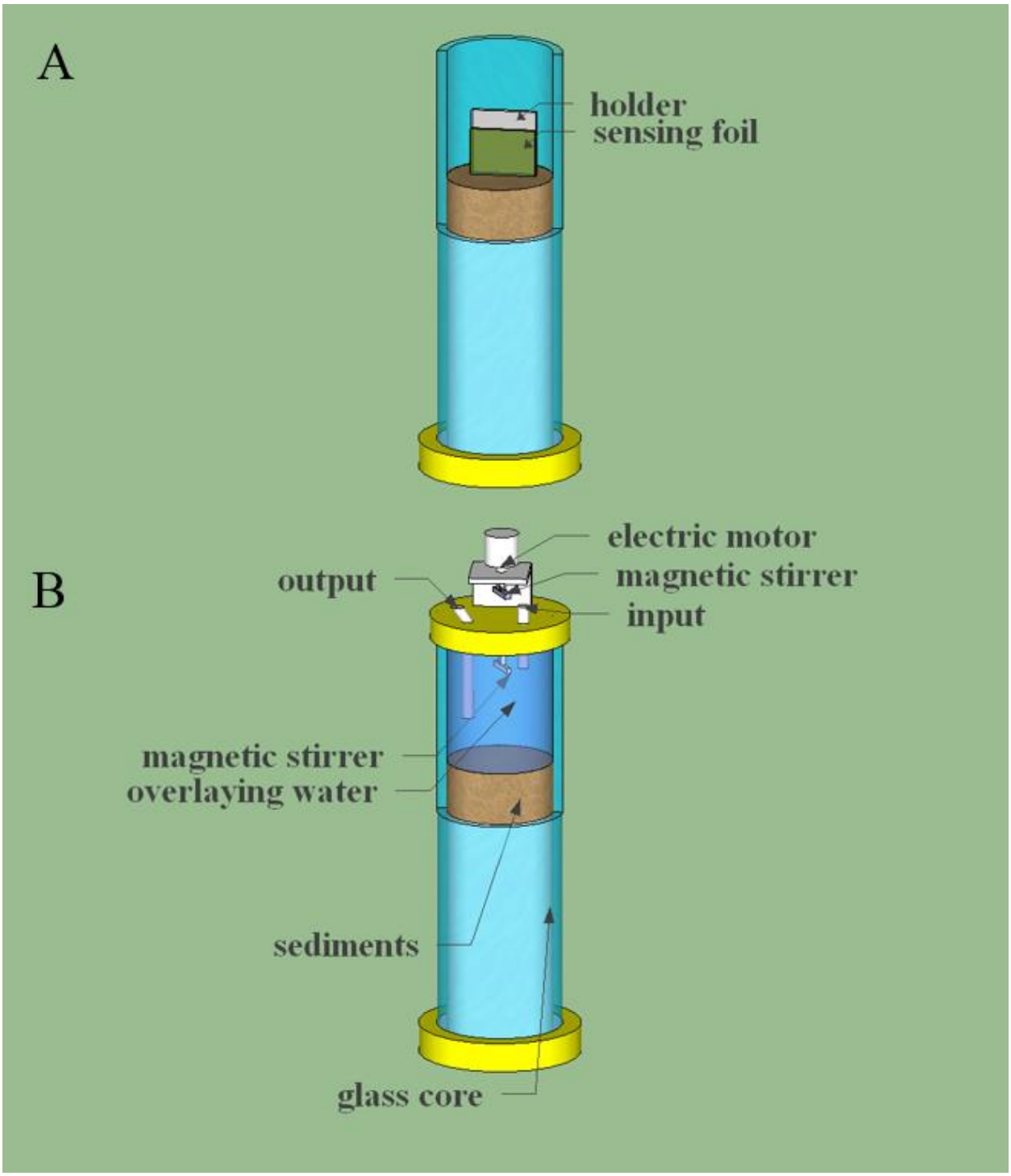
A
holder
sensing foil
B
electric motor
output
magnetic stirrer
input
magnetic stirrer
overlaying water
sediments
glass core

Figure 4.4

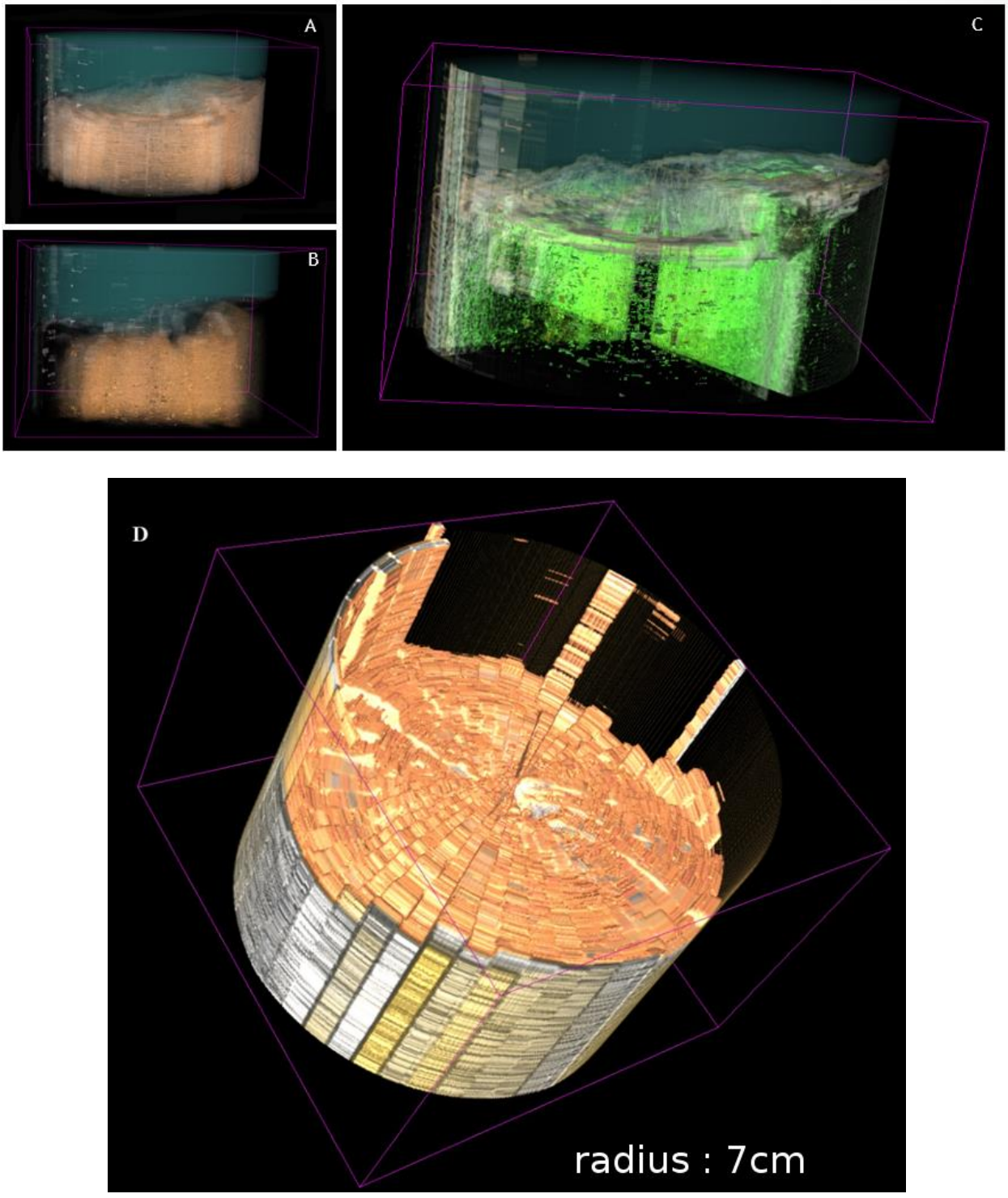

Figure 4.5

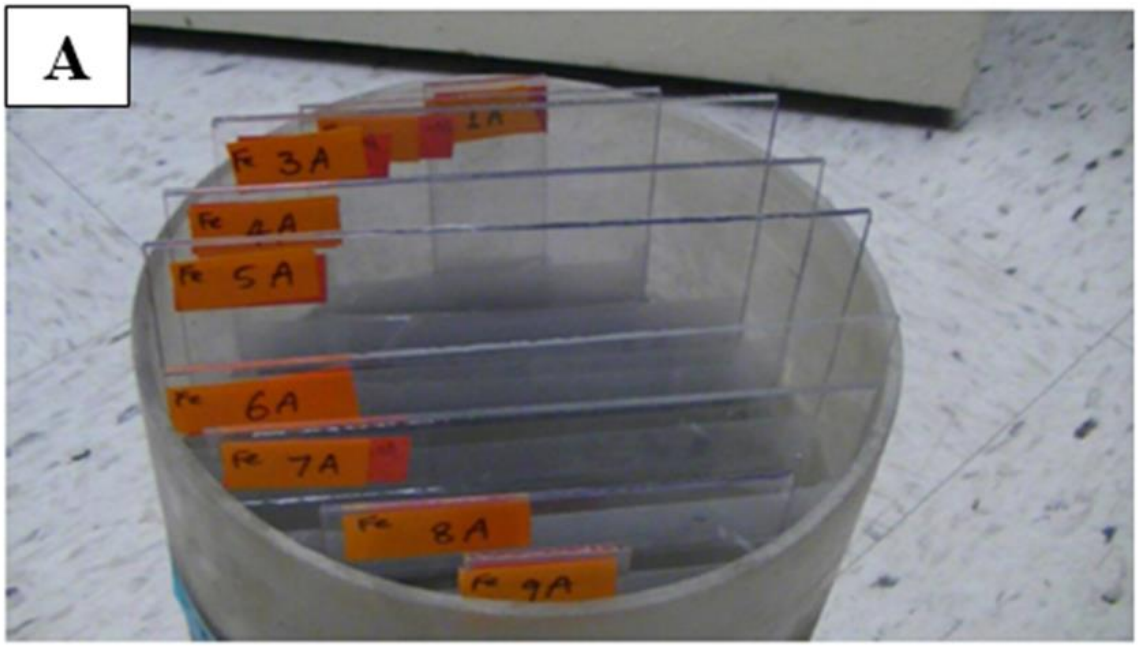
A
1A
Fe 3A
Fe 4A
Fe 5A
Fe 6A
Fe 7A
Fe 8A
Fe 9A

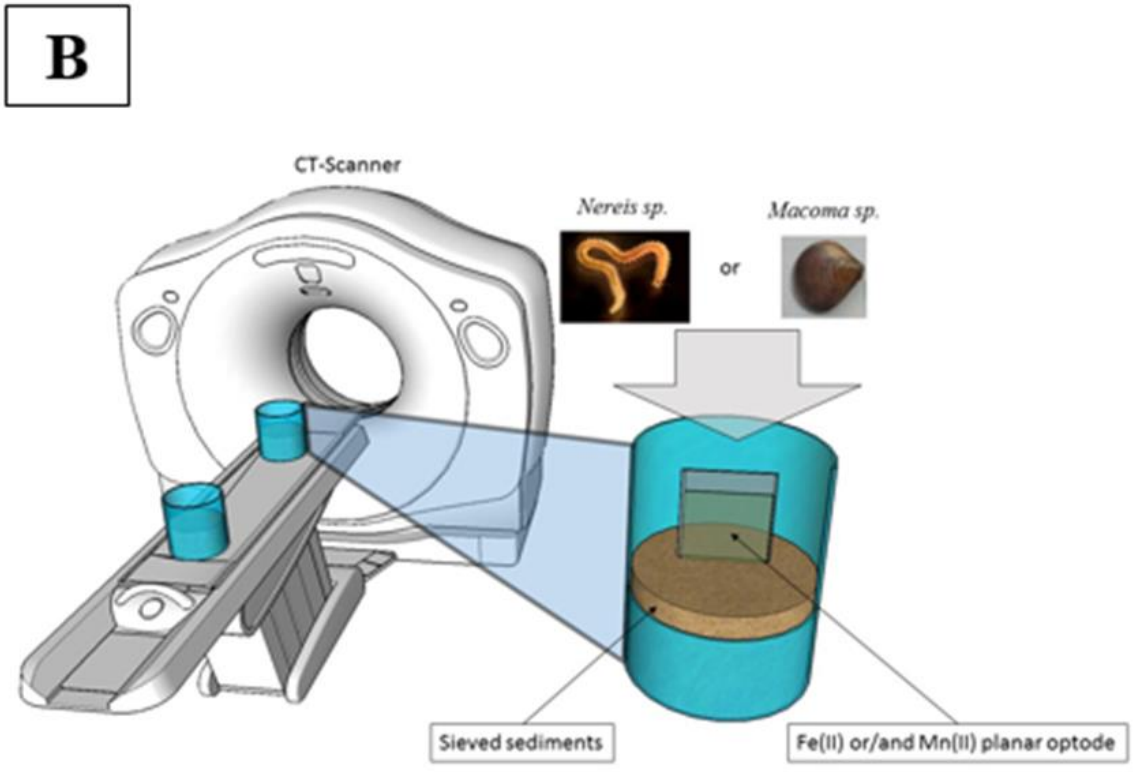
B
CT-Scanner
Nereis sp.
or
Macoma sp.
Sieved sediments
Fe(II) or/and Mn(II) planar optode

Figure 4.6

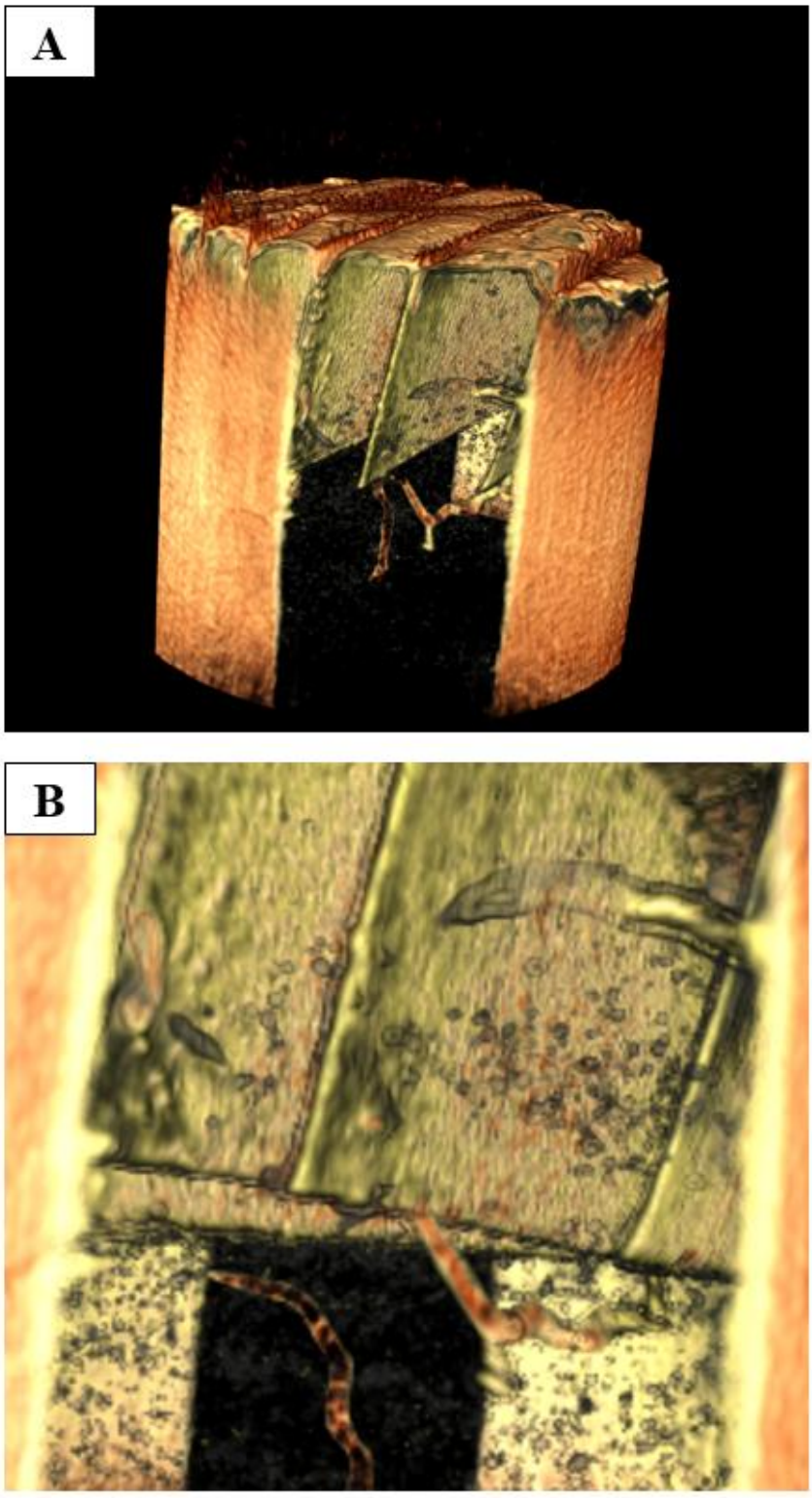

Figure 4.7

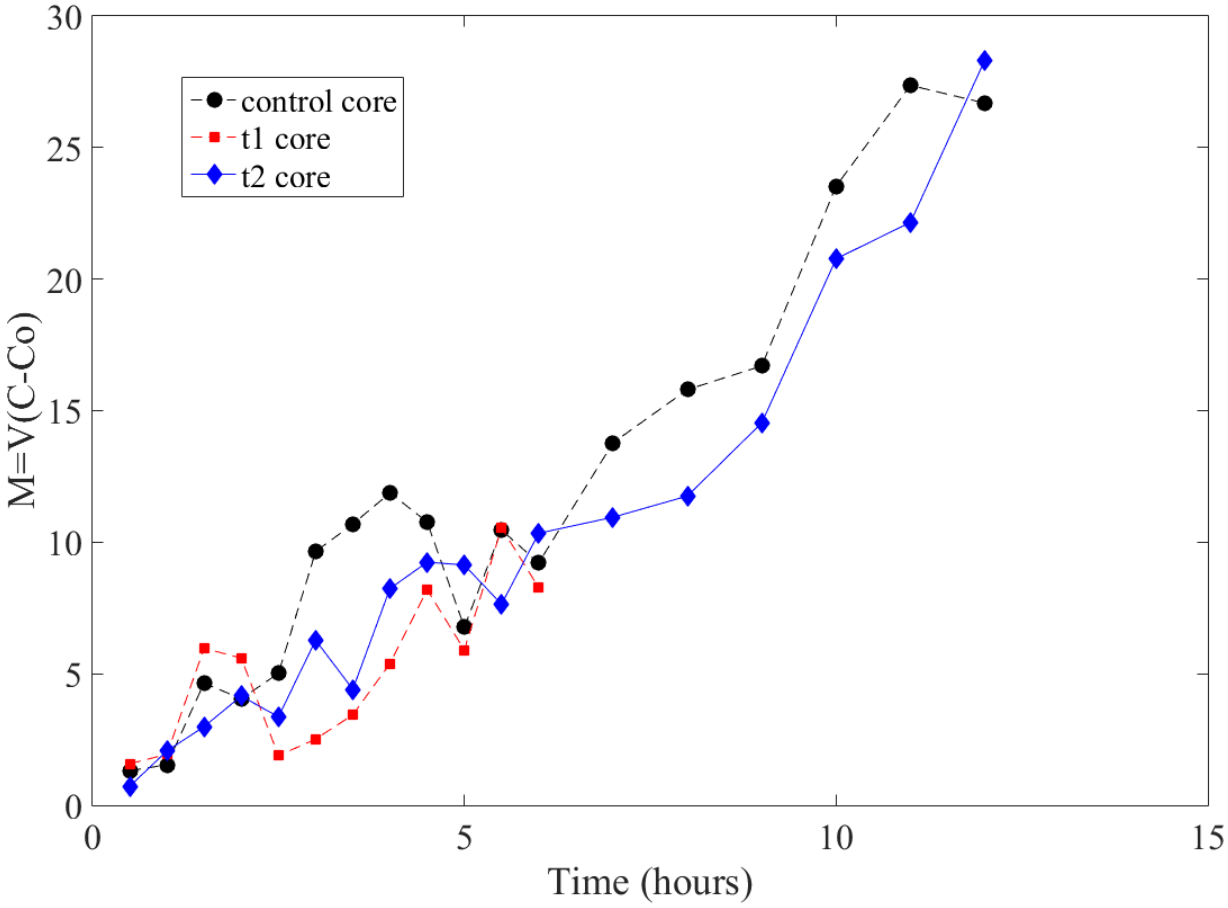

Figure 4.8

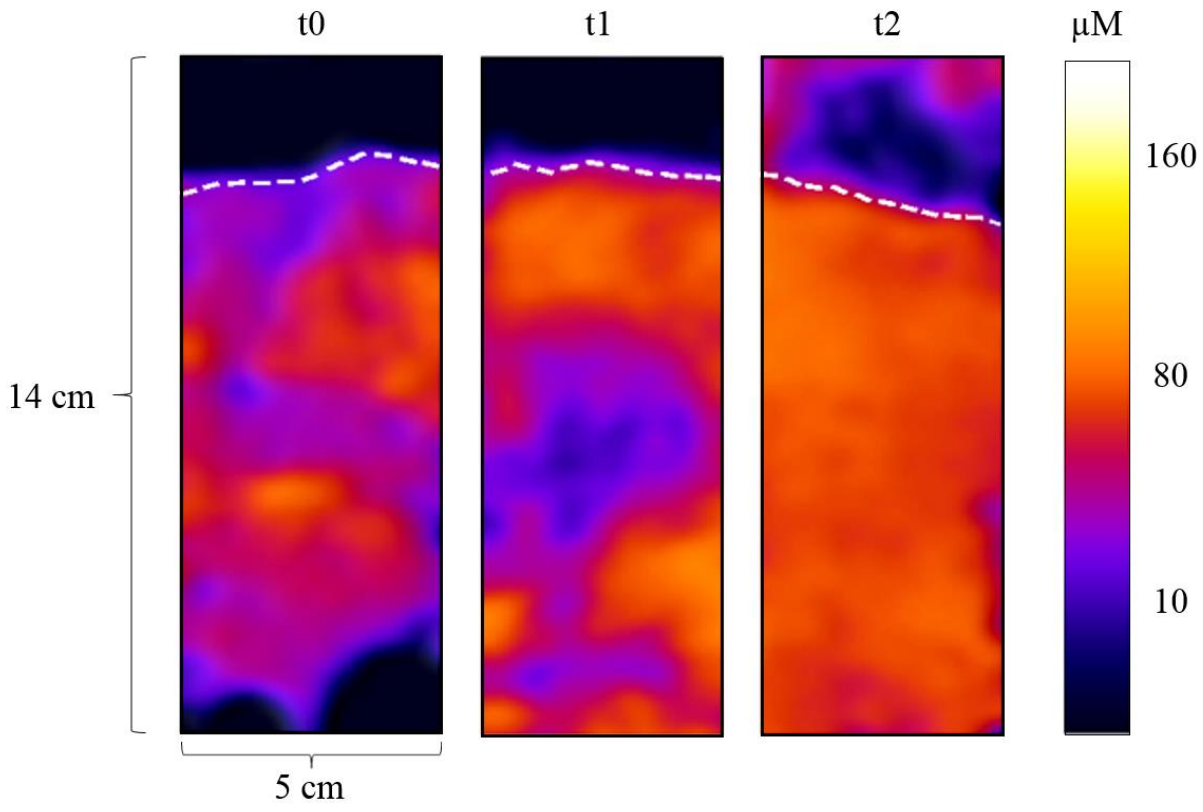

Figure 4.9

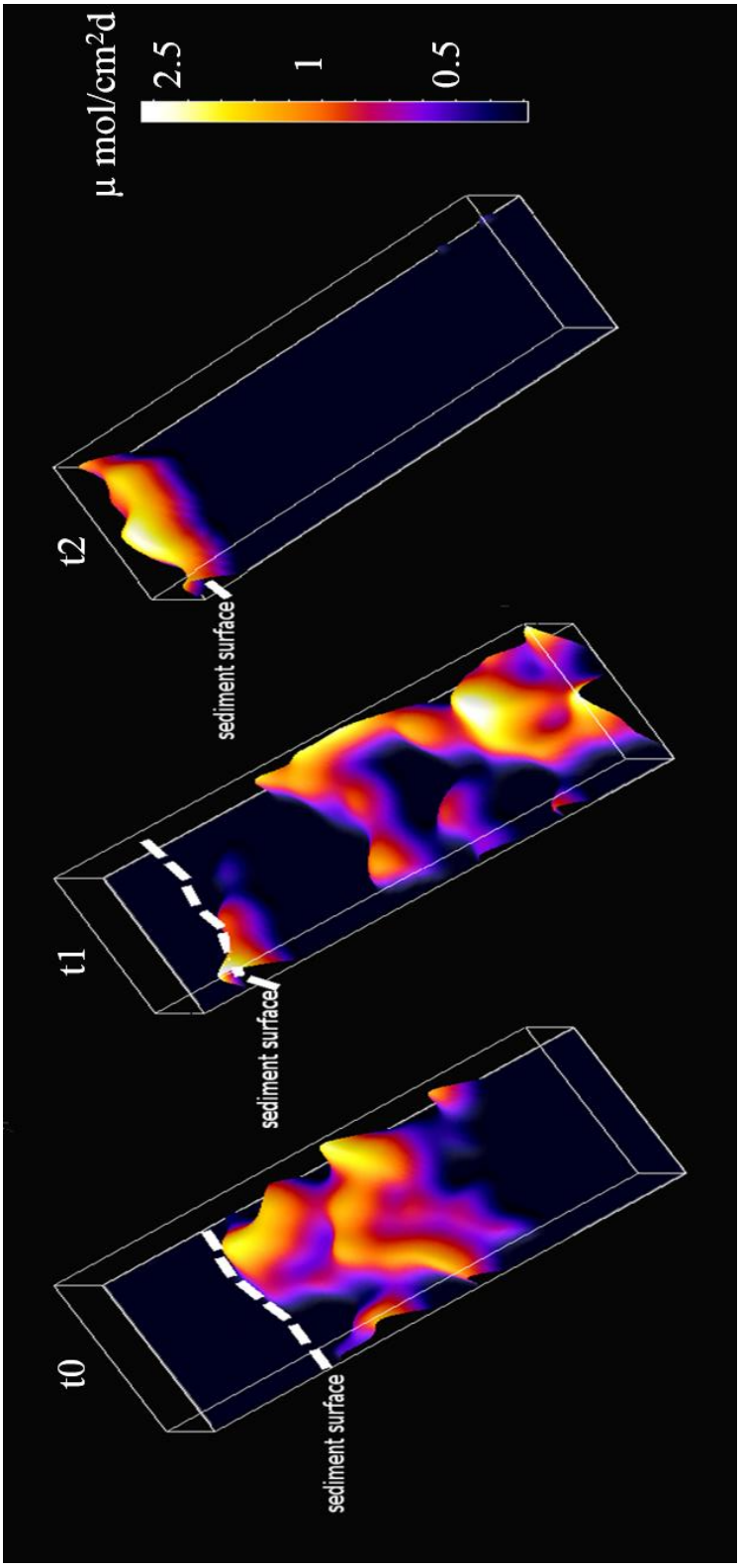
μ mol/cm²d
2.5
1
0.5
t2
t1
t0
sediment surface
sediment surface
sediment surface

Figure 4.10

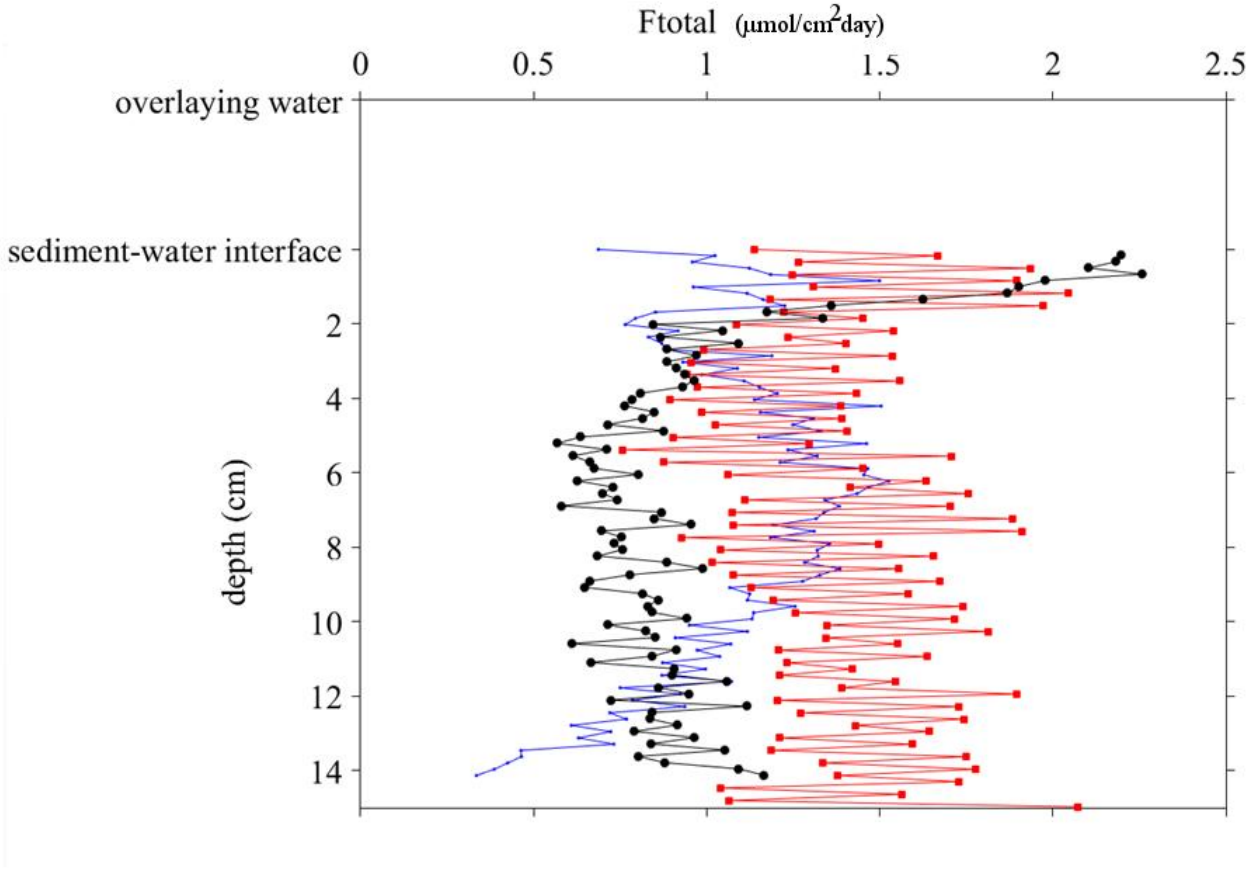
Ftotal (μmol/cm2day)
0
0.5
1
1.5
2
2.5
overlaying water
sediment-water interface
depth (cm)
2
4
6
8
10
12
14

Figure 4.11

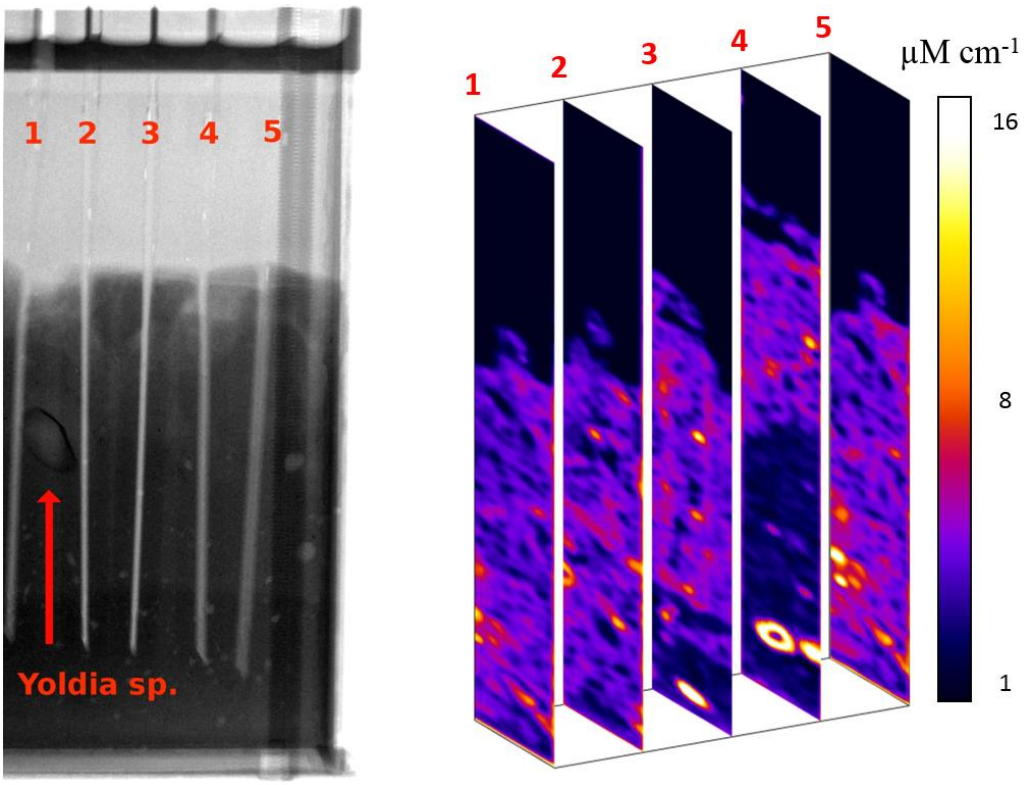

Figure 4.12

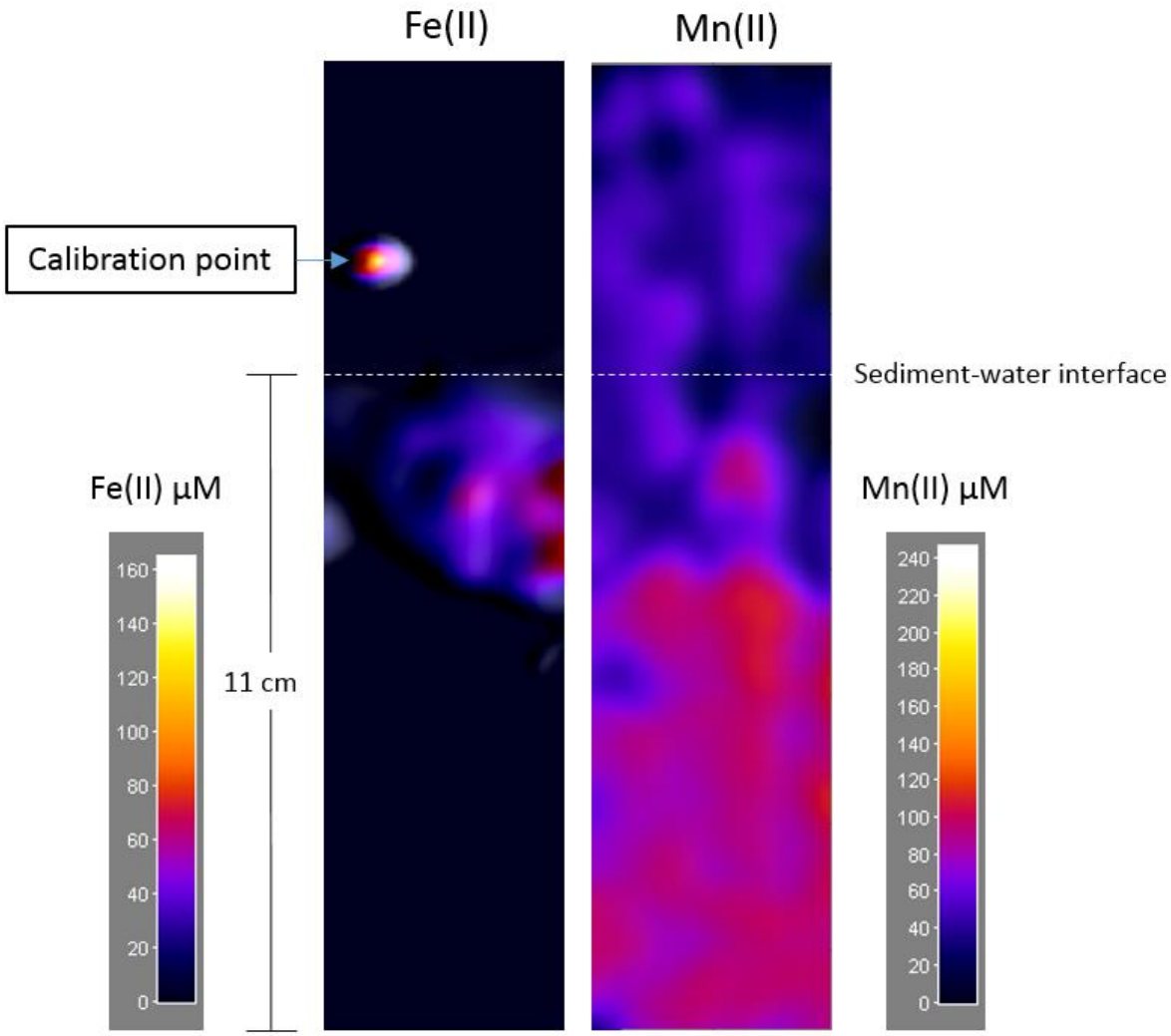
Fe(II)
Mn(II)
Calibration point
Sediment-water interface
Fe(II) µM
Mn(II) µM
11 cm
160
140
120
100
80
60
40
20
0
240
220
200
180
160
140
120
100
80
60
40
20
0

Figure 4.13

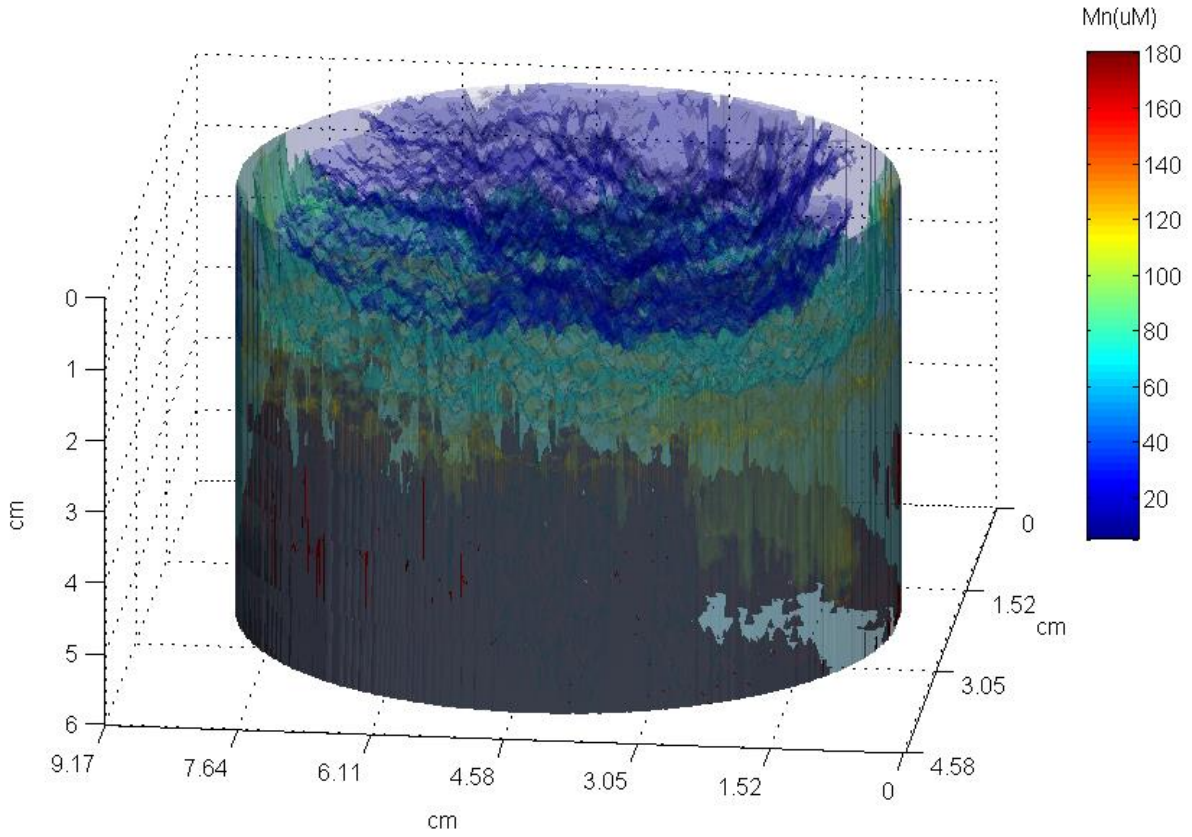
Mn(uM)
180
160
140
120
100
80
60
40
20
cm
0
1
2
3
4
5
6
9.17
7.64
6.11
4.58
3.05
1.52
0
cm
0
1.52
3.05
4.58
cm

Figure 4.14

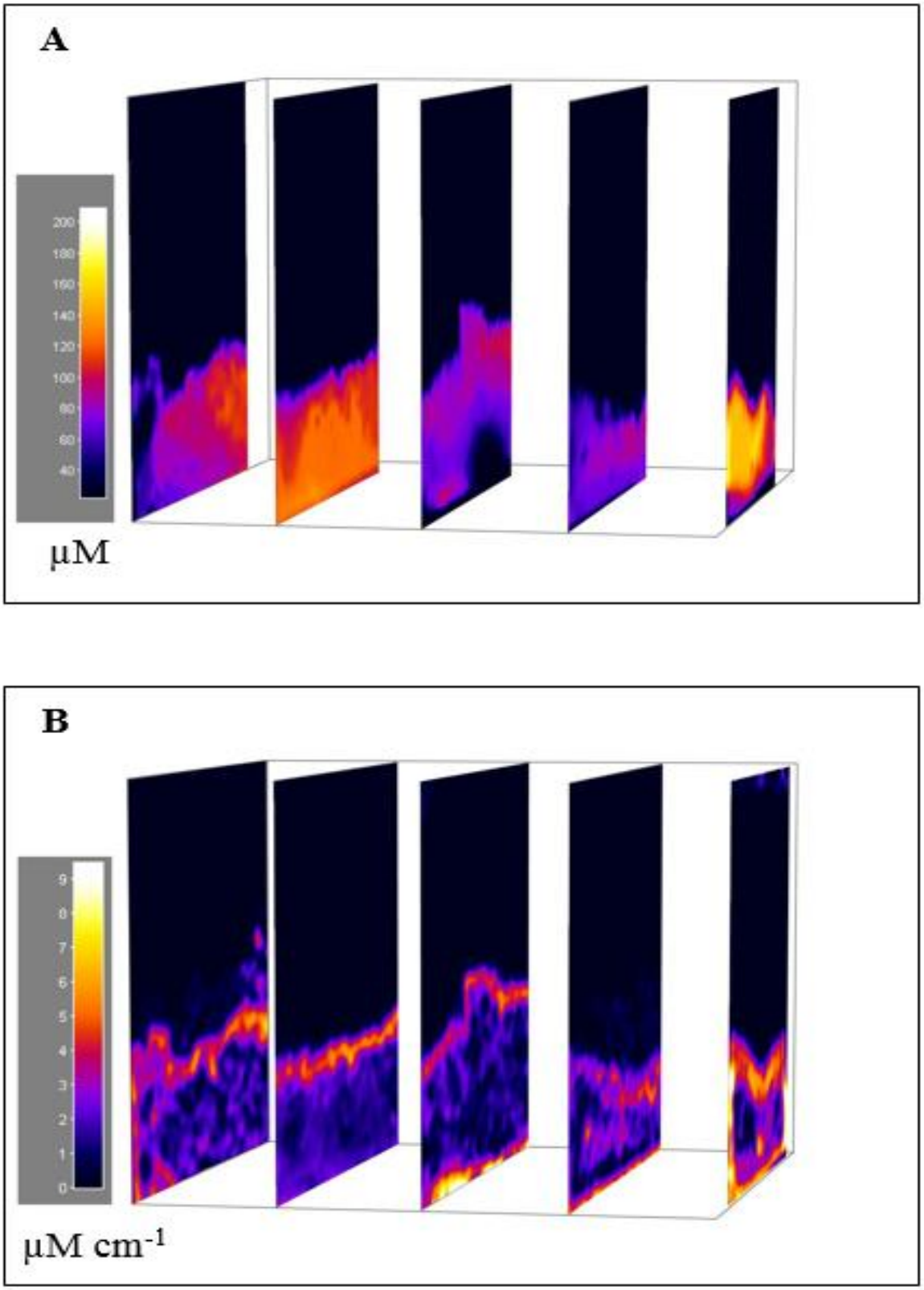

Figure 4.15

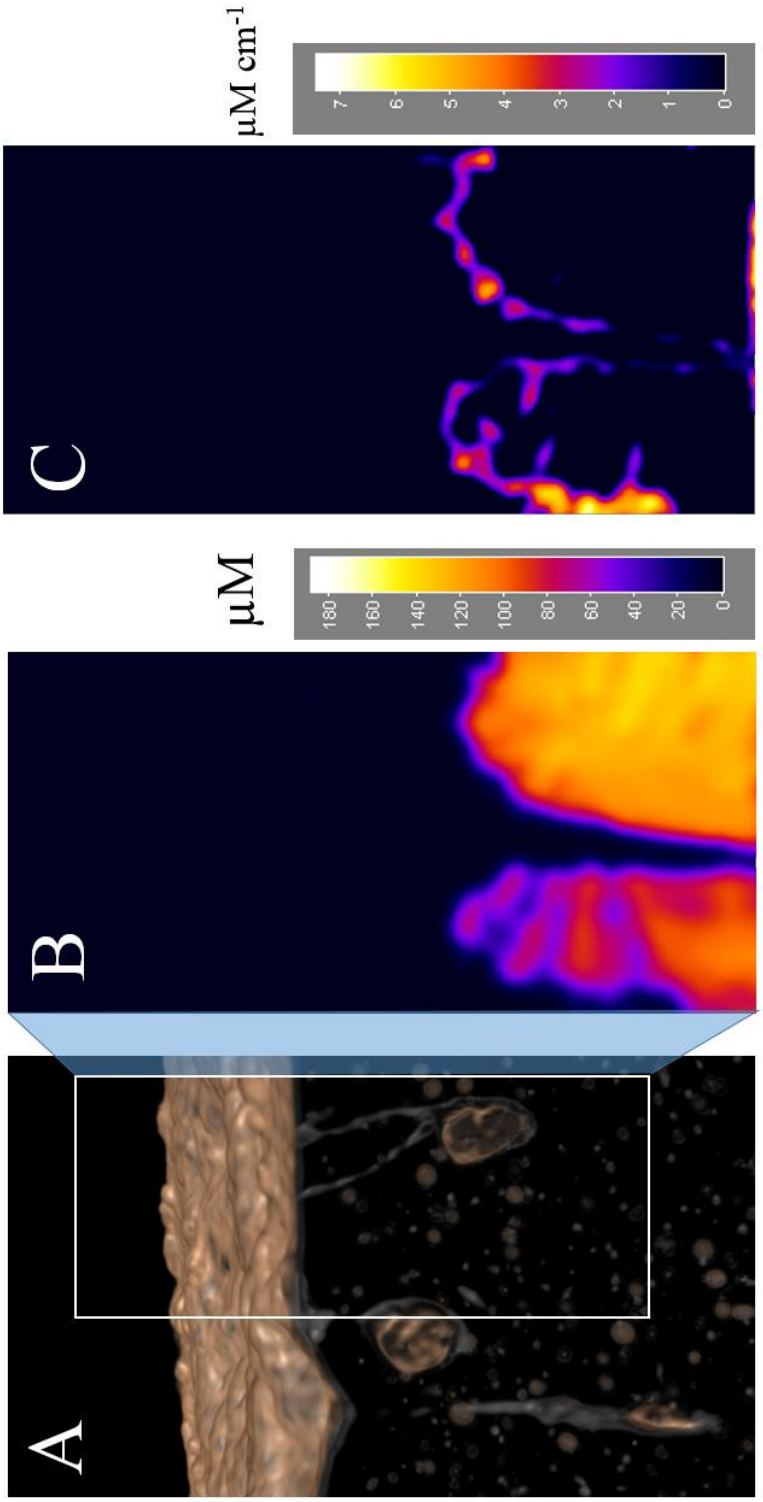

Figure 4.16

Tables

Table 2.1

Estimated parameters, fitting error (eq.14) and second derivative (eq. 15) values at 469 nm for Gaussian curves (eq. 13) fitted to the Mn-TSPP peak for each solution used in the calibration curve.

Gaussian fitting (eq. 3)	Mn(II) added (nmol)/well	7.5	3.750	1.875	0.938	0.469	0.234	0.117	0.059	mean	SD
	Ao	1.003	1.003	0.525	0.290	0.167	0.102	0.074	0.062		
	q	0.288	0.288	0.201	0.215	0.216	0.189	0.192	0.190	0.227	0.052
	w	15.97673	15.977	16.037	16.066	16.084	16.016	15.954	16.031	16.013	0.053
	Xo(nm)	469									
	d	-4Ln(2)									
	err (eq. 4)	0.003655	0.004	0.001	0.000	0.000	0.000	0.000	0.000	0.002	0.005
	2d derivative at 468 (eq. 5)	-0.03852	-0.022	-0.011	-0.006	-0.004	-0.002	-0.002	-0.001		

Table 2.2

The Effect of foreign ions on the determination of 10 μM Mn^{2+} solutions (2 nmol Mn/well; sample volume: 200 μL; T=298.15ºK; pH 8 and 35 psu).

Foreign ions	Concentration (μM)	Relative error (%)	
		2nd deriv.	Single absorbance
Pb^{2+}	1	0.06	1.09
Al^{3+}	1	0.03	0.05
Fe^{2+}	24.88	0.07	2.53
Li^{+}	100	0.33	4.99
Ni^{2+}	100	0.32	0.67
Sr^{2+}	100	0.37	6.42
Zn^{2+}	1	0.19	11.22
Cu^{2+}	1	0.13	8.75
Cr^{3+}	1	0.13	16.15
Co^{2+}	1	0.08	12.56

Table 2.3

Comparison of proposed 2nd derivative and single absorbance methods with formaldoxime method for determination of Mn^{2+} in oxidized and filtered porewater matrixes.

Oxidized Porewater	Added $[Mn^{2+}]$ (μM)	Recovered $[Mn^{2+}]$ ± SD (μM), (n=4)		
		2nd Derivative method	Single absorbance ($\Delta A_{469-490}$)	Formaldoxime Method
1	9.40	9.44±0.20	9.52±0.22	11.40±0.76
2	10.00	9.99±0.13	10.09±0.13	10.78±0.62
3	9.40	9.61±0.39	9.59±0.40	9.20±0.22

Table 2.4

Determination of Mn^{2+} in pore water from Great Peconic Bay and Long Island Sound using both formaldoxime and proposed Cd-TSPP methods (single absorbance and 2nd derivative).

Sample site	Methods Mean (µM) ±SD (n=4)		
	Formaldoxime	Single absorbance	2nd derivative
Great Peconic Bay	65.3±2.1	64.4±0.54	65.3±0.83
Long Island Sound	90.48±2.9	95.7±1.51	96.8±2.08

Table 3.1

Combinations of supporting material (S), immobilizing agent (IA; IA1: D4 and IA2: alcohol blocked D4) and indicator solution (IN; undiluted (IN_{stock}), in water (IN1), in a ethyl alcohol 97% (IN2), and modified porphyrin (IN3)) utilized to prepare sensing foils for each tested immobilization sub-scheme.

Sub-scheme	S	IA		IN			
		IA1	IA2	IN_{stock}	IN1	IN2	IN3
Sch1	X	X		X			
Sch2	X	X			X		
Sch3	X	X				X	
Sch4	X		X		X		
Sch5	X		X			X	
Sch6	X		X				X

Table 3.2

Summary of indicator release from entrapment attemps using the different sub-schemes proposed in this study (n.d: non detectable).

Sub-scheme	Indicator release from entrapment
Sch1	Low
Sch2	Low
Sch3	n.d
Sch4	Very high
Sch5	Very high
Sch6	n.d

Table 3.3

Summary of reactivity test results for each sub-scheme proposed in this study, excepting Sch 4 and Sch5, which were discarded because their profuse release of chemical indicator into the immersing solution.

Sub-scheme	Sub-scheme response to Mn(II) (reactivity test)
Sch1	No response
Sch2	Slow reaction rate
Sch3	Slow reaction rate
Sch4	non tested (immobilization issues)
Sch5	non tested (immobilization issues)
Sch6	Positive response (useful reaction rate for Mn(II) determinations

Table 4.1

Summarized schedule of core sealing (X), overlying water sampling (S), and opening & two dimensional sensor deployment (2DS) for cores used during flux experiments.

Core	t: 0 hrs.	$t \in]0,6[\ hrs.$	t: 6hrs	$t \in]6,12[\ hrs.$	T: 12 hrs.
'control'	X,S	S	S	S	S
't0'	2DS				
't1'	X,S	S	2DS		
't2'	X,S	S	S	S	2DS